

# CELL SEPARATION IN AQUEOUS TWO-PHASE SYSTEMS – DEVELOPMENT OF AN INTEGRATED HIGH-THROUGHPUT SCREENING PLATFORM FOR DOWNSTREAM PROCESS DEVELOPMENT FOR CELL-BASED PRODUCTS

zur Erlangung des akademischen Grades eines  
DOKTORS DER INGENIEURWISSENSCHAFTEN (Dr.-Ing.)

der Fakultät für Chemieingenieurwesen und Verfahrenstechnik des  
Karlsruher Instituts für Technologie (KIT)  
vorgelegte

genehmigte  
DISSERTATION

von  
M.Sc. Sarah Zimmermann (geb. Nagel)  
aus Landau in der Pfalz

Referent: Prof. Dr. Jürgen Hubbuch  
Korreferent: Prof. Dr. Eric Gottwald  
Tag der mündlichen Prüfung: 03.02.2017



---

## Acknowledgments

During the past years, I received support from many people to which I would like to express my gratitude.

Firstly, I would like to express my gratitude to my doctoral advisor Prof. Dr. Jürgen Hubbuch for the opportunity to conduct my dissertation in his group and the continuous financial and intellectual support during my dissertation. I am sincerely grateful for the opportunity to work on this cutting edge research project and the support on conference participations and industrial and academic collaborations. Moreover, I very much appreciated the freedom I was given to shape this project and realize my own ideas.

Moreover, I would like to express my sincere gratitude to my second referee Prof. Dr. Eric Gottwald for the support during my dissertation, his professional advice, continuous support, and great discussions.

Furthermore, I would like to thank Dr. Stefan Oelmeier and Dr. Anna Osberghaus for mentoring me during my dissertation. Many thanks to Dr. Stefan Oelmeier for introducing me to high-through experimentation, aqueous two-phase systems, and the quirks of Chantalle, and to Dr. Anna Osberghaus for the many great discussions, her encouragement, and her continuous support on statistical data analysis and scientific writing.

My sincere thank goes to my advisors from Novo Nordisk A/S, Arne Staby, Are Bogsnes, Mattias Hansson, Tino Klein, Nicolaj Strøyer Christophersen, and Lina Thorén for their continuous support during my thesis, the great discussions, and the warm welcome in Denmark. Especially, I would like to thank Are for inviting us tyskere to a wonderful dinner!

My sincere thank also goes to Prof. Dr. Andrea Hartwig, Dr. Sarah Fremgaard Risnes, Dr. Barbara Koch, Dr. Christopher-Tilman Krüger, Elena Maser, and Rebecca Schilling for sharing their laboratories and research facilities with us, helping me out with cell lines and reagents, and supporting me with my flow cytometry analyses. Without their support it would not have been possible to conduct this project.

I would like to thank my fellow labmates and all other members of the Biomolecular Separation Engineering Group for being great colleagues during the past years. In particular, I would like to thank Sarah Gretzinger for keeping me company during the many long days in the cell culture lab and for helping me to bring our last project to a successful ending. I would like to thank Christopher Ladd Effio very much for introducing me to the world of CPC, even though my cells took a particular dislike in this method. Finally, I would like to thank my office colleagues Frieder Kröner, Pascal Baumann, Kai Baumgärtner, and Frank Hämmerling, for many great and funny hours in the office.

I would also like to thank my students Sarah Gretzinger, Marie-Luise Schwab, Anna-Lena Winkler, Eva Conraths, and Christian Scheeder, who all contributed to the success of this work.

---

Moreover, I would like to thank the Karlsruhe House of Young Scientist (KHYS) for awarding me with a Research Travel Grant, which enabled me to conduct my research stay in Denmark.

Last but not the least, I would like to thank my family: my parents and my brother and his girlfriend, to whom I could always come home to after a long and stressful week. Moreover, I would like to thank all my friends for being there for me during the past years, and significantly contributing to me keeping my sanity.

But most of all, I would like to thank my husband Philipp for always being there for me during the past eleven years and believing in me much more than I did. Without your love and support I am absolutely certain that I wouldn't be where I am today.

---

## Abstract

Emerging cell-based therapeutics hold promise to revolutionize the way we treat diseases, and the field has gained considerable momentum in the past decade. As a consequence, many cell-based therapeutics have reached clinical development. The availability of clinical-scale downstream processing strategies for cell-based products presents a critical juncture between basic research and clinical development. Cell-based therapeutics need to be provided in high purities, since certain contaminants can cause severe adverse reactions. Aqueous two-phase systems (ATPS) facilitate the label-free, scalable, and cost-effective separation of cells, and present a promising tool for downstream processing of cell-based therapeutics. ATPS have been subject of research since the 1950s, nonetheless, the knowledge about the mechanisms underlying cell partitioning is limited. As a result, the development of effective downstream processes requires the optimization of many different parameters, and, even though the applicability of ATPS for preparative-scale cell separation is well established, laborious empirical process optimizations have hampered widespread application of ATPS in cell purification.

This thesis is centered around the development of preparative-scale downstream processing strategies for cell-based products. The scope of the first part of this thesis is the development of an integrated high-throughput screening (HTS)-platform for downstream process development for cell-based therapeutics using ATPS. The second part of this thesis describes the application of this HTS-platform to study mechanisms in ATPS-mediated cell separation, determine key process parameters, and conduct case studies on downstream process design.

The first section of this thesis deals with the evaluation of analytical technologies for high-throughput (HT)-downstream process development for cell-based products. In order to design novel HTS-platforms for downstream processing of cell-based drugs, robust, accurate, and sensitive HT-cell quantification assays are required. It is crucial that the utilized assays are robust towards changes in buffer composition and produce reliable results over a wide range of medium densities and viscosities. Accordingly, a comparative study on HT-cell quantification assays was performed, where sensitivity, dynamic range, and precision were evaluated for a number of methods that differ in their respective mechanism. In addition, the performance of these methods was assessed over a range of buffer compositions, medium densities, and viscosities, to evaluate assay robustness. This benchmark study was designed as a guide for selecting HT-cell quantification assays for a specific application. The study revealed that both CellTiter-Glo<sup>TM</sup> and HT-flow cytometry are excellent tools for HT-cell quantification. Both methods showed broad working ranges, high precision, and excellent robustness. Moreover, HT-flow cytometry enables the simultaneous analysis of multiple parameters, such as cell viability, cell cycle distribution, and the expression of surface markers, to identify various cell types in complex mixtures. HT-flow cytometry is thus an ideal tool for cell quantification and analysis in HT-downstream process development for cell-based products.

The second section of this thesis describes the development and validation of an automated robotic screening that enables HT-cell partitioning analysis in ATPS. The availability of miniaturized and fully automated screening-platforms presents a crucial enabling technology for downstream processing of cell-based products. The reduction in time and material consumption enables the systematic investigation of key parameters in cell parti-

---

tioning and thus facilitates more directed downstream process development. Moreover, it will enable researchers to gain a more detailed understanding of the mechanisms underlying cell partitioning in ATPS. The screening was implemented on a robotic liquid-handling station and comprises a fully automated screening process, from ATPS preparation to cell quantification and analysis using HT-flow cytometry. The study demonstrates that this setup enables fast and systematic investigation of factors influencing cell partitioning. In a first case study, separation conditions for the differentiable promyelocytic cell line HL-60 in polyethylene glycol (PEG)-dextran ATPS were examined, and it was shown that the separation of CD11b-positive and CD11b-negative HL-60 cells is possible after partial DMSO-mediated differentiation towards the granulocytic lineage. The influence of salt composition, pH, and tie-line length on the resolution of CD11b-positive and CD11b-negative HL-60 was evaluated, and separation conditions were optimized. Using a countercurrent distribution (CCD)-model, optimal separation conditions for a multi-stage purification process were investigated. The modeling data indicate that complete peak separation is possible with 30 transfers, and > 93% of CD11b-positive HL-60 cells can be recovered with > 99% purity.

The third section of this thesis describes the application of the previously developed screening-platform to investigate the influence of polymer molecular weight and tie-line length on the resolution of five model cell lines in charge-sensitive PEG-dextran ATPS, which enable cell separation based on surface charge-associated properties. In order to enable multiplexing of HT-partitioning analysis in ATPS, a barcoding strategy using different CellTracker<sup>TM</sup> dyes in a combinatorial fashion was developed. This enabled a substantial reduction in time and material consumption, and it was shown that CellTracker<sup>TM</sup> dyes are an excellent tool for multiplexing in screenings investigating cell surface properties, as they are retained inside living cells and do not alter cell surface properties. The study describes how polymer molecular weight and tie-line length influence cell partitioning in charge-sensitive ATPS, and that the combination of low molecular weight PEGs and high molecular weight dextrans enable the highest resolution of the five cell lines. Furthermore, the study demonstrates that the separability of each cell line from the mixture is highly dependent on the polymer molecular weight composition and tie-line length. Finally, it was shown that cell surface charge-dependent cell partitioning due to an interfacial Donnan potential is the major driving force in ATPS containing phosphate, independent of polymer molecular weight and tie-line length. Using a CCD-model it was demonstrated that the conducted screenings yielded conditions that enable the isolation of four of the five cell lines with high purity (>99.9%) and high yield in a single CCD-run.

The final section of this thesis describes the design of a purification strategy for the two model cell lines HL-60 and L929 based on HTS-data and CCD-modeling using PEG-dextran ATPS. Subsequently, the CCD-model was experimentally validated, showing excellent congruence between model and experimental data. The study showed that CCD-models are highly accurate and, in combination with HTS-data, present a powerful tool in downstream process development. Finally, the influence of cell cycle phase on cell partitioning and the resolution of HL-60 and L929 was analyzed, which may interfere with the robustness of a purification process. As cells pass through the cell cycle, a multitude of changes takes place, such as changes in cell volume, density, DNA content, protein expression, and consequently cell surface properties. The study revealed that while cell

---

cycle phase is a significant factor in cell partitioning, cell type-specific differences in surface properties were the main driving force. Constant growth conditions are, however, a means to further increase process robustness.

In summary, the HTS-method developed in this work enables faster, cheaper, and more directed downstream process development for cell-based products, and presents a powerful enabling technology for translational research. The conducted case studies identified key parameters in cell separation and provide a benchmark for future applications. Future exploitation of this platform will enable a more detailed understanding of cell separation using ATPS.

---

---

## Zusammenfassung

Innovative Zelltherapien versprechen die Behandlung von Krankheiten zu revolutionieren und das Feld der Zelltherapeutika hat im letzten Jahrzehnt bedeutend an Dynamik gewonnen. Infolgedessen sind viele Zelltherapeutika inzwischen in der klinischen Entwicklung angelangt. Die Verfügbarkeit von Aufarbeitungs (*engl.* Downstream Processing)-Strategien für Zelltherapeutika im klinischen Maßstab stellt eine kritische Schnittstelle zwischen Grundlagenforschung und klinischer Entwicklung dar. Zelltherapeutika müssen in hoher Reinheit vorliegen, da bestimmte Kontaminanten schwerwiegende Nebenwirkungen hervorrufen können. Wässrige Zweiphasensysteme (*engl.* aqueous two-phase systems (ATPS)) ermöglichen die Marker-freie, skalierbare und kosteneffiziente Separation von Zellen und stellen somit eine vielversprechende Methode für die Aufarbeitung von Zelltherapeutika dar und obwohl ATPS bereits seit den 1950er Jahren Gegenstand der Forschung sind, ist das Wissen über die zugrunde liegenden Mechanismen bisher begrenzt. Daher ist zur Entwicklung von effektiven Aufbereitungsverfahren die Optimierung einer Vielzahl von Parametern notwendig. Obwohl die Anwendbarkeit von ATPS zur präparativen Zellseparation bereits vielfach aufgezeigt wurde, verhinderte die arbeitsintensive empirische Prozessoptimierung bisher die breite Anwendung.

Das zentrale Thema dieser Dissertation ist die Entwicklung von präparativen Aufbereitungsverfahren für Zell-basierte Produkte. Der erste Teil dieser Arbeit beschreibt die Entwicklung einer integrierten Hochdurchsatz-Screening (*engl.* high-throughput screening (HTS))-Plattform für die Entwicklung von Aufbereitungsverfahren für Zelltherapeutika mittels ATPS. Im zweiten Teil der Arbeit wird diese HTS-Plattform angewandt um die der Zellseparation mittels ATPS zugrunde liegenden Mechanismen zu untersuchen, Schlüsselparameter zu identifizieren und Fallstudien zur Entwicklung von Aufbereitungsprozessen mit verschiedenen Modellsystemen durchzuführen.

Im ersten Abschnitt dieser Arbeit wurden verschiedene analytische Methoden für die Hochdurchsatz (HT)-Aufarbeitungsprozessentwicklung für Zell-basierte Produkte evaluiert. Um neue HTS-Plattformen für die Aufarbeitung von zell-basierten Produkten zu entwickeln, werden robuste, präzise und sensitive HT-Zellquantifizierungsmethoden benötigt. Außerdem ist es entscheidend, dass die verwendeten Methoden robust gegenüber Veränderungen in der Pufferzusammensetzung sind, sowie verlässliche Ergebnisse unabhängig von Mediendichte und Viskosität liefern. Diesbezüglich wurde eine Vergleichsstudie mit diversen HT-Zellquantifizierungsmethoden durchgeführt, um die Sensitivität, den dynamischen Bereich und die Präzision der Methoden zu ermitteln. Außerdem wurde die Leistung dieser Methoden in Abhängigkeit der Pufferzusammensetzung, Mediendichte und Viskosität untersucht, um die Robustheit der einzelnen Methoden zu validieren. Diese Studie wurde konzipiert, um die Auswahl geeigneter HT-Zellquantifizierungsmethoden für spezifische Anwendungen zu ermöglichen. Der Methodenvergleich ergab, dass sowohl CellTiter-Glo<sup>TM</sup> als auch HT-Durchflusszytometrie exzellente Methoden für die HT-Zellquantifizierung sind. Beide Methoden zeigten einen breiten Arbeitsbereich sowie hohe Präzision und Robustheit. Zudem ermöglicht die HT-Durchflusszytometrie die gleichzeitige Analyse mehrerer Parameter, wie Zellvitalität, Zellzyklusverteilung, sowie die Expression von Oberflächenmarkern zur Identifizierung verschiedener Zellarten in komplexen Zellpopulationen. HT-Durchflusszytometrie ist somit eine ideale Methode zur Zellquan-

---

tifizierung und -analyse in der HT-Aufarbeitungsprozessentwicklung von Zell-basierten Produkten.

Der zweite Abschnitt der Arbeit beschreibt die Entwicklung und Validierung eines automatisierten robotergestützten Screeningverfahrens, das die HT-Analytik der Zellverteilung in ATPS ermöglicht. Die Verwendung von miniaturisierten und vollautomatisierten Screeningplattformen stellt eine wichtige Grundlagentechnologie in der Aufarbeitung von Zell-basierten Produkten dar. Die daraus resultierende Zeit- und Kostenreduktion ermöglicht die systematische Untersuchung von Schlüsselparametern in der Zellseparation und somit eine zielgerichtete Aufarbeitungsprozessentwicklung. Zudem ermöglicht die Verwendung von HTS-Technologien es Wissenschaftlern ein detailliertes mechanistisches Verständnis der Zellverteilung in ATPS zu erlangen. Die Screeningmethode wurde auf einer Pipettierroboterplattform etabliert und beinhaltet einen vollautomatisierten Screeningprozess, von der ATPS-Präparation bis hin zur Zellquantifizierung und -analyse mittels HT-Durchflusszytometrie. Die Studie zeigte, dass dieser Versuchsaufbau eine schnelle und systematische Untersuchung von Schlüsselfaktoren in der Zellverteilung ermöglicht. In einer ersten Fallstudie wurden Separationsbedingungen für die differenzierbare promyelozytische Zelllinie HL-60 in Polyethylenglycol (PEG)–Dextran ATPS untersucht, und es konnte gezeigt werden, dass die Separation von CD11b-positiven und CD11b-negativen HL-60 Zellen nach partieller DMSO-induzierter granulozytischer Differenzierung möglich ist. Im Rahmen der Studie wurde der Einfluss von Salzzusammensetzung, pH-Wert und Konodenlänge auf die Verteilung von CD11b-positiven und CD11b-negativen HL-60 Zellen evaluiert und die Separationsbedingungen optimiert. Durch die Verwendung eines Gegenstromverteilungs (*engl.* countercurrent distribution (CCD)) -Modells wurden optimale Separationsbedingungen für einen mehrstufigen Aufreinigungsprozess validiert. Die Modelldaten zeigen, dass eine Auftrennung in 30 Verteilungsschritten möglich ist und dass >93% der Cd11b-positiven HL-60 Zellen mit einer Reinheit von >99% isoliert werden können.

Im dritten Abschnitt dieser Arbeit wurde die zuvor entwickelte Screeningmethode eingesetzt um den Einfluss von Polymermolekulargewicht und Konodenlänge auf die Separation von fünf Modellzelllinien in ladungsabhängigen (*engl.* charge-sensitive) PEG-Dextran ATPS zu untersuchen, welche die Zellseparation basierend auf Oberflächenladungs-assoziierten Eigenschaften ermöglichen. Um die gleichzeitige Verteilungsanalyse mehrerer Zelllinien zu ermöglichen, wurde eine 'Barcoding'-Strategie entwickelt, welche auf dem kombinatorischen Einsatz der CellTracker<sup>TM</sup> Farbstoffen beruht und eine signifikante Reduktion des Zeit- und Materialverbrauchs ermöglicht. Es konnte gezeigt werden, dass CellTracker<sup>TM</sup>

Farbstoffe hervorragend für Screenings geeignet sind, welche die Untersuchung von Zelloberflächeneigenschaften zum Ziel haben, da die Farbstoffe im Inneren der Zelle in ein zellimpermeables Reaktionsprodukt umgesetzt werden und somit keine Veränderung der Zelloberflächeneigenschaften zur Folge haben. Diese Studie beschreibt, wie das Polymermolekulargewicht und die Konodenlänge die Zellseparation in ladungsabhängigen ATPS beeinflussen und dass die Kombination aus niedermolekularen PEGs und hochmolekularen Dextranen die höchste Auflösung der fünf Zelllinien ermöglicht. Außerdem konnte gezeigt werden, dass die Separierbarkeit der einzelnen Zelllinie aus der Mischung stark abhängig

---

von der Zusammensetzung der Polymermolekulargewichte und der Konodenlänge ist. Weiterhin wurde in der Studie gezeigt, dass die oberflächenladungsabhängige Zellverteilung aufgrund der Ausbildung eines Donnan-Potentials ein Hauptfaktor in der Zellverteilung in phosphathaltigen ATPS ist, unabhängig von Polymermolekulargewicht und Konodenlänge. Durch die Verwendung eines CCD-Modells konnten Separationsbedingungen identifiziert werden, welche die Isolierung von vier der fünf Zelllinien mit hoher Reinheit (>99,9%) und hoher Ausbeute in einem CCD-Lauf ermöglichen.

Im letzten Abschnitt dieser Arbeit wurde eine Aufarbeitungsstrategie für die Modellzelllinien HL-60 und L929 in PEG-Dextran ATPS, basierend auf HTS-Daten und CCD-Modellen entwickelt. Die experimentelle Validierung des CCD-Modells ergab eine exzellente Übereinstimmung von experimentellen und Modelldaten. Die Studie zeigte, dass CCD-Modelle sehr akkurat sind und in Kombination mit HTS-Daten eine wichtige Methode in der Entwicklung von Aufarbeitungsprozessen darstellen. Abschließend wurde der Einfluss der Zellzyklusphase auf die Verteilung und Auflösung von HL-60 und L929 analysiert, da dies die Robustheit des Aufreinigungsprozesses beeinflussen kann. Im Laufe des Zellzyklus finden eine Vielzahl an zellulären Veränderungen, wie z.B. die Änderung des Zellvolumens, der Dichte, des DNA-Gehalts, der Proteinexpression und somit der Oberflächeneigenschaften statt. Die Studie ergab, dass obwohl die Zellzyklusphase ein signifikanter Faktor in der Zellverteilung ist, die Zellseparation primär von Zelltyp-spezifische Unterschieden der Oberflächeneigenschaften abhängig ist. Konstante Wachstumsbedingungen sind jedoch ein geeignetes Mittel um die Prozessrobustheit zu steigern.

Zusammenfassend ermöglicht die hier entwickelte HTS-Methode eine schnellere, kostengünstigere und zielgerichteter Entwicklung von Aufbereitungsverfahren für Zell-basierte Produkte und stellt somit eine wichtige Technologie für die translationale Forschung dar. Die durchgeführten Fallstudien identifizierten Schlüsselparameter in der Zellseparation und stellen einen Bezugspunkt für zukünftige Anwendungen dar. Die zukünftige Nutzung dieser Plattform wird ein detaillierteres Verständnis der Zellseparation in ATPS ermöglichen.



---

# Contents

<b>1</b>	<b>Introduction</b>	<b>15</b>
1.1	Cell-based therapeutics . . . . .	16
1.1.1	Manufacturing of cell-based therapeutics . . . . .	19
1.2	Downstream processing of cell-based therapeutics . . . . .	19
1.3	Cell separation methods . . . . .	20
1.3.1	Immunoaffinity-based cell separation methods . . . . .	20
1.3.2	Physical cell separation methods . . . . .	21
1.4	Aqueous two-phase systems (ATPS) . . . . .	22
1.4.1	Cell partitioning in aqueous-two phase systems (ATPS) . . . . .	23
1.4.2	Multi-stage countercurrent distribution (CCD) . . . . .	24
1.4.3	Modeling countercurrent distribution (CCD) . . . . .	25
1.5	High-throughput process development (HTPD) . . . . .	26
1.5.1	HT-cell quantification methods . . . . .	26
<b>2</b>	<b>Research Proposal</b>	<b>29</b>
<b>3</b>	<b>Publications &amp; Manuscripts</b>	<b>31</b>
	High-throughput cell quantification assays for use in cell purification develop- ment – enabling technologies for cell production . . . . .	32
	High-throughput downstream process development for cell-based products using aqueous two-phase systems . . . . .	53
	Cell separation in aqueous two-phase systems – Influence of polymer molecular weight and tie-line length on the resolution of five model cell lines . . . . .	81
	High-throughput downstream process development for cell-based products using aqueous two-phase systems – A case study . . . . .	105
<b>4</b>	<b>Conclusion &amp; Outlook</b>	<b>123</b>
<b>5</b>	<b>References</b>	<b>125</b>
<b>6</b>	<b>Abbreviations</b>	<b>131</b>

## CONTENTS

---

---

# 1 Introduction

Fueled by the invention of genetic engineering technologies, the emergence of biologics more than three decades ago has revolutionized medicine, which has long been dominated by small-molecule drugs. Today, countless peptide- and protein-based therapeutics have been licensed. Their huge success stems from their highly specific biological functions, which cannot be mimicked by small molecules. As a result, biologics have improved therapeutic effects, enable the treatment of formerly incurable diseases, and cause considerably less adverse reactions. The emergence of cell-based therapeutics presents the next turning point for pharmaceutical industry. The use of living cells as therapeutic agents holds great promise for medicine, as cells are capable of performing complex biological functions, can sense diverse biological signals and perform a series of biological responses (Fischbach et al., 2013; Leader et al., 2008). While most immunosuppressive drugs, for example, massively and non-specifically suppress immune reactions, rendering patients prone to infections, regulatory T-cells can be employed as "smart" therapeutic agents. Regulatory T-cells are capable of selectively controlling immune responses by controlling the activity of various immune cells in an antigen-specific manner. Thus, they can for example mediate highly specific immune tolerance for an organ graft, leaving the patient's immune response against pathogens intact (Tang and Bluestone, 2013). Today, cell-based therapeutics for numerous diseases and from a variety of cell sources have made their way to clinical development (Ratcliffe et al., 2013; Trounson and McDonald, 2015). A critical juncture between research and translational science is the availability of clinical-scale downstream processing strategies for cell-based products, since therapeutic cells need to be provided in high purities to ensure product safety.

Aqueous two-phase systems (ATPS) present a gentle, cost-effective, label-free, and scalable method for cell purification, and are well established in downstream processing of biopharmaceuticals (Albertsson, 1986; Soares et al., 2015; Walter et al., 1985). Moreover, polyethylene-glycol (PEG)-dextran ATPS have been successfully used to separate cells according to their surface properties with high selectivity and resolution (Albertsson, 1986; Walter et al., 1985). Using multi-step partitioning, such as countercurrent distribution (CCD), even complex cell mixtures could be effectively separated (Albertsson and Barid, 1962; Walter et al., 1985). Nonetheless, the development of efficient downstream processes requires the optimization of many different parameters, hampering widespread application of ATPS in cell purification. In the past decade, high-throughput screening (HTS)-technologies have become state-of-the-art in downstream process (DSP) development of biopharmaceuticals, such as protein- and DNA-based drugs (Łacki, 2014). These technologies have facilitated miniaturized, parallelized, and fully automated experimental setups, and have consequently enabled faster, cheaper, and more directed DSP development. In combination with Design of Experiments (DoE) and modelling tools, they present a powerful instrument to elicit mechanisms underlying separation and design purification strategies for novel targets. The implementation of HTS-tools in DSP development for cell-based therapeutics will likewise open up new possibilities for process design, and thus presents a crucial enabling technology for the translation of cell-based therapeutics.

## 1.1 Cell-based therapeutics

While the idea of using living cells as therapeutic agents is as old as the invention of blood transfusion, the progress in stem cell technology and molecular biology in the past decade has opened up an entirely new perspective on cell-based therapeutics. Today, cell-based therapeutics for a variety of diseases and from a variety of cell sources have made their way into clinical trials (Ratcliffe et al., 2013; Trounson and McDonald, 2015). Presently, approximately 1900 clinical trials on cell-based therapeutics are ongoing worldwide, and the cell therapy market is estimated to reach annual commercial sales of \$20 billion by 2025 (Buckler et al., 2016; Ratcliffe et al., 2013).

The field of cell-based therapeutics, while still in its infancy, is vast and extremely diverse. The most common form of cell-based therapy is cell replacement therapy, where lost cell types, e.g. hematopoietic stem cells or pancreatic beta-cells, are replaced. A special form of cell replacement therapy is tissue engineering, where tissues, and eventually entire organs, are rebuilt. Successful examples are skin, bone, and cartilage grafts, which have been approved almost a decade ago (Dodson and Levine, 2015). In addition, there are cell-based immunotherapies, where various cell types of the immune system are used to trigger, modulate, or suppress specific immune reactions. Cancer vaccines, for example, employ specifically engineered immune cells, such as dendritic cells (DC), natural killer (NK) cells, or cytotoxic T-cells, to target cancer cells and eradicate them by triggering a specific immune response. Finally, there are numerous approaches for cell-based drug delivery, where cells are specifically engineered to deliver biologics. Studies show that the cell-based delivery of therapeutic proteins enables the administration of steady protein concentrations over prolonged timespans, with improved therapeutic effects and considerably simpler treatment plans for the patients (Dove, 2003; Fliervoet and Mastrobattista, 2016; Pierigè et al., 2008; Ye and Mahato, 2008).

Cell-based therapies can be further classified into allogenic and autologous therapies. Autologous cell-based therapies use the patient's own cells as the therapeutic agent, while allogenic cell-based therapies use cells from a donor. While the allograft approach enables large-scale production of cell-based drugs, specific strategies are required to circumvent graft rejection. Autologous cell-based therapies, on the other hand, do not require immune protection as they are custom made for each patient from their own cells, which in turn creates a variety of economic, regulatory, and logistic obstacles (Dove, 2003). Moreover, cell-based therapeutics can be simple transplants or transfusions, or cells which have been specifically engineered for a therapeutic application, so called Advanced Therapy Medicinal Products (ATMPs) (Mount et al., 2015).

The emergence of stem cell technologies and the invention of induced pluripotent stem cells (iPSC) about a decade ago, has provided a novel source for numerous cell-based therapeutics (Daley and Scadden, 2008; Fischbach et al., 2013; Takahashi and Yamanaka, 2006). Embryonic stem cells (ESC) possess the unique ability of unlimited self-renewal and the ability to differentiate into to all cell types of the body (pluripotency). The ability to generate pluripotent stem cells (PSC) by directed reprogramming of somatic cells towards induced pluripotent stem cells (iPSC) has alleviated the ethical concerns associated with ESC, and thus represents one of the most crucial enabling technologies for modern regenerative medicine. iPSC thus provide a unique and potentially unlimited source for both autologous and allogenic cell-based therapeutics. A particularly promis-

ing approach is the use of iPSC-banks for HLA haplotype-matched allografts (Daley and Scadden, 2008; Turner *et al.*, 2013). In the past decade numerous differentiation protocols for PSC have been established, paving the way countless novel cell-based therapeutics. As a consequence, clinical trials for various stem cell-based therapeutics are presently conducted (Trounson and McDonald, 2015). In **Table 1** examples of cell-based therapeutics that have been approved by the authorities or are currently undergoing clinical trials are summarized (Dodson and Levine, 2015; Fliervoet and Mastrobattista, 2016; Mount *et al.*, 2015; Ratcliffe *et al.*, 2013; Trounson and McDonald, 2015).

# 1 INTRODUCTION

**Table 1:** Overview and current status of cell-based therapeutics for various indications and from different cell sources that have been approved by the authorities or are currently undergoing clinical trials (Dodson and Levine, 2015; Fliervoet and Mastrobattista, 2016; Mount et al., 2015; Ratcliffe et al., 2013; Trounson and McDonald, 2015). PBMC: peripheral blood mononuclear cells; ALL: acute lymphoblastic leukemia; ALS: amyotrophic lateral sclerosis; ASC: adult stem cells; CAR: chimeric antigen receptor; CNS: central nervous system; GvHD: graft-vs-host disease; hESC: human embryonic stem cells; MSC: mesenchymal stem cells; NSC: neural stem cells.

<b>Trial Sponsor</b>	<b>Indication</b>	<b>Cell type</b>	<b>Status</b>	<b>Reference</b>
<i>somatic cell therapeutics</i>				
Vericel (MA, USA)	cartilage defects	autologous chondrocytes (Catricel <sup>®</sup> )	FDA approved	(vcel.com)
Dendreon (WA, USA)	advanced prostate cancer	autologous reprogrammed PBMC (Provenge <sup>®</sup> )	FDA approved	(www.dendreon.com)
U.S. STEMCELL (FL, USA)	congestive heart failure	autologous myoblasts (MyoCell <sup>®</sup> ) / modified autologous myoblasts expressing angiogenic proteins (MyoCell <sup>®</sup> SDF-1)	phase II/III / phase I	(us-stemcell.com)
National Cancer Institute (NCI), National Institute of Health (NIH) (MD, USA)	ALL	CAR-modified T-cells targeting CD-19	phase I	(Lee et al., 2015)
<i>ASC-derived cell therapies</i>				
NuVasive, Inc. (CA, USA)	bone regeneration	allogenic (Osteocele <sup>®</sup> )	MSC FDA approved	(www.nuvasive.com)
Osiris Therapeutics, Inc. (MD, USA) / Mesoblast, Ltd. (Australia)	GvHD	allogenic (Prochymal <sup>®</sup> )	MSC Approved in Canada & New Zealand	(osiris.com), (www.mesoblast.com)
Neuralstem Inc. (MD, USA)	ALS	fetal-derived NSC	phase II	(www.neuralstem.com)
ReNeuron Ltd. (UK)	stroke & lower limb ischemia	hNSC	phase II	(www.reneuron.com)
Stem Cells Inc. (CA, USA)	multiple applications, including macular degeneration and spinal cord injury	human CNS stem cells	phase I/II	(www.stemcellsinc.com)
TRANSEURO (UK)	Parkinson's disease	fetal-derived dopaminergic cells	phase I	(www.transeuro.org.uk)
Brainstorm Cell Therapeutics, Inc. (NY, USA)	ALS	autologous MSC differentiated to express neurotrophic factors (MSC-NCF) (NurOwn <sup>™</sup> )	phase II	(www.brainstorm-cell.com)

## 1.2 Downstream processing of cell-based therapeutics

Trial Sponsor	Indication	Cell type	Status	Reference
<i>hESC-derived cell therapeutics</i>				
ViaCyte (CA, USA)	type I diabetes mellitus	hESC-derived pancreatic endodermal cells	phase I/II	(viacyte.com)
Pfizer UK/ Cell Cure Neurosciences Ltd. (Israel), ChabioTech Co. Ltd. (S. Korea)	macular degeneration	hESC-derived pigmented epithelial cells	phase I/II	(cellcureneurosciences.com; en.chabio.com)
Assistance Publique-Hopitaux de Paris (France)	heart failure	hESC-derived CD15+ Isl-1+ progenitors	phase I	(Trounson and McDonald, 2015)
International Stem Cell Corp. (Australia)	Parkinson's disease	human parthenogenetic-derived NSC	phase I/II	(internationalstemcell.com)
Asterias Biotherapeutics (CA, USA)	spinal cord injury	hESC-derived oligodendrocyte precursor cells	phase I/II	(asteriasbiotherapeutics.com)

### 1.1.1 Manufacturing of cell-based therapeutics

As an industry, cell-based therapies are still in their infancy, and manufacturing protocols are still in early stages of development (Heathman *et al.*, 2015). Nonetheless, scalable manufacturing processes need to be developed in parallel with clinical assessment, and the final manufacturing process needs to be in place before the products enter phase III clinical trials (Heathman *et al.*, 2015). Thus, it is essential that scalable and economically viable up- and downstream processing strategies are available as cell-based therapeutic enter clinical development. Manufacturing protocols for cell-based therapeutics are as diverse as the cell sources they are derived from. While hematopoietic stem cells from HLA-matched donors require small-scale isolation and purification protocols, iPSC-derived allografts require complex expansion, differentiation, harvesting, purification, and encapsulation protocols (Darkins and Mandenius, 2013; Sart *et al.*, 2014). Pancreatic progenitors for the treatment of type I diabetes, for example, are manufactured by a complex expansion and differentiation protocol (Schulz, 2015; Schulz *et al.*, 2012). In the first stage of the process hESC are expanded using a suspension-based feeder-free culture method. Subsequently, a step-wise differentiation protocol towards pancreatic endoderm is used by mimicking embryonic development. Finally, the cells are encapsulated for transplantation to ensure immune protection of the allograft (Schulz, 2015). Moreover, the scale varies significantly, depending on the number of patients to be treated, which can range from single-dose manufacturing processes for autologous cell-based therapies to large-scale bioprocesses for allografts.

## 1.2 Downstream processing of cell-based therapeutics

Downstream processing strategies for cell-based products are a critical juncture between basic research and translational science. The requirements on DSP are highly dependent on cell source and application. Following an initial enrichment step, several specific positive- and negative-selection steps may be required to further enrich the target cell type and deplete critical contaminants (Al-Rubeai and Naciri, 2014; Amos *et al.*, 2012; Rodrigues *et al.*, 2015; Stemberger *et al.*, 2012). When, for example, employing hESC or hiPSC-derived cell-based therapeutics, the propensity of tumor formation by residual

undifferentiated or partially differentiated cells presents a key regulatory issue (Rodrigues et al., 2015; Schriebl et al., 2010; Weil and Veraitch, 2014). Moreover, the differentiation of PSC usually results in a mix of different cell types and differentiation stages, which are often not fully characterized. The large size and complexity of mammalian cells, along with the inherent heterogeneity of differentiated cell populations, presents a major challenge for both DSP development and regulatory processes (Rodrigues et al., 2015; Willoughby, 2009). Thus, novel cell-based therapeutics need to be assessed carefully in order to evaluate potential risks and to design suitable purification strategies. Overall process requirements are high purities and yields. Moreover, maintaining cell viability, functionality, therapeutic potential, and ensuring overall safety are key requirements (Heathman et al., 2015; Rodrigues et al., 2015; Willoughby, 2009). During the translation of the first phase of cell-based therapeutics a key manufacturing issue was to keep manufacturing costs at a level that allows for commercial success (Dodson and Levine, 2015; Heathman et al., 2015).

### 1.3 Cell separation methods

At present there are a variety of cell separation methods available that differ in their specific mechanism, throughput, and selectivity (Tomlinson et al., 2013; Zhu and Murthy, 2013). They can be categorized into physical and immunoaffinity-based cell separation methods (**Figure 1**). While physical cell separation technologies exploit differences in physical properties such as density, size, surface charge or hydrophobicity, immunoaffinity-based cell separation methods use specific-antibodies to isolate the target cell population. For certain applications, e.g. the purification of hESC-derived cardiomyocytes, the specific metabolic properties of the target cells can be used for highly selective and cost-effective cell purification (Tohyama et al., 2013).

#### 1.3.1 Immunoaffinity-based cell separation methods

The antibody-mediated capture of cells based on the expression of specific surface antigens is highly selective, and the specificity and diversity of monoclonal antibodies makes them a powerful tool in cell purification. Thus, it is not surprising that these methods are the most widely applied (Amos et al., 2012; Weil and Veraitch, 2014). In addition to fluorescence activated cell sorting (FACS), immunoaffinity-based cell separation methods are available in many different formats, including magnetic, surface, column, and bead-based devices (Weil and Veraitch, 2014).

Magnetic activated cell sorting (MACS), a trademark name of Miltenyi Biotech for a magnetic bead-based immunoaffinity-purification system, for example, is applied in many clinical settings, such as the isolation of CD34+ hematopoietic stem cells (HSC) from mobilized peripheral blood apheresis products, and regulatory T-cells (Tregs) and NK-cells from peripheral blood mononuclear cells (PBMC) (Bluestone et al., 2015; Dahlberg et al., 2015; Hoffmann et al., 2006; Spohn et al., 2015; Tang and Bluestone, 2013).

While immunoaffinity-based cell separation methods are usually highly selective, scalable, and gentle with regards to cell viability, they have several drawbacks. Firstly, the use of large amounts of clinical-grade antibodies renders the method one of the most cost-intensive. Secondly, if several consecutive separation steps are required, purity and yield

can be significantly reduced. Even in single-marker MACS protocols, purities and yields vary considerably between batches, e.g. 30-90% purity, for the isolation of CD34+ HSC from mobilized peripheral blood apheresis products (Weil and Veraitch, 2014). Moreover, scalability and obtainable purities and yields are highly dependent on the format of the method (Al-Rubeai and Naciri, 2014; González-González et al., 2012). While FACS e.g. provides higher purities than other immunoaffinity-based cell separation techniques, the scalability is highly limited (Amos et al., 2012; González-González et al., 2012; Tomlinson et al., 2013). Thirdly, the use of positive-selection strategies poses considerable regulatory obstacles for the treatment of patients, as antibody-labels may cause adverse cellular reactions (Amos et al., 2012; Chen et al., 2014; Fernandes et al., 2014; Rodrigues et al., 2015; Tomlinson et al., 2013). Finally, there are a significant number of therapeutically relevant cell types that lack a specific surface antigen (Weil and Veraitch, 2014).

### 1.3.2 Physical cell separation methods

Physical cell separation technologies exploit differences in physical properties, such as density, size, surface charge, and hydrophobicity for cell separation.

Centrifugation techniques, such as density gradient centrifugation, exploit differences in cell density and size for cell separation. Density gradients and apheresis, for example, are applied in many clinical settings, such as the isolation of mononuclear cells from peripheral blood or bone marrow (Diogo et al., 2012; Tomlinson et al., 2013). Other methods include membrane filtration, dielectrophoresis (DEP), field flow fractionation (FFF), and ATPS, as summarized in **Figure 1** (Al-Rubeai and Naciri, 2014; González-González et al., 2012; Tomlinson et al., 2013; Zhu and Murthy, 2013). While membrane filtration separates cells based on their size (Al-Rubeai and Naciri, 2014), dielectrophoretic cell separation is based on the application of an electrical field, enabling cell separation based on electro-physical properties, as well as cell size and density (González-González et al., 2012; Zhu and Murthy, 2013). In FFF, a laminar flow mobile phase is used to separate cells. In gravitational FFF, e.g., cells position within the laminar flow according to their mass, density, and size, and can thus be separated. In addition, FFF can be combined with DEP or centrifugation to enhance resolution (González-González et al., 2012; Zhu and Murthy, 2013). The partitioning of cells in ATPS is based on their surface properties, i.e. charge and hydrophobicity, and has successfully been combined with immunoaffinity-purification (González-González et al., 2012; Sousa et al., 2011).

Physical cell separation methods have significantly lower selectivity than immunoaffinity-based cell purification methods, but have been successfully applied as initial enrichment steps (Rodrigues et al., 2015). In addition, they can be used in an orthogonal and/or multi-stage fashion for increased selectivity. All of these methods have the great advantage of being label-free, cost-effective and scalable, even though there are differences in scalability. While membrane filtration, ATPS, and centrifugation techniques are highly scalable, the scalability of DEP and FFF are more limited and these methods are mostly applied in microfluidic applications (González-González et al., 2012; Tomlinson et al., 2013; Zhu and Murthy, 2013). To date, most of these methods are still in early stages of development and have only been applied in laboratory settings (Tomlinson et al., 2013). Nonetheless, many of these methods hold great promise for future industrial-scale downstream processing of cell-based products.

# 1 INTRODUCTION

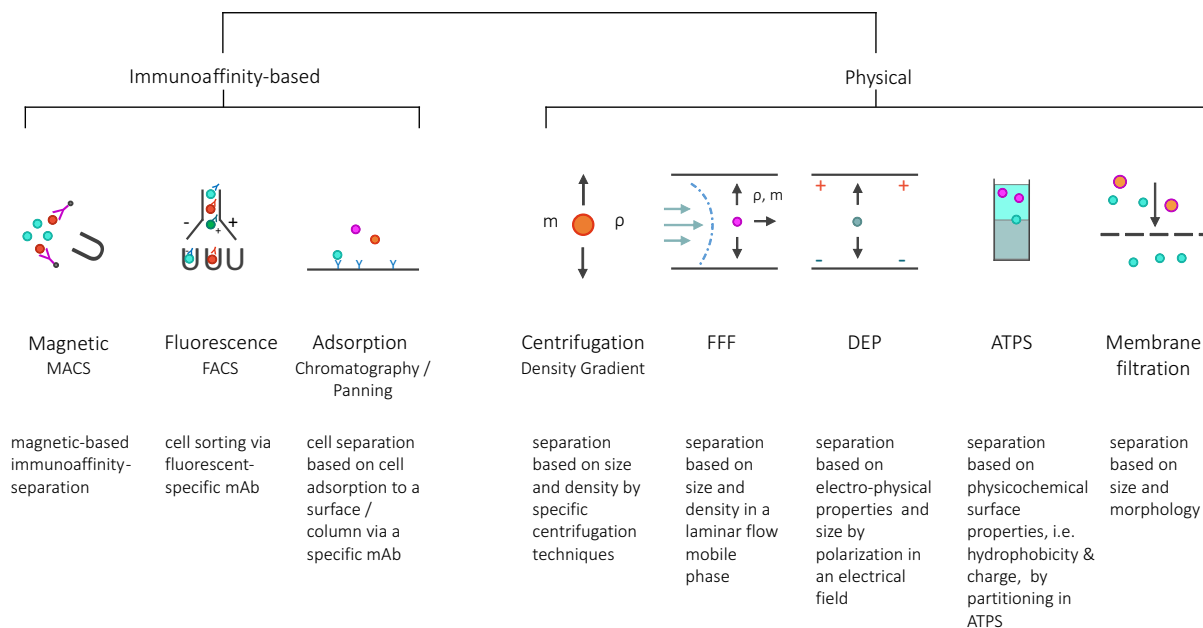


**Figure 1:** Overview of immunoaffinity-based and physical cell separation techniques. ATPS: aqueous two-phase systems; DEP: dielectrophoresis; FACS: fluorescence activated cell-sorting; FFF: field-flow fractionation; m: mass; mAb: monoclonal antibody; MACS: magnetic activated cell sorting;  $\rho$ : density.

## 1.4 Aqueous two-phase systems (ATPS)

ATPS have been successfully used in downstream processing of biomolecules, such as proteins, nucleic acids, viruses, cells, and cell organelles, for more than 50 years (Albertsson, 1986; Walter et al., 1985). ATPS-research was pioneered by Per-Åke Albertsson in 1956, who discovered phase formation when PEG was mixed with highly concentrated phosphate buffers (Walter et al., 1985). His work initiated intensive research on two-phase extraction of biological materials for analytical and preparative purposes, and ATPS-technology is now making its way towards industrial bioprocessing (Soares et al., 2015). ATPS can be formed by a variety of components, usually polymers and salts, which are immiscible above a certain critical threshold (e.g. concentration, temperature).

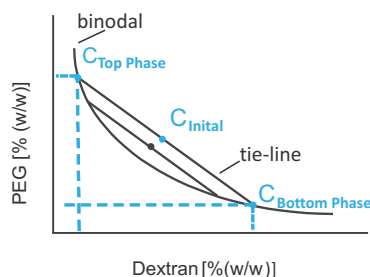


**Figure 2:** Schematic phase diagram of a PEG-dextran aqueous two-phase system (ATPS). The binodal curve marks the polymer concentrations above which phase separation occurs. The tie-lines connect systems with equal phase composition but varying volume ratios, and the nodes between binodal and tie-lines depict the compositions of top and bottom phase, respectively (Hatti-Kaul, 2000). C: concentration.

The phases are enriched in either of the components and exhibit different physicochemical properties. By now, a large number of compound pairs have been identified that are capable of phase formation. A schematic phase diagram for a PEG-dextran ATPS is depicted in **Figure 2**. The binodal curve marks the critical polymer concentrations for phase formation and the tie-lines connect systems with equal phase composition but varying volume ratios. The nodes between binodal and tie-lines depict the respective compositions of top and bottom phase (Hatti-Kaul, 2000; Walter et al., 1985). For cell separation, polymer-polymer ATPS, more specifically PEG-dextran ATPS, are the most widely applied. PEG-dextran ATPS can be buffered and made isotonic by the addition of salts.

#### 1.4.1 Cell partitioning in aqueous-two phase systems (ATPS)

The partitioning of molecules and particles in ATPS is, in addition to specific interactions with the phase-forming components, driven by Brownian motion and interfacial forces. While the Brownian motion distributes molecules or particles randomly within the ATPS, the interfacial tension acts to minimize the interfacial area. The adsorption of cells and other particles to the interface reduces the interfacial area, and consequently the total free energy of the system. As a result, cells and other particles above a certain diameter have a strong tendency to adsorb to the interface, in dependence of the interfacial tension. Thus, partitioning into either phase can only take place if the interaction with the cell surface is strong enough to "pull" the cells out of the interface. The higher the interfacial tension, the stronger the required interaction to enable partitioning (Albertsson, 1986; Forciniti et al., 1990; Walter et al., 1985). Depending on specific interactions, cells and other particles partition between either of the bulk phases, i.e. top and bottom phase, and the interface (Albertsson and Barid, 1962; Baird et al., 1961).

The partitioning coefficient  $P$  of a cell type can thus be defined as the ratio of cells in either of the bulk phases (**equation 1**).

$$P = \frac{C_{TP} \times V_{TP}}{C_{Ctr} \times V_{Ctr}} \quad (1)$$

*C: cell concentration; V: volume; TP: top phase; Ctr: control*

While the mechanisms underlying cell partitioning in ATPS are not entirely understood, two main factors in cell separation have been identified: surface charge and membrane lipid composition. Salts with polyvalent anions, e.g. phosphate, have a higher affinity for the dextran-rich bottom phase, while salts of halides, for example NaCl, partition almost equally between the phases. Unequal partitioning of a salt results in the generation of an interfacial electrostatic potential difference (Donnan potential), and molecules and particles partition in such ATPS according to their surface charge (Gascoine and Fisher, 1984; Reitherman et al., 1973; Vis et al., 2014; Walter et al., 1985). In PEG-dextran ATPS with moderate interfacial tensions containing phosphate, cells can therefore be separated based on their surface charge (charge-dependent partitioning). As cells have a negative net surface charge, they partition into the top phase in ATPS containing phosphate (Cabral, 2007; Reitherman et al., 1973). Charge-independent cell separation,

on the other hand, is possible in ATPS containing e.g. sodium chloride (charge-insensitive ATPS). More precisely, partitioning coefficients of distinct cell types in charge-insensitive ATPS have been correlated with their membrane lipid composition (Albertsson, 1986; Gascoine and Fisher, 1984; Walter, 1978; Walter et al., 1985).

Both interfacial tension and Donnan potential are dependent on polymer type, polymer molecular weight, tie-line length (TLL), temperature, salt type and concentration, and the presence of certain additives (Fan et al., 1998; Forciniti et al., 1990; King et al., 1988; Luther and Glatz, 1995; Walter et al., 1985).

Cell partitioning and the resolution of distinct cell populations is thus highly dependent on all of these parameters. However, the interaction of these parameters in respect to cell partitioning and the resolution of different cell populations remains unclear. By varying this multitude of factors, separation conditions can be optimized for a specific application. Since the partitioning of cells in ATPS is fully reversible, independent of their concentration and the presence of other cells types, CCD can be used for multi-stage separation processes (Albertsson and Barid, 1962; Baird et al., 1961).

#### 1.4.2 Multi-stage countercurrent distribution (CCD)

While a single purification step can yield good results in some cases, differences in partitioning coefficients do generally not suffice to obtain high purities in a single extraction step. In order to increase resolution between target cells and contaminants, multi-stage separation processes such as CCD can be applied. CCD was developed by Craig (Craig and Post, 1949) and is nowadays a well-established method in liquid-liquid extraction. In CCD the top phase is transferred stepwise while the bottom phase is retained (**Figure 3**). Between transfers, the ATPS are mixed and allowed to separate by gravity. Depending on the application, the interface can either be transferred or retained (Johansson, 1998). As cells partition between either of the bulk phases and the interface, the interface is retained when cells partition between top phase and interface, and transferred when the cells partition between interface and bottom phase. Cells that partition largely into the top phase e.g. move faster through the CCD-device than cells that partition largely to the interface, and the two cell populations can thus be separated. Even though numerous devices for liquid-liquid chromatography have been introduced, i.e. hydrodynamic countercurrent chromatography (CCC) and hydrostatic centrifugal partition chromatography (CPC), CCD has so far proven the most suitable for cell separation (Albertsson and Barid, 1962; Walter et al., 1985). Due to low pressures and shear forces, high cell viabilities can be obtained. In addition, settling by gravity enables cell separation according to surface properties, rather than densities, as it may be the case for centrifugation-based methods, depending on the mode of operation and centrifugation force.

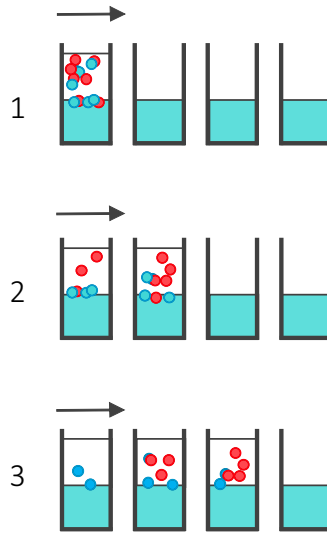


**Figure 3:** Scheme of the countercurrent distribution (CCD)-principle for aqueous two-phase systems (ATPS) in which cells partition between top phase and the interface. The top phase is transferred stepwise. Between the transfers ATPS are mixed and phases are separated by gravity (Johansson, 1998).

### 1.4.3 Modeling countercurrent distribution (CCD)

Based on partitioning ratios determined in batch experiments, CCD-curves can be modelled using **equation 2**:

$$F(r) = \frac{n!}{r!(n-r)!} P^r (1-P)^{n-r} \quad (2)$$

where  $F$  represents the fraction of the total cell population appearing in each theoretical cavity  $r$  of the CCD-apparatus,  $n$  represents the total number of transfers, and  $P$  represents the fraction of cells in either of the bulk phases. The fraction of cells in each cavity will be given by a binomial distribution (Walter et al., 1985). Based on given  $P$ -values, a purification process can be designed. Highly accurate models can be obtained if all relevant parameters, i.e. vessel geometry, volume, mixing intensity, mixing time, temperature, and phase separation time, are identical between batch and CCD-experiments. By increasing the number of transfers, the resolution can be increased as shown in **Figure 4**. However, processing time increases accordingly, which can reduce cell viability. By decreasing the temperature to 4°C, or the use of certain additives, prolonged processing times can be realized (Albertsson, 1986; Walter et al., 1985). This, however, needs to be considered during process development.

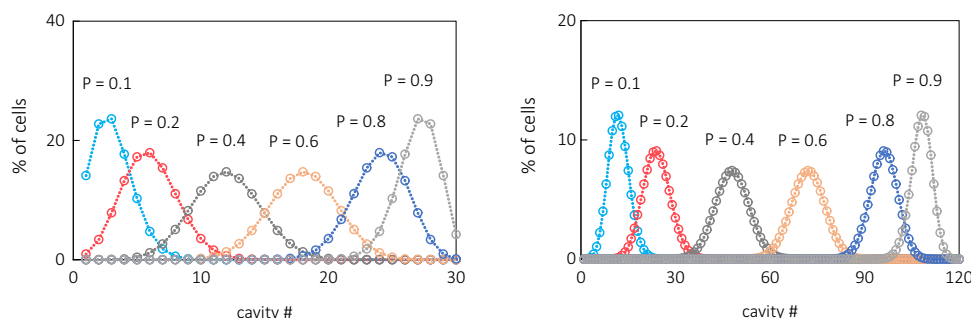


**Figure 4:** Predicted countercurrent distribution (CCD)-curves for different partitioning ratios ( $P$ ) with 30 (left) and 120 (right) transfers (Walter et al., 1985).

## 1.5 High-throughput process development (HTPD)

HTS-technology has been state-of-the-art in drug development for more than two decades, and automation, miniaturization, and parallelization of numerous methods has resulted in a significant increase in throughput and a concomitant reduction in time and material consumption. Likewise, HTS-platforms are used in various other scientific disciplines such as fundamental research, diagnostics, and biotechnology (An and Tolliday, 2010; Bensch et al., 2005; Hertzberg and Pope, 2000; Macarron et al., 2011). In the past decade, HTS-technologies have gained considerable importance in DSP development of biopharmaceuticals such as protein- and DNA-based drugs, and are, by now, available for most platform technologies e.g. column chromatography, crystallization, and ATPS (Bensch et al., 2005, 2007; Coffman et al., 2008; Oelmeier et al., 2012; Wiendahl et al., 2008; Zang et al., 2011). In combination with DoE, modeling, and simulation data, HTS-technologies present a powerful tool for the directed design of purification strategies (Coffman et al., 2008; Oelmeier et al., 2012). The knowledge gained in DSP development for complex biomolecules, such as therapeutic antibodies, is now expected to drive the development of industrial-scale downstream processing of cell-based pharmaceuticals (Ratcliffe et al., 2013).

### 1.5.1 HT-cell quantification methods

In order to design novel HTS-platforms for downstream processing of cell-based drugs, robust, accurate, and sensitive HT-cell quantification assays are required. Currently, a vast number of direct and indirect cell quantification methods are available (**Figure 5**). Direct cell quantification assays detect the cells themselves, while indirect cell quantification methods quantify intracellular targets. Direct cell quantification assays include light microscopy in combination with trypan blue staining (e.g. hemocytometer, Cedex (Roche)), impedance-based cell counting (e.g. Coulter Counter), and light scattering as performed in flow cytometry. The majority of cell quantification methods, though, are based on indirect means of cell enumeration, i.e. the quantification of genomic DNA (e.g. CyQuant<sup>®</sup>(LifeTechnologies<sup>™</sup>)), total protein (e.g. Bradford Assay), specific enzymes (e.g. CellTracker<sup>™</sup>, LiveDead Cell Viability Assay), or certain metabolites, for instance ATP (e.g. CellTiter-Glo<sup>™</sup>(Promega), ATPlite (Perkin Elmer)).

## 1.5 High-throughput process development (HTPD)

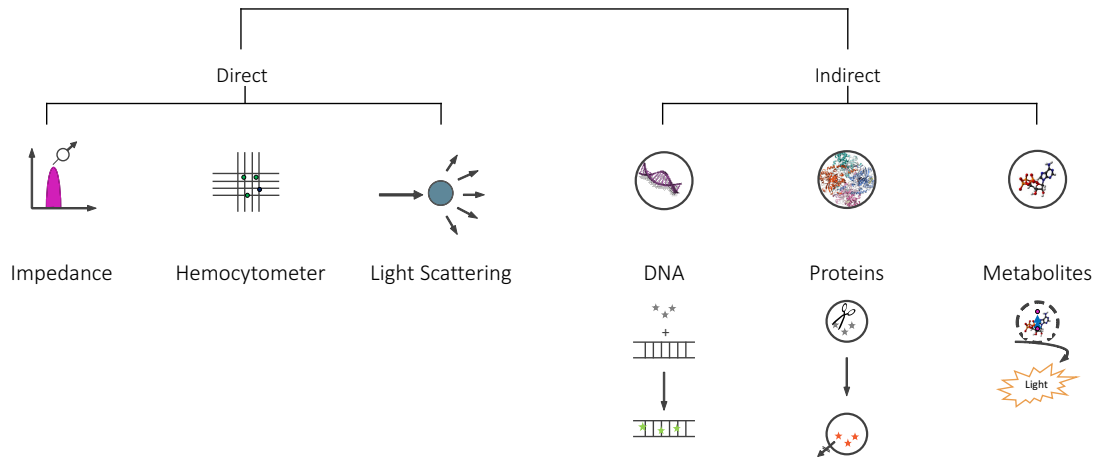


**Figure 5:** Overview of state-of-the-art direct and indirect cell quantification methods.

While some assays enable the exclusive quantification of live cells, other assays enable the discrimination between live and dead cells. Quantification of dead cells is usually performed by investigating membrane permeability using a dye that is impermeable to live, but not dead cells. Most assay types are further available with different readouts, such as absorbance, fluorescence, or luminescence, which in turn influences sensitivity and robustness.



---

## 2 Research Proposal

The availability of clinical-scale downstream processing strategies for cell-based products presents a critical juncture between basic research and clinical development. Due to the large size and inherent complexity of mammalian cells, the design of effective downstream processing strategies remains challenging. The requirements on downstream processes (DSP) are highly dependent on cell source and application. Following an initial enrichment step, several specific positive and negative selections steps may be required to further enrich the target cell type and deplete critical contaminants. Aqueous two-phase systems (ATPS) facilitate the label-free, scalable, and cost-effective separation of cells, and present a promising tool for downstream processing of cell-based therapeutics. They are especially promising as an initial enrichment step, since they are highly scalable and cost-effective. Nonetheless, the development of effective downstream processes requires the optimization of many different parameters, hampering widespread application of ATPS in cell purification. In the past decade, HTS-technologies have become state-of-the-art in DSP development of biopharmaceuticals such as protein- and DNA-based drugs. These technologies have facilitated miniaturized, parallelized, and fully automated experimental setups, and have consequently enabled faster, cheaper, and more directed DSP development. In combination with Design of Experiments (DoE) and modelling tools, they present a powerful instrument to elicit mechanisms underlying separation and design purification strategies for novel targets. The implementation of HTS-tools in DSP development for cell-based therapeutics will likewise open up new possibilities for process design, and thus presents a crucial enabling technology for the translation of cell-based therapeutics.

The present work focusses on the implementation of an integrated HTS-platform for DSP development for cell-based products using ATPS. In this context robust, accurate, and sensitive high-throughput (HT)-cell quantification assays are required. It is crucial that the utilized assays are robust towards changes in buffer composition and produce reliable results over a wide range of medium densities and viscosities.

The scope of the first part of this thesis is thus the implementation of analytical technologies for HT-DSP development for cell-based products. In this context a comparative study will be conducted that assesses state-of-the-art cell quantification methods regarding their applicability in HT-DSP development.

The focus of the second part of this thesis is the application of this HTS-platform to study mechanisms in ATPS-mediated cell separation, determine key process parameters, and conduct case studies on the design of a DSP. The vast number of process parameters in aqueous two-phase extraction presents a major bottleneck for effective DSP development. The utilization of a HTS-approach will enable the systematic investigation of numerous parameters, will help to identify their role in cell separation, and enable the determination of key parameters for efficient and directed DSP development. Likewise, a HTS-approach will enable us to assess the influence of numerous cellular parameters, e.g. cell cycle phase, on cell partitioning, and consequently their influence on process robustness.

The combination of DoE, HTS-data, and multi-stage process models will further enable the design of complex DSP based on batch-data with minimal time and material consumption. The knowledge gained from these screenings can further be used to develop a

more detailed mechanistic understanding of cell partitioning in ATPS, which will eventually enable the implementation of more model-based DSP development approaches. The overall objective of this thesis is the investigation of ATPS as a downstream processing tool for cell-based therapeutics. The use of a HTS-platform in combination with multi-stage models will enable the identification of key parameters in cell separation, resulting in more directed DSP development, and will finally help to provide a more detailed mechanistic understanding of cell partitioning in ATPS.

---

### 3 Publications & Manuscripts

1. **High-throughput cell quantification assays for use in cell purification development – Enabling technologies for cell production**

S. Zimmermann, S. Gretzinger, C. Scheeder, M.-L. Schwab, S.A. Oelmeier, A. Osberghaus, E. Gottwald, J. Hubbuch

*Biotechnol. J.* (2016), doi: 10.1002/biot.201500577

This article presents a comparative study on high-throughput (HT)-cell quantification assays for downstream process (DSP) development for cell-based products. Several cell quantification methods that differ in their respective mechanism were validated for their applicability in high-throughput screening (HTS)-platforms for DSP development. The compared methods differed significantly in sensitivity, dynamic range, robustness, and throughput, and the study provides a guideline for selecting the most suitable assay for a specific application.

2. **High-throughput downstream process development for cell-based products using aqueous two-phase systems**

S. Zimmermann, S. Gretzinger, M.-L. Schwab, C. Scheeder, P.K. Zimmermann, S.A. Oelmeier, E. Gottwald, A. Bogsnes, M. Hansson, A. Staby, J. Hubbuch

*J. Chrom. A.* (2016), doi: 10.1016/j.chroma.2016.08.025

This article describes the development and validation of an automated robotic screening that enables HT-cell partitioning analysis in aqueous two-phase systems (ATPS). In a first case study, separation conditions for the differentiable promyelocytic cell line HL-60 in PEG-dextran ATPS were examined, and it was shown that the separation of CD11b-positive and CD11b-negative HL-60 cells is possible after partial DMSO-mediated differentiation towards the granulocytic lineage. The influence of salt composition, pH, and tie-line length (TLL) on the resolution of the two cell populations was evaluated, and separation conditions were optimized using a countercurrent distribution (CCD)-model.

3. **Cell separation in aqueous two-phase systems – Influence of polymer molecular weight and tie-line length on the resolution of five model cell lines**

S. Zimmermann<sup>‡</sup>, S. Gretzinger<sup>‡</sup>, P.K. Zimmermann, A. Bogsnes, M. Hansson, J. Hubbuch (<sup>‡</sup>: contributed equally)

*J. Chrom. A*, submitted manuscript

This study explores the influence of polymer molecular weight and TLL on the resolution of five model cell lines in charge-sensitive PEG-dextran ATPS using a HTS-approach in combination with CCD-modelling. In addition, a barcoding-strategy was developed that enables multiplexing in cell partitioning analysis. The study demonstrates that the separability of each cell line from the mixture is highly depen-

dent on the polymer molecular weight composition and TLL. Finally, it was shown that cell surface charge-dependent cell partitioning due to an interfacial Donnan potential is the major driving force in ATPS containing phosphate, independent of polymer molecular weight and tie-line length.

#### 4. **High-throughput downstream process development for cell-based products using aqueous two-phase systems (ATPS) – A case study**

S. Zimmermann, C. Scheeder, P.K. Zimmermann, A. Bogsnes, M. Hansson, A. Staby, J. Hubbuch

*Biotechnol. J., submitted manuscript*

In this case study a purification strategy for two model cell lines based on HTS-data and CCD-modeling was designed and validated experimentally. The study showed excellent congruence between CCD-model and experimental data, indicating that CCD-models in combination with HTS-data are a powerful tool in downstream process development. Finally, the influence of cell cycle phase on cell partitioning and the resolution of the two model cell lines was analyzed, which may interfere with the robustness of a purification process. The study revealed that while cell cycle phase is a significant factor in cell partitioning, cell type-specific differences in surface properties were the main driving force.

---

High-throughput cell quantification assays for use in cell  
purification development - enabling technologies for cell  
production

**Sarah Zimmermann<sup>1</sup>, Sarah Gretzinger<sup>1</sup>, Christian Scheeder<sup>1</sup>, Marie-Luise Schwab<sup>1,3</sup>, Stefan A. Oelmeier<sup>1,4</sup>, Anna Osberghaus<sup>1</sup>, Eric Gottwald<sup>1</sup>, and Jürgen Hubbuch<sup>1,\*</sup>**

<sup>1</sup>: Karlsruhe Institute of Technology (KIT), Institute of Process Engineering in Life Science, Section IV: Biomolecular Separation Engineering (MAB), Karlsruhe, Germany

<sup>2</sup>: Karlsruhe Institute of Technology (KIT), Institute for Biological Interfaces (IBG 5), Eggenstein-Leopoldshafen, Germany

<sup>3</sup>: DIARECT AG, Department of Quality Assurance and Quality Control, Freiburg, Germany

<sup>4</sup>: Boehringer Ingelheim Pharma GmbH & Co. KG, Global Bioprocess & Pharmaceutical Development, Biberach, Germany

\*: Corresponding author. *E-mail-address*:juergen.hubbuch@kit.edu (J. Hubbuch)

## Abstract

High-throughput screening (HTS) technology is gaining increasing importance in downstream process development of cell-based products. The development of such HTS-technologies, however, is highly dependent on the availability of robust, accurate, and sensitive high-throughput cell quantification methods. In this article, we compare state-of-the-art cell quantification methods with focus on their applicability in HTS-platforms for downstream processing of cell-based products. Sensitivity, dynamic range, and precision were evaluated for four methods that differ in their respective mechanism. In addition, we evaluated the performance of these methods over a range of buffer compositions, medium densities, and viscosities, representing conditions found in many downstream processing methods. We found that CellTiter-Glo<sup>TM</sup> and flow cytometry are excellent tools for high-throughput cell quantification. Both methods have broad working ranges (3-4 log) and performed well over a wide range of buffer compositions. In comparison, CyQuant<sup>®</sup>Direct and CellTracker<sup>TM</sup> had smaller working ranges and were more sensitive to changes in buffer composition. For fast and sensitive quantification of a single cell type, CellTiter-Glo<sup>TM</sup> performed best, while for more complex cell mixtures flow cytometry is the method of choice. Our analysis will facilitate the selection of the most suitable method for a specific application and provides a benchmark for future HTS development in downstream processing of cell-based products.

**Keywords:** cell-based products, cell quantification assays, downstream processing, high-throughput screening (HTS)

---

# 1 Introduction

High-Throughput screening (HTS) technology has been state-of-the art in drug development for more than two decades, and, by now, most pharmaceutical companies use HTS in lead discovery. As a result, many of the recently approved small-molecule drugs and biopharmaceuticals have been identified by HTS [1,2]. Likewise, high-throughput screening platforms are used in various other scientific disciplines such as basic research, diagnostics, and biotechnology [1–4]. In the past decade, HTS-technology has also gained increasing importance in downstream process development of biopharmaceuticals, such as protein- and DNA-based drugs [4]. High-throughput platforms are currently available for most platform technologies, including column chromatography, crystallization, and aqueous two-phase systems (ATPS) [4–10]. These technologies have facilitated faster, cheaper, and more directed downstream process development. In combination with modeling and simulation data, they present a powerful tool for the directed design of purification strategies for novel targets.

As the development of cell-based pharmaceuticals is advancing, new scalable downstream processing strategies are required. The knowledge gained in downstream process development for complex biomolecules, such as therapeutic antibodies, is now expected to drive the development of downstream processing of cell-based pharmaceuticals [11]. This is supported by the fact that both chromatography as well as ATPS have been successfully used for cell separation [12–19]. In order to design novel HTS platforms for downstream processing of cell-based drugs, robust, accurate, and sensitive high-throughput cell quantification assays are required. For application of cell quantification assays in HTS platforms for cell separation, it is crucial that the utilized assays are robust towards changes in buffer composition, but should also give reliable results over a wide range of medium densities and viscosities.

Presently, a vast number of direct and indirect cell quantification methods are available [20]. Direct cell quantification assays detect the cells themselves, while indirect cell quantification methods quantify intracellular targets, such as genomic DNA, proteins or metabolites. Direct cell quantification assays include light microscopy in combination with trypan blue staining (e.g. hemocytometer, Cedex (Roche)), impedance based cell counting (e.g. Coulter Counter), and light scattering, as performed in flow cytometry. The majority of cell quantification methods, however, are based on indirect means of cell enumeration. Indirect cell quantification assays are based on quantification of genomic DNA (e.g. CyQuant®(LifeTechnologies™)), total protein (e.g. Bradford Assay), specific enzymes (e.g. CellTracker™, LiveDead Cell Viability Assay), or certain metabolites, for instance adenosine triphosphate (ATP), e.g. CellTiter-Glo™ (Promega), ATPlite (Perkin Elmer).

Some of these assays exclusively quantify live cells, while others are able to discriminate between live and dead cells. Identification of dead cells is performed by investigating membrane permeability using a dye that is impermeable to live, but not to dead cells. In addition, one can choose between different readouts for many of the assays formats, e.g. absorbance, fluorescence or luminescence. Likewise, this has a significant effect on the sensitivity and robustness of the assay. With such an abundance of assay types, it can be difficult to find the appropriate assay for the respective application, and it has been shown that each assay type has its limitations, depending on their mechanism of action

[20,21]. Therefore, it is important to understand the underlying principles and carefully validate different assays for a new application. To our knowledge, a comparative analysis of different cell quantification assays for high-throughput applications in downstream processing of cell-based products had not been conducted to date.

In this article, we compared four high-throughput cell quantification methods that differ in their respective mechanism. The following indirect high-throughput cell quantification methods were chosen: CellTiter-Glo<sup>TM</sup>, a luciferase reagent that quantifies intracellular ATP, CyQuant<sup>®</sup>Direct, a cell-permeant fluorescent nucleic acid stain, and the CellTracker<sup>TM</sup> dyes, which belong to the group of thiol-reactive esterase substrates. Moreover, we chose flow cytometry as a direct cell quantification method. We evaluated sensitivity, dynamic range, and precision for each of these four methods. In addition, we evaluated their performance over a range of buffer compositions, medium densities, representing conditions found in many downstream processing methods. Finally, we compared the four methods regarding assay time and material costs.

---

## 2 Materials & Methods

### 2.1 Disposables

For fluorescence measurements, 96-well UV-Star plates (Greiner Bio-One, Kremsmünster, Austria) and for luminescence measurements, LIA flat-bottom 96-well plates (Greiner Bio-One) were used. For flow cytometry, 96-well U-bottom plates (BD Falcon San Jose, CA, USA) were used. For all other purposes, polypropylene flat-bottom microplates (Greiner Bio-One) and 1.3 mL deep well plates (Nalgene Nunc, Rochester, NY, USA) were used.

### 2.2 Software

Excel 2013 (Microsoft, Redmond, WA, USA) was used as import format and for data storage, as well as for data evaluation and visualization. The Tecan Infinite<sup>®</sup>Pro M200 plate reader was controlled using iControl 1.9 (Tecan, Crailsheim, Germany). For statistical data analysis, Matlab R2014a (The MathWorks, Inc., Natick, ME, USA) was used. BD FACSDiva 8.0 was used to control the BD LSR Fortessa Cell Analyzer and for analysis of flow cytometry data (BD Biosciences, San Jose, CA, USA).

### 2.3 Preparation of buffers and stock solutions

Stock solutions of 5% Dextran 500,000 (Pharmacosmos A/S, Holbaek, Denmark, cat. 551005009007, Batch No.: HT3229) and 5% PEG 8,000 (Sigma Aldrich, St. Louis, MO, USA, cat. P2139, Batch No.: 059Ko121) were prepared in Dulbecco's Phosphate Buffered Saline (DPBS) (Life Technologies<sup>™</sup>, Carlsbad, CA, USA). All other buffers and stock solutions were prepared with ultra-pure water ( $0.55 \mu\text{S}/\text{cm}$ ) obtained from an Arium<sup>®</sup>proUV water system (Satorius, Göttingen, Germany). 500 mM phosphate buffer stock solutions were prepared by using di- (Merck Millipore, Darmstadt, Germany) and monobasic sodium phosphate (Sigma Aldrich) in varying ratios, in order to obtain specific pH-values (241 mM  $\text{Na}_2\text{HPO}_4$ , and 259.4 mM  $\text{NaH}_2\text{PO}_4$  for pH 6.6, 353 mM  $\text{Na}_2\text{HPO}_4$ , and 147.4 mM  $\text{NaH}_2\text{PO}_4$  for pH 7.0, 430 mM  $\text{NaH}_2\text{PO}_4$ , and 70.6 mM  $\text{NaH}_2\text{PO}_4$  for pH 7.4). Sodium chloride (Merck Millipore) was prepared as a 500 mM stock solution. A 500.8 mM citrate buffer stock solution, pH 6.6 was prepared using 495 mM sodium citrate (Sigma Aldrich) and 5.8 mM acetic acid (Merck Millipore). A 500 mM Tris-buffer, pH 7.0 was prepared using 473 mM Tris-HCl (AppliChem, Darmstadt, Germany) and 26.8 mM sodium hydroxide (Merck Millipore). 1 x Hank's Balanced Salt Solution (HBSS), pH 7.0, was prepared using 5.33 mM potassium chloride (VWR, Darmstadt, Germany), 0.49 mM magnesium chloride (Sigma Aldrich), 1.26 mM calcium chloride, 0.41 mM magnesium sulfate, 0.44 mM potassium phosphate, monobasic, 4.17 mM sodium bicarbonate, 137.93 mM sodium chloride, 0.34 mM sodium phosphate, dibasic, and 5.56 mM D-glucose (Merck Millipore). Working solutions were prepared at 129 mM sodium phosphate pH 6.6, 118 mM sodium phosphate pH 7.0, 111 mM sodium phosphate pH 7.4, 150 mM sodium chloride, 150 mM Tris-buffer, and 100 mM citrate buffer, respectively, to obtain physiological osmolarities. Osmolarities were verified using a VAPRO<sup>®</sup> 5600 vapor pressure osmometer (Wescor Inc., Logan, UT, USA), and all buffers had osmolarities within the physiological range (290-310 mOs). All buffers and polymer solutions were

filtrated ( $\varnothing$  0.22  $\mu\text{m}$  PES, VWR). Buffers were stored at room temperature and polymer solutions were stored at 4  $^{\circ}\text{C}$ .

## 2.4 Cell culture

The promyelocytic cell line HL-60 was purchased from CLS (Cell lines Service, Eppelheim, Germany) and propagated at 37  $^{\circ}\text{C}$  in a humidified 5%  $\text{CO}_2$  incubator. Cell culture media and supplements were purchased from Life Technologies<sup>TM</sup>. Cells were grown in RPMI 1640 with GlutaMAX-1, supplemented with 15% fetal bovine serum (FBS), 1% sodium pyruvate, 1% non-essential amino acids (NEAA), and 0.5% Penicillin/ Streptomycin. Cells were split to a concentration of  $2 \times 10^5$  cells per mL every 3-4 days. For assay calibration, HL-60 cells were counted using a Neubauer improved hemocytometer (Marienfeld, Land-Königshofen, Germany).

## 2.5 Cell quantification assays

### 2.5.1 Cell quantification using CellTracker<sup>TM</sup> dyes

CellTracker<sup>TM</sup> Orange CMRA (9'-(4 [and 5]-chloromethyl-2-carboxyphenyl)-7'-chloro-6'-oxo-1,2,2,4-tetramethyl-1,2-dihydropyrido [2',3'-6]xanthene), (Life Technologies<sup>TM</sup>) was prepared as recommended by the manufacturer, and staining was performed with 10  $\mu\text{M}$  CellTracker<sup>TM</sup> Orange CMRA at 37  $^{\circ}\text{C}$  for 30 minutes. Subsequently, fluorescence intensity was measured using a Tecan Infinite<sup>®</sup>Pro M200 plate reader (Ex.: 548 nm, Em.: 576 nm).

### 2.5.2 Cell quantification using CyQuant<sup>®</sup> Direct Cell Proliferation Assay

Cell quantification with CyQuant<sup>®</sup> Direct Cell Proliferation Assay (Life Technologies<sup>TM</sup>) was performed according to the manufacturer's instructions, and DNA-bound dye molecules were quantified by fluorescence measurement using a Tecan Infinite<sup>®</sup>Pro M200 plate reader (Ex: 480 nm, Em.: 535 nm).

### 2.5.3 Cell quantification using CellTiter-Glo<sup>TM</sup> Luminescent Cell Viability Assay

CellTiter-Glo<sup>TM</sup> Luminescent Cell Viability Assay Kit (Promega, Madison, WI, USA) was used according to the manufacturer's instructions. Luminescence intensity was measured with a 500 ms integration time using a Tecan Infinite<sup>®</sup>Pro M200 plate reader.

### 2.5.4 Cell quantification using flow cytometry

Flow cytometry was performed using a LSR Fortessa from BD Bioscience equipped with a BD<sup>TM</sup> High Throughput Sampler (HTS). The high throughput sampler was operated at the following settings: sample flow rate: 3  $\mu\text{L}/\text{s}$ , sample volume: 100  $\mu\text{L}$ , mixing volume: 100  $\mu\text{L}$ , mixing speed: 200  $\mu\text{L}/\text{s}$ , and four mixing cycles. For cell quantification, cells were diluted with 2x FACS staining buffer (DPBS with 1% (w/v) bovine serum albumin (BSA) (Miltenyi Biotec, Bergisch Gladbach, Germany) and 4 mM EDTA (Life Technologies<sup>TM</sup>)). Discrimination between live and dead cells was performed using forward (FSC) and side

(SSC) scatter signal. Dead cells were gated using a control sample with heat-inactivated cells (70 °C, 10 minutes).

## 2.6 Validation of assay performance

The respective cell quantification assays were validated in regards to sensitivity, linear range, precision, and robustness, according to the recommendations of the ICH guidelines [22].

### 2.6.1 Linearity and calibration

For calibration, a dilution series of  $10^7$  to  $10^2$  cells per mL, with a total of 12 to 19 calibration points including a blank control, was prepared and quantified with the respective method. All measurements were performed in technical triplicates. As cell quantification was assessed over several orders of magnitude, homoscedasticity was not given in most cases, as confirmed by the application of an F-Test. Thus, weighted least squares linear regression (WLSLR) was performed as described by Almeida et al. [23]. The following weighting factors ( $w_i$ ) were compared:  $1/x^{0.5}$ ,  $1/x$ ,  $1/x^2$ ,  $1/y^{0.5}$ ,  $1/y$ ,  $1/y^2$ . Relative errors (%RE) were calculated using equation (1), and residuals were visualized in order to assess the effectiveness of the weighted regression.

$$\% RE = \left( \frac{\sum \left( \frac{C_{found} - C_{nom}}{C_{nom}} \right)}{n} \right) \times 100 \quad (1)$$

$C_{found}$ , regressed concentration

$C_{nom}$ , nominal standard concentration

### 2.6.2 Limit of detection and quantitation

The limits of detection (DL) and quantitation (QL) were calculated using equations (2) and (3) [23].

$$DL = \frac{3.3 \times (SD_{Blank})}{S} \quad (2)$$

$$QL = \frac{10 \times (SD_{Blank})}{S} \quad (3)$$

S, slope of calibration function

SD, standard deviation of the response

### 2.6.3 Range

The linear range was defined as the range of concentrations above the detection limit, where a linear correlation between cell number and readout was observed ( $R^2 > 0.995$ ). The working range was defined as the section of the linear range where the variation coefficient (CV) was below 10%.

#### 2.6.4 Robustness

Robustness was evaluated by quantifying  $10^5$  cells per mL in the presence of different salts and polymers. PEG 8000 and Dextran 500 000 were used at final concentrations between 0.5 and 2%. Buffers containing different salts and pH-values were used at physiological osmolarities, undiluted, as well as 10-fold diluted with DPBS. The recovery rate was calculated as the percentage of cells detected compared to the DPBS controls. To determine if the recovery was altered significantly, pairwise Student's *t*-test was performed, provided that equal variances could be asserted by using an F-test. A difference in means was considered significant for p-values  $< 0.01$ .

### 3 Results

In the present work, we compare four cell quantification methods regarding their applicability in high throughput downstream process development for cell-based products. Thus, we evaluated the assays with regards to their performance over a range of buffer compositions, medium densities, and viscosities.

#### 3.1 High-throughput flow cytometry, CellTiter-Glo™, CyQuant® Direct, and the CellTracker™ dyes are suitable assays for high-throughput cell quantification in downstream processing applications

A pre-selection of assays was performed taking the following criteria into account: Firstly, the measured parameters should correlate linearly with cell number to facilitate the use of an internal standard with two or three data points. Thereby, the influence of batch to batch variations can be eliminated, which ensures that data are comparable over a large set of experiments [24]. Secondly, it is essential that the assay has a broad working range, high sensitivity, and short processing times. Furthermore, the assay handling and readout need to be compatible with automated liquid handling.

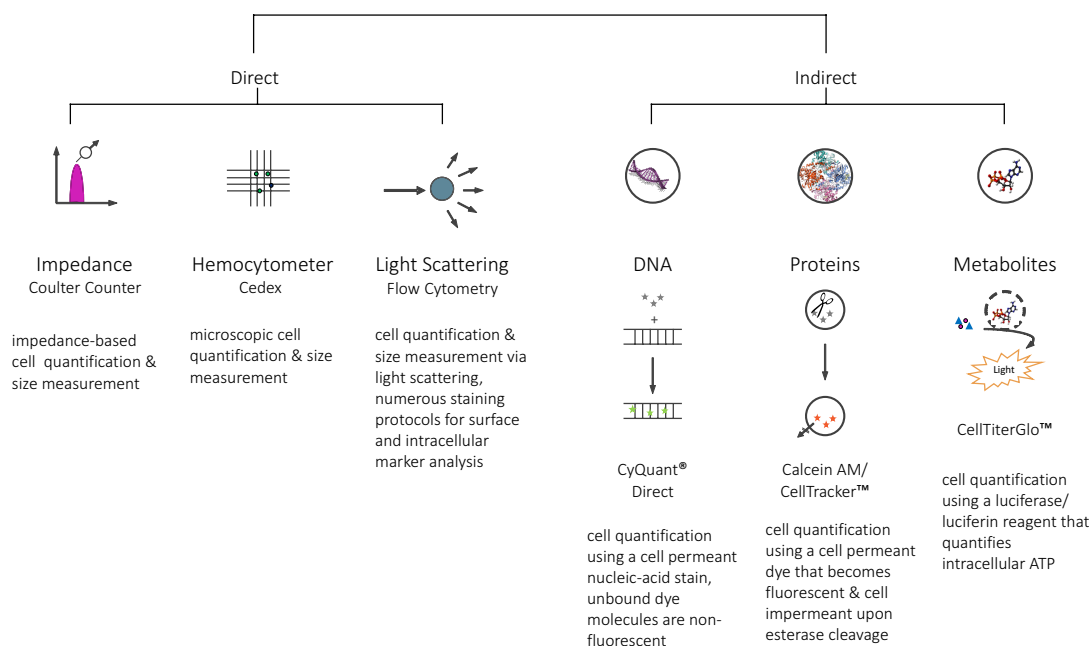


**Figure 1:** Overview of state-of-the-art cell quantification methods.

Thirdly, it is crucial that the utilized assay is not only robust towards changes in buffer composition, but should also give reliable results over a wide range of medium densities and viscosities. Moreover, working with different medium densities makes the use of centrifugation steps challenging, since cells cannot easily be sedimented at medium

densities similar to the cell's density. Therefore, an add-mix-and-measure type of assay is favorable. This, likewise, is of great advantage regarding simplicity of handling and reproducibility. Based on these criteria, we chose the following indirect cell quantification methods: CellTiter-Glo™, CyQuant®Direct, and the CellTracker™ dyes. Moreover, we chose flow cytometry as a direct cell quantification method, since it is suitable for high throughput applications and allows the discrimination between numerous cell populations based on the staining of specific intracellular and extracellular markers. Since cellular DNA content is highly regulated, nucleic acid stains are known to be a reliable tool for cell quantification [20,25]. From the many nucleic acid stains available, CyQuant®Direct was chosen, since this assay was developed for high throughput applications and is therefore designed as a simple add-mix-and-measure assay. Moreover, it has been shown to be more sensitive than many other nucleic acid stains [25–27]. Another advantage of this assay is that it contains a dye quenching reagent that is excluded from living cells, thus, only live cells are quantified. However, it is important to consider the influence of cell cycle on cell proliferation assays based on DNA quantification. If there is a change in the distribution between the different cell cycle phases, there will be an over- or underestimation of cell numbers [25,28].

Another commonly used type of fluorescent dyes for determining the number of viable cells are esterase substrates (e.g. Calcein AM, Cell Tracker™ dyes) [29]. Cell Tracker™ dyes are live cell stains that are retained within living cells and belong to the group of thiol-reactive esterase substrates. These dyes were chosen, since they offer a versatile and simple means of cell tracking and quantification. CellTracker™ Green CMFDA and CellTracker™ orange CMRA are non-fluorescent unless retained inside the cells where they become transformed into a cell impermeant fluorescent product [30]. This allows cell quantification without washing steps in a simple add-mix-and-measure format, since excess dye molecules are non-fluorescent, and, therefore, do not interfere with the read-out. In addition, these dyes can be easily combined with live cell impermeant nucleic acid stains (e.g. Sytox stains, Ethidium homodimer-1) for dead cell quantification.

The most widely applied cell quantification assays are based on the quantification of metabolic activity and assays like MTT, MTS, and Alamar Blue™, and are commonly used in toxicity studies [20,28]. From this assay category we chose the CellTiter-Glo™ Luminescent Cell Viability Assay, which determines intracellular ATP levels by a luciferin/ luciferase reaction. The assay exclusively quantifies living cells, as ATP is rapidly degraded upon cell death. This assay is, like the others, a simple and fast add-mix-and-measure type of assay. A potential drawback of this assay is a bias due to changes in metabolic activity, which needs to be evaluated for each application [20,28]. Flow cytometric enumeration of cells is a standard analytical technique in clinical diagnostics [31,32]. This, however, is only possible, if the flow cytometer is equipped with precision pumps or if counting beads are used. Using counting beads, however, gives additional uncertainty, since the pipetting of accurate bead number is challenging [31]. Thus, we evaluated if accurate cell counting is nonetheless possible using a high throughput sampler which can analyze defined sample volumes (**Figure 1 & Table 1**).

**Table 1:** Summary of different properties of the evaluated cell quantification assays.

Method	Properties					Parameter						
	Principle	Readout	Discrimination between live and dead cells	Quantification of dead cells	Cell lysis	Assay time [min] <sup>a)</sup>	Material costs <sup>b)</sup>	Refs.	Linear Range [cells/mL]	Working Range [cells/mL]	LoD [cells/mL]	LoQ [cells/mL]
CellTracker™	dye activation & retention in living cells upon esterase cleavage	fluorescence	+	additional dead cell staining possible	-	40	++	29	10 <sup>4</sup> -5x10 <sup>5</sup>	10 <sup>4</sup> -5x10 <sup>5</sup>	10 <sup>4</sup>	10 <sup>4</sup>
CyQuant Direct®	dsDNA <sup>c)</sup> -binding cyanine dye	fluorescence	+	additional dead cell staining possible	-	70	++	20,25-28	10 <sup>3</sup> -10 <sup>5</sup>	10 <sup>3</sup> -10 <sup>5</sup>	10 <sup>3</sup>	5x10 <sup>3</sup>
CellTiter-Glo™	quantification of intracellular ATP	luminescence	+	-	+	20	++	20,28	10 <sup>2</sup> -10 <sup>6</sup>	5x10 <sup>2</sup> -10 <sup>6</sup>	<10 <sup>2</sup>	<10 <sup>2</sup>
Flow cytometry	direct cell counting	light scattering	+	+	-	80	+	31,32	10 <sup>2</sup> -5x10 <sup>5</sup>	5x10 <sup>2</sup> -5x10 <sup>5</sup>	2.5x10 <sup>2</sup>	10 <sup>3</sup>

a) Average assay time for 96 samples. Assay time in flow cytometry is highly dependent on sample flow rate and sample volume. b) Material costs were compared for the analysis of 96 samples in 96-well format (costs were compared for consumables and reagents only). c) dsDNA: double-stranded DNA.

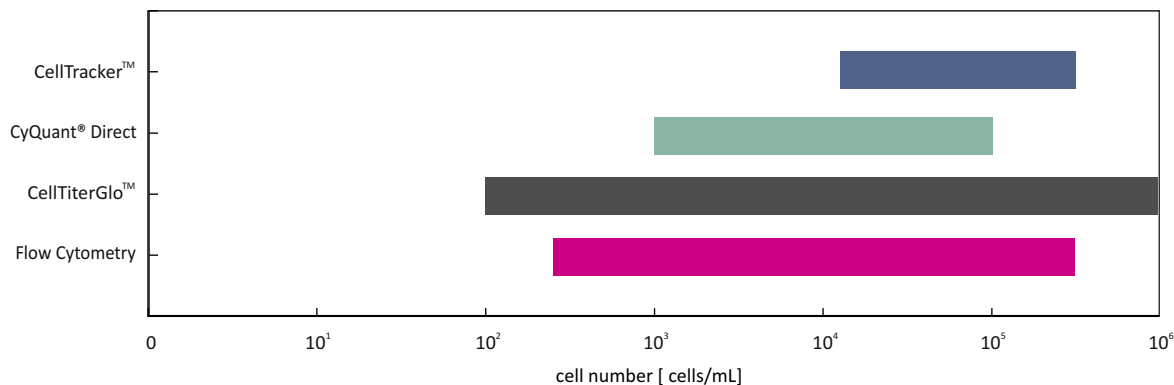


**Figure 2:** Working ranges of CellTracker™, CyQuant® Direct, CellTiter-Glo™, and flow cytometry. A dilution series of  $10^7$  to  $10^2$  cells per mL, including a blank control, was prepared and quantified with the respective method ( $n = 3$  technical replicates), followed by determination of working ranges.

### 3.2 Sensitivity and working range differ significantly between assay-types

For high-throughput cell quantification in downstream processing of cells, it is essential that the assay has a broad working range and high sensitivity. Therefore, we evaluated sensitivity and working range by preparing a dilution series between  $10^7$  and  $10^2$  cells per mL and subsequent quantification using the respective assay. From these data, the detection limit and working range were determined. Moreover, calibration was performed using linear least-square regression analysis. If variances between the highest and lowest concentration of the working range were not equal, weighted least squares regression analysis was performed. Regression parameters as well as working ranges of the respective methods are summarized in **Table 1 & Table 2**. As shown in **Figure 2**, the working ranges of the evaluated assays differed significantly.

**Table 2:** Summary of regression parameters.

Method	F-Test	Weighting Factor	% RE	R <sup>2</sup>	Mean CV (%)	Slope <sup>a)</sup>	Intercept <sup>a)</sup>
CellTracker™	>0.05	none	1.67	0.9996	4.7	0.0165 (0.0155–0.0175)	34600 (34300–34800)
CyQuant Direct®	<0.01	1/x <sup>2</sup>	0.01	0.9989	4.5	0.3518 (0.3302–0.3735)	8393 (8348–8439)
CellTiter-Glo™	<0.01	1/x	0.01	0.9998	4.3	1.772 (1.745–1.799)	372.7 (232.6–512.7)
Flow cytometry	<0.01	1/x	-0.02	0.9993	2.9	0.1079 (0.1058–0.11)	58.72 (25.97–91.58)

<sup>a)</sup> Values for 95% prediction bounds are shown in parentheses

CellTracker™ and CyQuant® Direct showed working ranges of 1.5 and 2 orders of magnitude, and limits of detection of  $10^4$  and  $10^3$  cells per mL, respectively (**Figure 3, A+B, & Table 2**). However, it should be noted that the regression curve for CellTracker™ showed a comparably small slope, thus, the assay is less sensitive to small changes in cell number. CellTiter-Glo™ and flow cytometry showed larger working ranges with 3 and 4 orders of magnitude, respectively. The detection limits were comparable with  $<10^2$  and

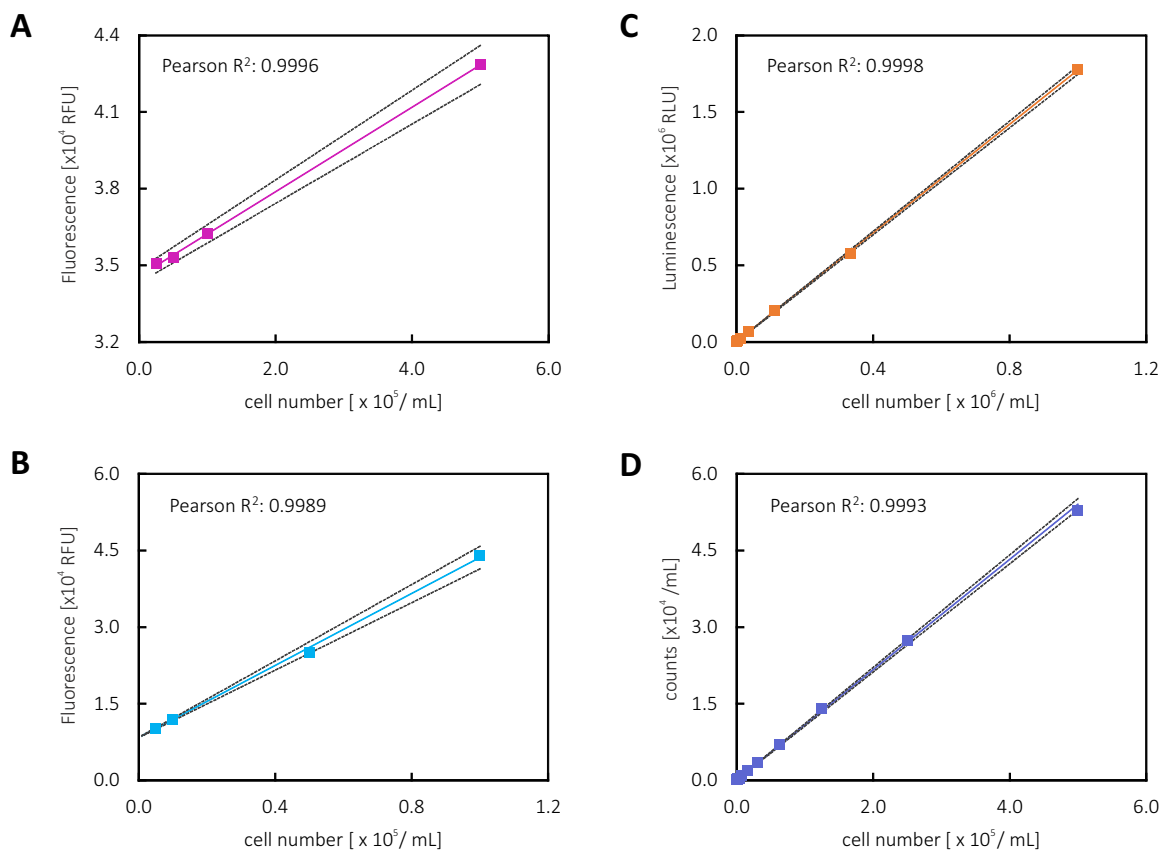


**Figure 3:** Regression analysis of HL-60 cells quantified with CellTracker<sup>TM</sup> (A), CyQuant<sup>®</sup> Direct (B), CellTiter-Glo<sup>TM</sup> (C), and flow cytometry (D). A dilution series of  $10^7$  to  $10^2$  cells per mL, including a blank control, was prepared and quantified with the respective method ( $n=3$  technical replicates). Calibration curves were calculated using weighted least squares linear regression and 95% confidence intervals and coefficients of determination were calculated. Curve fit (color) and 95% confidence intervals (grey, dotted) are depicted in each plot. RFU: relative fluorescence units, RLU: relative luminescence units.

$5 \times 10^2$  cells per mL (**Figure 3, C+D & Table 2**). All assays showed high linearity ( $R^2 > 0.998$ ) and %RE were below 0.02%, except for CellTracker<sup>TM</sup> which was significantly higher with 1.67%.

### 3.3 Assay precision is primarily dependent on liquid handling precision

Precision was evaluated by comparing coefficients of variation over the working range of the four assays (**Table 2**). Mean variation coefficients ranged from 4.3 to 4.7%, and were comparable for all indirect cell quantification assays. For flow cytometry the mean variation coefficient was slightly lower with 2.9%. This, however, is most likely due to the smaller number of pipetting steps. Our data indicate that precision of the four assays is mostly dependent on liquid handling precision, which can be much higher for automated liquid-handling.

### 3.4 Flow cytometry shows higher robustness than plate-based assays

Assay robustness is an important factor in high-throughput screening development. Particularly in downstream processing of cell-based products, robustness towards changes in buffer compositions, pH, and the presence of different polymers is a prerequisite. Fluorescence and luminescence detection, as well as enzymatic reactions, can be influenced by changes in pH, ionic composition, and light scattering. It is, however, unclear to what extent such changes influence the performance of the assays. Moreover, changes in viscosity can influence liquid handling as well as mixing and diffusion kinetics. We thus evaluated the robustness of each assay by quantifying  $10^5$  cells per mL in the presence of different salts and polymers that are commonly used in chromatography and aqueous two-phase systems. All buffers were used undiluted and 10-fold diluted with DPBS. The recovery rate was calculated as the percentage of cells detected compared to the DPBS controls. All three indirect cell quantification assays were to some degree sensitive to changes in buffer composition and pH, while flow cytometry was insensitive to all tested buffers and polymers. Buffer effects were the most distinct for CyQuant<sup>®</sup>Direct and the CellTracker<sup>™</sup> dyes. Here, all tested buffers reduced the number of detected cells by 30 to 50%. The CellTiter-Glo<sup>™</sup> assay, on the other hand, was sensitive to the presence of phosphate buffers of varying pH as well as sodium citrate, but not to other buffers, such as HBSS and Tris-HCl. Buffer effects were, however, not observed when the buffers were 10-fold diluted with DPBS (**Figure 4, E–G**). Moreover, we observed a significant effect ( $p < 0.01$ ) of both PEG 8,000 and dextran 500,000 on cell quantification with CyQuant<sup>®</sup>Direct and CellTracker<sup>™</sup> at concentrations above 1% (w/w), where the number of detected cells was reduced by up to 17%. Both, CellTiter-Glo<sup>™</sup> and flow cytometry were, however, not significantly influenced by up to 2% (w/w) of PEG 8,000 and dextran 500,000 (**Figure 4, A–C**). It should be noted though that higher polymer concentrations will result in inaccurate results (data not shown).

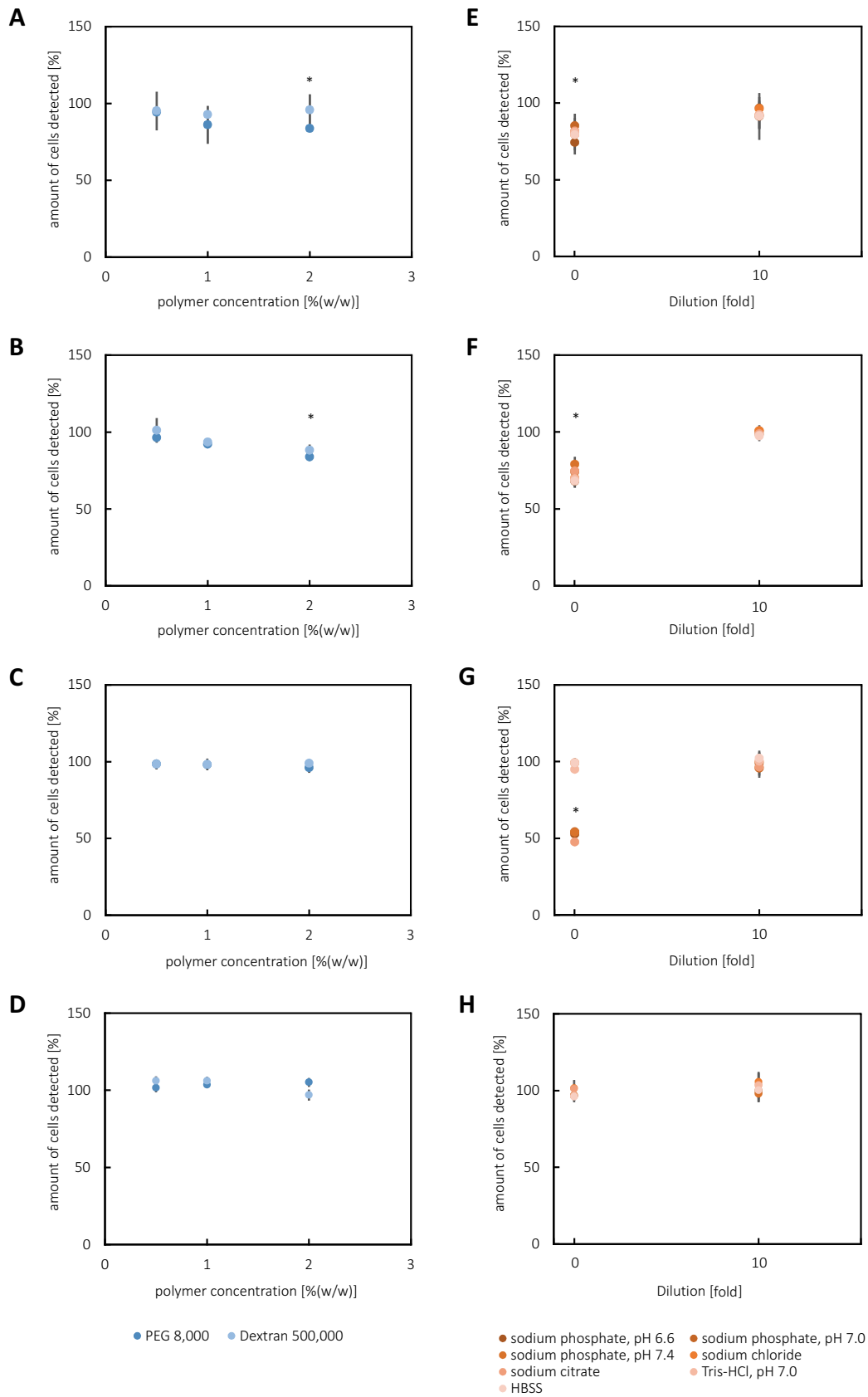


**Figure 4:** Influence of different polymers (A–D) and salts (E–H) on quantification of HL–60 cells.

**Figure 4:** (*continued*) Influence of different polymers (A–D) and salts (E–H) on quantification of HL-60 cells. A+E: CellTracker<sup>TM</sup>; B+F: CyQuant<sup>®</sup>Direct; C+G: CellTiter-Glo<sup>TM</sup>; D+H: flow cytometry. Robustness was evaluated by quantifying  $10^5$  cells per mL in the presence of different salts and polymers. Buffers containing different salts and pH-values were used at physiological osmolarities, undiluted, as well as 10-fold diluted with DPBS. Error bars indicate standard deviation of  $n = 3$  technical replicates. Asterisks indicate significant changes in detected cell numbers ( $p < 0.01$ ) as determined by Student's  $t$ -test.

## 4 Discussion

We compared four distinct high-throughput cell quantification methods that differ in their respective mechanisms (**Figure 1**).

We found significant differences between the working ranges (**Figure 2**) and robustness (**Figure 4**) of the evaluated methods. Both CellTiter-Glo<sup>TM</sup> and flow cytometry are excellent tools for high throughput cell quantification. Both methods have broad working ranges (3 and 4 log) (**Table 1, Figure 2**), and performed well over a wide range of buffer compositions, medium densities, and viscosities (**Figure 4**). Even though the utilized BD<sup>TM</sup> LSR Fortessa is not equipped with precision pumps, we found that when using a high throughput sampler, accurate cell quantification is possible without the use of counting beads. In comparison, CyQuant<sup>®</sup>Direct and the CellTracker<sup>TM</sup> dyes had smaller working ranges and were more sensitive to changes in buffer composition (**Table 1**). As expected, CellTiter-Glo<sup>TM</sup> was the most sensitive cell quantification assay, since luminescence-based assays are very sensitive due to the strong signal amplification. Interestingly, flow cytometry showed comparable sensitivity. CyQuant<sup>®</sup>Direct, however, showed significantly lower sensitivity, with a detection limit about one order of magnitude higher than CellTiter-Glo<sup>TM</sup> and flow cytometry, while the CellTracker<sup>TM</sup> dyes showed the lowest sensitivity, with a detection limit about two orders of magnitude higher than CellTiter-Glo<sup>TM</sup>. Even though all assays except CellTiter-Glo<sup>TM</sup> do not include a signal amplification step, flow cytometry is more sensitive than the two fluorescence-based assays (**Figure 2**).

With the exception of flow cytometry, all assays were susceptible to changes in buffer composition. This is due to the fact that both enzymatic reactions as well as fluorescence and luminescence detection are sensitive to changes in pH and ionic composition. These influences, however, could be eliminated by 10-fold dilution with DPBS (**Figure 4**). In addition, the fluorescence-based assays CyQuant<sup>®</sup>Direct and CellTracker<sup>TM</sup> were sensitive towards the presence of polymers, which is most likely due to increased light scattering [33]. This was not observed when using CellTiter-Glo<sup>TM</sup>, which can tolerate moderate polymer concentrations.

Even though, flow cytometry is based on light scattering and fluorescence measurement, cells can be quantified reliably in the presence of different salts and polymers. This is most likely due to mode of operation, as cells are hydrodynamically focused in a fluid stream, thereby being further diluted, and pass the lasers individually, which in turn gives much higher sensitivity.

Using high-throughput flow cytometry for cell quantification has the advantage that other parameters such as the expression of surface antigens can be analyzed simultaneously, if robust, no-wash staining protocols are available. Thus, even complex cell mixtures can

---

be analyzed in a single experiment, while the other cell quantification methods require additional experiments to quantify different subpopulations of complex cell mixtures. The evaluated methods also vary in assay time and cost of material. In 96-well format the required processing time for CellTiter-Glo<sup>TM</sup>, the CellTracker<sup>TM</sup> dyes and CyQuant<sup>®</sup>Direct differ only in the incubation time of the respective reagents. Here, CellTiter-Glo<sup>TM</sup> is substantially faster than the other methods (**Table 1**). Using an interlaced experimental design, the impact on total processing time can however be minimized, and since luminescence and fluorescence measurement of a 96-well plate takes less than two minutes, sample preparation is most likely the limiting factor. Using a Tecan Freedom Evo liquid handling station, pipetting one compound in different volumes into 96-wells takes 5–10 minutes, depending on the viscosity of the liquid. Equal volumes can be pipetted using a 96-channel arm, which takes less than a minute. In high-throughput flow cytometry the processing time is highly dependent on the flow cytometer settings (i.e. sample volume and flow rate). The settings described here are optimized for high sensitivity, thus, the processing time for a 96-well plate is comparably long. In high-throughput mode, a 96-well plate can be analyzed in less than 15 minutes, however, due to the decreased sample volume, the sensitivity decreases and the working range shifts towards higher cell numbers (data not shown). In 384-well format the differences in processing time increase, while fluorescence and luminescence measurement take 4–8 minutes, depending on the integration time, flow cytometric analysis of a 384-well plate takes almost an hour in high-throughput mode. However, there are strategies to increase throughput dramatically using cell barcoding which is not an option for plate-based assays [34]. As for the plate-based assays, the influence of sample preparation on total processing time can be minimized using an interlaced experimental design. While flow cytometry has significantly higher instrumentation costs, the cost of material are comparably low (**Table 1**). The choice of an assay or a combination of assays is, thus, highly dependent on the application and the dynamic range, robustness, and throughput needed. In summary, we showed that both CellTiter-Glo<sup>TM</sup> and flow cytometry are excellent tools for high-throughput cell quantification in downstream process development for cell-based products. Both methods have broad working ranges and perform well over a wide range of buffer compositions, medium densities, and viscosities. In addition, both assays can be performed in 96- and 384-well format. For fast and sensitive quantification of a single cell type, CellTiter-Glo<sup>TM</sup> is the method of choice, while for more complex cell mixtures and analysis of additional parameters, such as apoptosis, flow cytometry is the method of choice.

## 5 References

- [1] Hertzberg, R. P., Pope, A. J., High-throughput screening: New technology for the 21st century. *Curr. Opin. Chem. Biol.*, 2000, **4**, 445–451.
- [2] Macarron, R., Banks, M. N., Bojanic, D., Burns, D. J. et al., Impact of high-throughput screening in biomedical research. *Nat. Rev. Drug Discov.*, 2011, **10**, 188–195.
- [3] Mayr, L. M., Bojanic, D., Novel trends in high-throughput screening. *Curr. Opin. Pharmacol.*, 2009, **9**, 580–588.
- [4] Lacki, K. M., High-throughput process development in biomanufacturing. *Curr. Opin. Chem. Eng.*, 2014, **6**, 25-32.
- [5] Wiendahl, M., Oelmeier, S. A., Dismer, F., Hubbuch, J., High-throughput screening-based selection and scale-up of aqueous two-phase systems for pDNA purification. *J. Sep. Sci.*, 2012, **35**, 3197-3207.
- [6] Oelmeier, S. A., Ladd Effio, C., Hubbuch, J., High throughput screening based selection of phases for aqueous two-phase system-centrifugal partitioning chromatography of monoclonal antibodies. *J. Chromatogr. A*, 2012, **1252**, 104-114.
- [7] Oelmeier, S. A., Dismer, F., Hubbuch, J., Application of an aqueous two-phase systems high-throughput screening method to evaluate mAb HCP separation. *Biotechnol. Bioeng.*, 2011, **108**, 69-81.
- [8] Zang, Y., Kammerer, B., Eisenkolb, M., Lohr, K., Kiefer, H., Towards protein crystallization as a process step in downstream processing of therapeutic antibodies: screening and optimization at microbatch scale. *PLoS One*, 2011, **6**, e25282.
- [9] Welsh, J., Pushing the limits of high-throughput chromatography process development : current state and future directions. *Pharm. Bioprocess.*, 2015, **1**, 1-3.
- [10] Lacki, K. M., High-throughput process development of chromatography steps: advantages and limitations of different formats used. *Biotechnol. J.*, 2012, **70**, 1192-1202.
- [11] Trounson A., McDonald C., Stem Cell Therapies in Clinical Trials: Progress and Challenges. *Cell Stem Cell*, 2015, **17**, 11-22.
- [12] Kumar, A., Srivastava, A., Cell separation using cryogel-based affinity chromatography. *Nat. Protoc.*, 2010, **5**, 1737-1747.
- [13] Kumar, A., Kamihira, M., Galaev, I. Y., Mattiasson, B., Iijima, S., Type-specific separation of animal cells in aqueous two-phase systems using antibody conjugates with temperature-sensitive polymers. *Biotechnol. Bioeng.*, 2001, **75**, 570-580.

- 
- [14] Kumar, A., Bhardwaj, A., Methods in cell separation for biomedical application: cryogels as a new tool. *Biomed. Mater.*, 2008, **3**, 034008.
- [15] Ujam, L. B., Clemmitt, R. H., Clarke, S. A., Brooks, R. A. et al., Isolation of Monocytes From Human Peripheral Blood Using Immuno-Affinity Expanded-Bed Adsorption. *Biotechnol. Bioeng.*, 2003, **83**, 554-566.
- [16] Johansson, G., Walter, H., Partitioning and concentrating biomaterials in aqueous phase systems. *Int Rev Cytol.*, 2000, **192**, 33-60.
- [17] Cabral, J. M. S., Cell Partitioning in Aqueous Two-Phase Polymer Systems. *Adv. Biochem. Eng. Biotechnol.*, 2007, **106**, 151-171.
- [18] Diogo, M. M., da Silva, C. L., Cabral, J. M. S., Separation technologies for stem cell bioprocessing. *Biotechnol. Bioeng.*, 2012, **11**, 2699-2709.
- [19] Sousa, A. F., Andrade, P. Z., Pirzgalska, R. M., Galhoz, T. M. et al., A novel method for human hematopoietic stem/progenitor cell isolation from umbilical cord blood based on immunoaffinity aqueous two-phase partitioning. *Biotechnol. Lett.*, 2011, **33**, 2373-2377.
- [20] Quent, V. M. C., Loessner, D., Friis, T., Reichert, J. C., Hutmacher, D. W., Discrepancies between metabolic activity and DNA content as tool to assess cell proliferation in cancer research. *J. Cell. Mol. Med.*, 2010, **14**, 1003-1013.
- [21] Kepp, O., Galluzzi, L., Lipinski, M., Yuan, J., Kroemer, G., Cell death assays for drug discovery. *Nat. Rev. Drug Discov.*, 2011, **10**, 221-237.
- [22] ICH Harmonized Tripartiate Guidelines: Validation of Analytical Procedures: Text and Methodology, 2005, Q2(R1).
- [23] Almeida, A. M., Falcao, A. C., Linear regression for calibration lines revisited: weighting schemes for bioanalytical methods. *J. Chrom. B.*, 2002, **774**, 215-222.
- [24] Wu, G., Doberstein, S. K., HTS technologies in biopharmaceutical discovery. *Drug Discov. Today*, 2006, **11**, 718-724.
- [25] Jones, L. J., Gray, M., Yue, S. T., Haugland, R. P., Singer, V. L., Sensitive determination of cell number using the CyQUANT cell proliferation assay. *J. Immunol. Methods*, 2001, **254**, 85-98.
- [26] Otto, R., Fields, I., Fluorimetric DNA Assay for Cell Growth. *Anal. Biochem.*, 1992, **192**, 186-192.
- [27] Abraham, V. C., Towne, D. L., Waring, J. F., Warrior, U., Burns, D. J., Application of a High-Content Multiparameter Cytotoxicity Assay to Prioritize Compounds Based on Toxicity Potential in Humans. *J. Biomol. Screen.*, 2008, **13**, 527-537.

- [28] Chan, G. K. Y., Kleinheinz, T. L., Peterson, D., Moffat, J. G., A simple high-content cell cycle assay reveals frequent discrepancies between cell number and ATP and MTS proliferation assays. *PLoS One*, 2013, **8**, e63583.
- [29] Mueller, H., Kassack, M. U., Wiese, M., Comparison of the usefulness of the MTT, ATP, and calcein assays to predict the potency of cytotoxic agents in various human cancer cell lines. *J. Biomol. Screen.*, 2004, **9**, 506-515.
- [30] Lulevich, V., Shih, Y.-P., Lo, S. H., Liu, G.-Y., Cell tracing dyes significantly change single cell mechanics. *J. Phys. Chem. B*, 2009, **113**, 6511-6519.
- [31] Barnett, D., Granger, V., Whitby, L., Storie, I., Reilly, J. T., Absolute CD4+ T-lymphocyte and CD34+ stem cell counts by single-platform flow cytometry: the way forward. *Br. J. Haematol.*, 1999, **106**, 1059-1062.
- [32] Gratama, J. W., Sutherland, D. R., Keeney, K., Flow cytometric enumeration and immunophenotyping of hematopoietic stem and progenitor cells. *Semin. Hematol.*, 2001, **38**, 139-144.
- [33] Ahmed, S. A., Zang, Z., Yoo, K. M., Ali, M. A., Alfano, R. R., Effect of multiple light scattering and self-absorption on the fluorescence and excitation spectra of dyes in random media. *Appl. Opt.*, 1994, **33**, 2746-2750.
- [34] Krutzik, P. O., Clutter M. R., Trejo A., Nolan G. P. Fluorescent cell barcoding for multiplex flow cytometry. *Curr. Protoc. Cytom.*, 2011, DOI:10.1002/0471142956.cy0631s55.

---

## High-throughput downstream process development for cell-based products using aqueous two-phase systems

**Sarah Zimmermann<sup>a</sup>, Sarah Gretzinger<sup>a,b</sup>, Marie-Luise Schwab<sup>a,c</sup>, Christian Scheeder<sup>a</sup>, Philipp K. Zimmermann<sup>a</sup>, Stefan A. Oelmeier<sup>a,d</sup>, Eric Gottwald<sup>e</sup>, Are Bogsnes<sup>f</sup>, Mattias Hansson<sup>g</sup>, Arne Staby<sup>h</sup> & Jürgen Hubbuch<sup>a,\*</sup>**

<sup>a</sup> : Karlsruhe Institute of Technology (KIT), Institute of Process Engineering in Life Science, Section IV: Biomolecular Separation Engineering (MAB), Engler–Bunte–Ring 3, 76131 Karlsruhe, Germany

<sup>b</sup> : Karlsruhe Institute of Technology (KIT), Institute of Functional Interfaces (IFG), Hermann–von–Helmholtz–Platz 1, 76344 Eggenstein–Leopoldshafen, Germany

<sup>c</sup> : DIARECT AG, Department of Quality Assurance and Quality Control, Bötzingen Straße 29 B, Freiburg, Germany

<sup>d</sup> : Boehringer Ingelheim Pharma GmbH & Co. KG, Global Bioprocess & Pharmaceutical Development, Birkendorfer Straße 65, 88397 Biberach an der Riss, Germany

<sup>e</sup> : Karlsruhe Institute of Technology (KIT), Institute for Biological Interfaces (IBG 5), Hermann–von–Helmholtz–Platz 1, 76344 Eggenstein–Leopoldshafen, Germany

<sup>f</sup> : Novo Nordisk A/S, Biopharm Purification Development & Virology, Hagedornsvej 1, 2820 Gentofte, Denmark

<sup>g</sup> : Novo Nordisk A/S, Diabetes Research, Novo Nordisk Park, 2760 Måløv, Denmark

<sup>h</sup> : Novo Nordisk A/S, CMC Project Planning & Management, Smørmosevej 17, 2880 Bagsværd, Denmark

\* *Correspondence to Prof. Dr. Jürgen Hubbuch, telephone: +49 721 608 47526; fax: + 49 721 608 46240; e-mail: juergen.hubbuch@kit.edu*

## Abstract

As the clinical development of cell-based therapeutics has evolved immensely within the past years, downstream processing strategies become more relevant than ever. Aqueous two-phase systems (ATPS) enable the label-free, scalable, and cost-effective separation of cells, making them a promising tool for downstream processing of cell-based therapeutics. Here, we report the development of an automated robotic screening that enables high-throughput cell partitioning analysis in ATPS. We demonstrate that this setup enables fast and systematic investigation of factors influencing cell partitioning. Moreover, we examined and optimized separation conditions for the differentiable promyelocytic cell line HL-60 and used a countercurrent distribution-model to investigate optimal separation conditions for a multi-stage purification process. Finally, we show that the separation of CD11b-positive and CD11b-negative HL-60 cells is possible after partial DMSO-mediated differentiation towards the granulocytic lineage. The modeling data indicate that complete peak separation is possible with 30 transfers, and > 93% of CD11b-positive HL-60 cells can be recovered with > 99% purity. The here described screening platform facilitates faster, cheaper, and more directed downstream process development for cell-based therapeutics and presents a powerful tool for translational research.

**Keywords:** high-throughput screening (HTS); downstream processing of cell-based products; label-free cell separation; aqueous two-phase systems (ATPS); high-throughput flow cytometry

---

# 1 Introduction

High-throughput screening (HTS) technologies are state-of-the art in various scientific disciplines, such as basic research, diagnostics, and biotechnology [1–4]. In the past decade, HTS-technologies have gained increasing importance in downstream process development of biopharmaceuticals, such as protein- and DNA-based drugs, and are currently available for most platform technologies, including column chromatography, crystallization, and aqueous two-phase systems (ATPS) [4–11]. These technologies have facilitated faster, cheaper, and more directed downstream process development. In combination with modeling and simulation data, they present a powerful tool to elicit mechanisms underlying separation and design purification strategies for novel targets.

As cell-based therapeutics are entering the market, new scalable downstream processing strategies are required. For clinical applications, cell-based products need to be provided in high purities, since certain contaminants can cause severe adverse effects, such as teratoma formation or graft-versus-host-disease (GvHD) [12–17]. The most widely applied cell separation methods use cell surface antigens for affinity-purification. These methods, however, require large amounts of clinical-grade antibodies, resulting in extremely high costs. Antibody-labels that remain on the cell surface, pose considerable regulatory obstacles for the treatment of patients, as they can cause adverse reactions [15,16,18,19]. ATPS offer a gentle, cost-effective, label-free, and scalable means of cell purification, and are well established in downstream processing of biopharmaceuticals [20–22]. ATPS are aqueous solutions consisting of different phase forming compounds, e.g. polymers, which form two immiscible phases above a certain threshold. The two phases have distinct physicochemical properties, and biomolecules partition between them according to their physicochemical properties. It is well established that polyethylene-glycol (PEG)-dextran ATPS can be used to separate cells according to their surface properties. It has been shown that ATPS can be used to separate different cell types with high selectivity and resolution. Using multi-step partitioning, such as countercurrent distribution (CCD), even complex cell mixtures can be separated [21,23]. Nonetheless, the development of effective downstream processes requires the optimization of many different parameters, hampering widespread application of ATPS in cell purification.

In this work, an automated HTS-platform for the investigation of cell partitioning in ATPS was developed and validated. The screening was implemented on a robotic liquid-handling station (LHS), and includes all steps from ATPS preparation to cell quantification and analysis using HT-flow cytometry. In a first case study, the partitioning of the differentiable cell line HL-60 was evaluated in a number of ATPS. HL-60 was chosen since it can be partially differentiated towards neutrophil granulocytes by DMSO-treatment, and monitored using an anti-CD11b-antibody [24]. The influence of salt composition, pH, and tie-line length (TLL) on the resolution of CD11b-positive and CD11b-negative HL-60 was evaluated, and separation conditions were optimized. Using a CCD-model, we investigated optimal separation conditions for a multi-stage purification process. Overall, we show that the here described HTS-platform enables fast and directed downstream process development for cell-based products and will permit the systematic investigation of mechanisms underlying cell separation in ATPS.

## 2 Materials & Methods

### 2.1 Disposables

For absorbance measurements, UV–Star plates (Greiner Bio–One, Kremsmuenster, Austria) were used. For flow cytometry, 96–well U bottom plates (BD Falcon<sup>™</sup>, Franklin Lakes, NJ, USA) were used. ATPS were prepared in 1.3 mL deep well plates (Nalgene Nunc, Rochester, NY). For all other purposes, polypropylene flat–bottom microplates (Greiner Bio–One) were used.

### 2.2 Software and data processing

The Tecan Freedom Evo 200 was controlled using Evoware 2.5 SP2 standard (Tecan, Crailsheim, Germany), and the Tecan Infinite<sup>®</sup> Pro M200 plate reader was controlled via Magellan 7.1 SP 1 (Tecan). For advanced applications such as sampling and cell resuspension, visual basic scripts were generated and fed into Evoware. Excel 2013 (Microsoft, Redmond, WA, USA) was used as import format and for data storage. Data evaluation and visualization was performed with Excel 2013 and Matlab R2014a (The MathWorks, Natick, ME, USA). For statistical data analysis Matlab R2014a was used. BD FACSDiva 8.0 (BD Biosciences, San Jose, CA, USA) was used to control the BD LSR Fortessa Cell Analyzer and for raw data analysis. For visualization of flow cytometry data, Flow Jo V10 (Tree Star, Ashland, OR, USA) was used.

### 2.3 Preparation of buffers and stock solutions

All buffers and stock solutions were prepared with ultra–pure water (0.55  $\mu\text{S}/\text{cm}$ ) obtained from an Arium<sup>®</sup> proUV water system (Sartorius Stedim Biotech, Goettingen, Germany). Stock solutions of 2% and 20% dextran 500,000 (Pharmacosmos A/S, Holbæk, Denmark, cat. 5510 0500 9007, Batch No.: HT3229) and 30% PEG 8,000 (Sigma Aldrich, St. Louis, MO, USA, cat. P2139, Batch No.: 059Ko121) were prepared and dissolved on a magnetic stirrer overnight. 500 mM sodium phosphate (NaPi) buffer stock solutions were prepared by using di– (Merck Millipore, Billerica, MA, USA) and monobasic sodium phosphate (Sigma Aldrich) in varying ratios, in order to obtain specific pH-values (241 mM  $\text{Na}_2\text{HPO}_4$  and 259.4 mM  $\text{NaH}_2\text{PO}_4$  for pH 6.6, 353 mM  $\text{Na}_2\text{HPO}_4$  and 147.4 mM  $\text{NaH}_2\text{PO}_4$  for pH 7.0, 430 mM  $\text{Na}_2\text{HPO}_4$  and 70.6 mM  $\text{NaH}_2\text{PO}_4$  for pH 7.4). 1 M NaPi buffers were prepared analogously. NaCl (Merck Millipore) was prepared as 1 M and 500 mM stock solutions. A 1 mM methyl violet 2B stock solution (Sigma Aldrich) was prepared in ultra–pure water. All buffers and polymer solutions were filtered ( $\varnothing$  0.22  $\mu\text{m}$ ). Buffers were stored at room temperature and polymer solutions were stored at 4°C. Osmolarities of the distinct ATPS were verified using a VAPRO<sup>®</sup> 5600 vapor pressure osmometer (Wescor, Logan, UT, USA), and all ATPS had osmolarities within the physiological range (290–310 mOs). FC–staining buffer consisted of phosphate buffered saline (PBS) supplemented with 2 mM EDTA (Life Technologies<sup>™</sup>, Carlsbad, CA, USA) and 0.5% bovine serum albumin (BSA) (Miltenyi Biotech, Bergisch Gladbach, Germany).

---

## 2.4 Cell culture

All cell culture reagents were purchased from Life Technologies<sup>TM</sup>. The promyelocytic cell line HL-60 and the murine fibroblast cell line L929 were purchased from CLS (Cell lines Service, Eppelheim, Germany) and propagated at 37°C in a humidified 5% CO<sub>2</sub> incubator. HL-60 cells were grown in RPMI 1640 with GlutaMAX supplemented with 15% fetal bovine serum (FBS), 1% sodium pyruvate, 1% non-essential amino acids (NEAA), and 0.5% Penicillin/ Streptomycin. L929 cells were grown in DMEM with GlutaMAX supplemented with 10% FBS and 1% Penicillin/ Streptomycin.

## 2.5 Granulocytic differentiation of HL-60 cells

Granulocytic differentiation of HL-60 was induced by the addition of DMSO [24]. For each differentiation experiment, cells were seeded at a density of 2.5 x 10<sup>5</sup> cells/mL in culture medium supplemented with 1.25% (v/v) DMSO (Sigma Aldrich) and cultured for 7 days. During this time, cell growth was monitored and medium was changed after 3 days.

## 2.6 Cell Tracker<sup>TM</sup>, antibody and viability staining

In spiking experiments and to discriminate between the two cell lines, HL-60 cells were stained with CellTracker<sup>TM</sup> Orange CMRA (Life Technologies<sup>TM</sup>). 1 x 10<sup>6</sup> cells per mL were resuspended in RPMI with GlutaMAX and stained with 0.5 μM dye at 37°C for 30 min. The cells were subsequently resuspended in culture medium, and incubated at 37°C for 30 min to inactivate unbound dye molecules.

For detection of differentiated HL-60 cells, a FITC-conjugated rat-anti-human-CD11b antibody (Miltenyi Biotech) [24] was used at a dilution of 1:100. For staining, up to 1 x 10<sup>6</sup> cells per mL were resuspended in 100 μL of FC-staining buffer, and incubated at 4°C in the dark for 10 min. For analysis of cell viability, cells were stained with LIVE/DEAD Green Fixable Dead Cell Stain (Life Technologies<sup>TM</sup>) according to the manufacturer's instructions.

## 2.7 Cell quantification using high-throughput flow cytometry

Cells were quantified using flow cytometry as previously described [25], by analyzing a defined sample volume. Thereby, the number of counted events can be correlated with the cell concentration by least squares linear regression. Flow cytometry was performed using a LSR Fortessa from BD Bioscience equipped with a BD<sup>TM</sup> High Throughput Sampler (HTS). The high throughput sampler was operated at the following settings: sample flow rate: 3 μL/s, sample volume: 100 μL, mixing volume: 100 μL, mixing speed: 200 μL/s, and four mixing cycles.

## 2.8 Liquid-handling calibration

Liquid-handling calibration was performed for all stock solutions as described previously [6]. For each stock solution 12 different volumes were pipetted onto the analytical balance

in octuplicates. Pipetting parameters were optimized until an  $r^2$  of  $> 0.999$  was reached, residuals were evenly distributed and deviated less than 3.5% from the nominal volume. Variation coefficients were below 1.6% for aqueous solutions and below 2% for the viscous polymer solutions (**Table A1**).

## 2.9 HT–binodal and tie–line determination

Manual and HTS–based binodal determination was performed using a cloud point approach that has previously been established in our group [6,26]. ATPS were prepared with increasing PEG and dextran concentrations in 0.25% (w/w) steps in 1.3 mL deep well plates. After an initial mixing step (1,300 rpm, 8 min) using the integrated orbital shaker, phase separation was determined by visual inspection. The curve was fitted as described before [27,28] using least square regression. Tie–lines were determined by measuring the phase volumes of a set of ATPS with increasing distance from the binodal. Tie–lines were then calculated using the lever arm rule as described before [26]. Tie–line length (TLL) and tie–line slope (STL) were determined based on concentration differences of the phase–forming polymers in top and bottom phase as described before [20,21].

## 2.10 Automated high–throughput screening of cell partitioning in aqueous two–phase systems

The automated high–throughput method was modified from Oelmeier *et al.* [6]. The entire high–throughput screening was performed on a Tecan Freedom Evo<sup>®</sup> 200 liquid–handling station (LHS), and sample plates were transferred to the HT–sampler of the BD LSR Fortessa for cell quantification and analysis. The LHS is equipped with an 8–port liquid–handling arm (LiHa), a standard robotic plate handling arm (RoMa) equipped with a centric gripper, an integrated centrifuge (Rotana 46RSC, Hettich), a rotational shaker (Te–shake<sup>™</sup>, Tecan), a 96–channel liquid–handling arm (MultiChannelArm<sup>™</sup> (MCA 96), Tecan) with an eccentric gripper, and an integrated spectrophotometer (Infinite<sup>®</sup> M200 Pro, Tecan).

ATPS were prepared in a 1.3 mL 96–well plate with a total volume of 637  $\mu\text{L}$ . After a first mixing step (1,300 rpm, 8 min), the plate was centrifuged (4,000 rpm, 20 min) to achieve phase separation. An intermediate mixing step was performed (1,300 rpm, 5 min), to reduce shear stress on the cells, before the cells were resuspended (3 cycles, aspiration volume: 50% of total volume, pipetting speed: 182  $\mu\text{L}/\text{s}$ , aspiration position: well bottom, dispense position: liquid surface) and added to the ATPS ( $5 \times 10^5$  cells per well in 13  $\mu\text{L}$  PBS). Subsequently, a final mixing step was performed (1,300 rpm, 2 min) and phase separation was achieved by settling (30 min, RT). A set of internal standards containing a defined cell number were included in each experiment. After phase separation, samples of both phases were taken and diluted 5–fold in staining buffer. Sampling was performed as described by [6], with the following exception: a delay of 5 s and a retraction speed of 10 mm/s were used during bottom phase sampling. The optimized pipetting parameters are summarized in **Table A2**. Prior to all cell handling steps, a partitioning volume of 100  $\mu\text{L}$  PBS was aspirated followed by an air gap, to protect the cells from contaminations with system liquid (deionized water).

---

## 2.11 Statistical data analysis

Screening data were pre-processed by excluding values below the detection limit. We showed that  $1.25 \times 10^2 - 5 \times 10^5$  events per  $100 \mu\text{L}$  of a labeled cell type can be quantified without bias in a cell mixture (**Figure 2g**). The detection limit was thus chosen accordingly. Outliers occur randomly in automated liquid-handling and are typically due to technical issues, such as the aspiration of air bubbles. To identify outliers above the detection limit, the modified  $z$ -score was applied with a  $z$ -score of  $>3.5$  considered significant [29,30]. To determine differences in means, a two-sided Student's  $t$ -test was performed, provided that equal variances could be asserted by an  $F$ -test. To determine significant differences between multiple means one-way analysis of variances (ANOVA) was performed, provided that equal variances could be asserted by a Levene-test. Error propagation was considered in all analyses [31]. Unless stated otherwise,  $n$  represents the number of technical replicates.

## 3 Results & Discussion

### 3.1 HTS-development and validation

We developed a fully automated screening set-up that integrates cell partitioning in ATPS on a Tecan LHS and cell quantification and analysis at the single cell level using HT-flow cytometry. Briefly, ATPS are prepared, and cells are added from a concentrated stock solution. After mixing and phase separation, samples are taken from top and bottom phase, diluted, and stained with specific antibodies to discriminate between the respective cell populations (**Fig. 1**). A major concern in ATPS research is the lack of reproducibility [32]. As shown in previous studies [6], liquid handling calibration is essential to enable accurate and precise liquid handling, and was thus performed for all stock solutions (**Table A1**). For automated liquid-handling of cells, resuspension steps were implemented and validated regarding accuracy and precision of transferred cell numbers, and cell viability. With optimized resuspension settings, accurate cell numbers could be transferred in a volume of 13  $\mu\text{L}$  over several resuspension cycles with good precision ( $\text{CV} \leq 7\%$ ). Cell viability was  $> 94\%$  and not significantly decreased compared to manual resuspension over 6 resuspension cycles ( $p > 0.05$ ) (**Fig. 2a & 2b**).

Sampling of top and bottom phase was performed as shown in previous work [6], and pipetting parameters were optimized with regard to precision, accuracy, and carry-over (**Table A2 & A3**). Using these pipetting parameters, we obtained variation coefficients of  $< 2.1\%$  for top phase sampling and  $< 1.63\%$  for bottom phase sampling. With a series of spiking experiments, we showed that there is no detectable carry-over during bottom phase sampling (**Fig. 2c**).

One of the most critical parameters in HTS-applications for ATPS research is sufficient mixing of the viscous polymer solutions which has thus been intensively investigated in our group [6,26]. We established that adequate mixing is possible for PEG-phosphate ATPS with the here described setup. It has been shown that the interfacial tension and viscosity are the main parameters influencing mixing efficiency [26]. Since the interfacial tension of PEG-dextran ATPS is very low ( $1\text{--}100 \mu\text{J}/\text{m}^2$ ) compared to other types of two-phase systems [33,34] the only limiting factor might be the comparably high viscosity of the polymers. We thus evaluated whether sufficient mixing is possible for different TLL of PEG-dextran ATPS by evaluating if the dye methyl violet is distributed homogeneously in the sample. We showed that 8 minutes mixing time is sufficient to achieve homogeneous dye distribution even at high TLL (**Fig. 2d & 2e**). In analogy to previous experiments [26], we evaluated whether the same partitioning coefficients for methyl violet are obtained when shaking on an orbital shaker and on an over-head shaker. The experiment was performed at intermediate and long tie-lines, representing high viscosities. No significant difference between partitioning coefficients was observed, and variation coefficients of the determined partitioning coefficients were below 5% (**Fig. 2f**). We thus concluded that sufficient mixing is possible under the same conditions as published before [6].

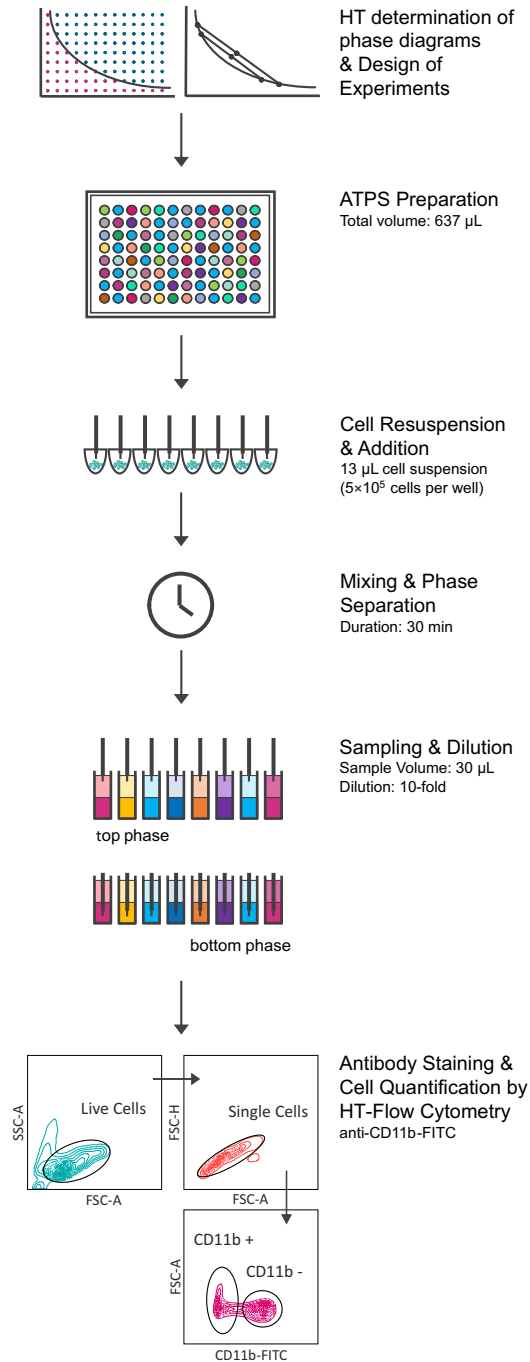


**Figure 1:** Overview of the developed HTS-platform. After phase diagrams are determined in high-throughput, ATPS are selected for the screening. ATPS are prepared in deep-well plates, and cells are added from a concentrated stock solution, after resuspension. After mixing and phase separation, samples are taken from top and bottom phase, diluted, and stained with an anti-CD11b-FITC antibody to discriminate between the two cell populations. FSC-A: forward scatter peak area, SSC-A: side scatter peak area, FSC-H: Forward scatter peak height.

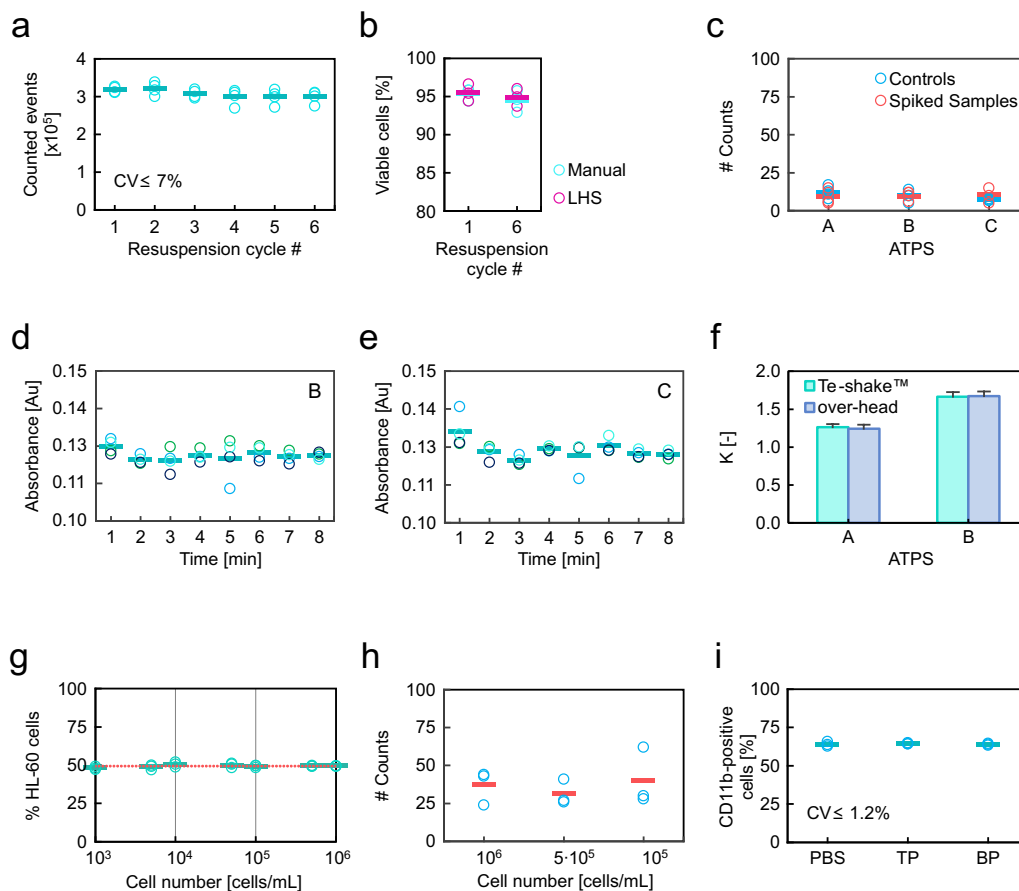


**Figure 2:** HTS development and validation. (a–b) Evaluation of cell resuspension efficiency and impact on cell viability. (a) Transferred cell numbers over six resuspension cycles ( $n=4$ ). One-way ANOVA showed no significant differences between mean transferred cell numbers ( $p > 0.05$ ). (b) Influence of cell resuspension on cell viability. The percentage of viable cells was determined over six resuspension cycles and compared to manual resuspension ( $n=3$ ). One-way ANOVA showed no significant changes in cell viability ( $p > 0.05$ ). (c) Evaluation of carry-over during bottom phase sampling. Top phase, spiked with  $5 \times 10^5$  CellTracker™ Orange CMRA stained HL-60 cells, was carefully layered on top of an equal volume of bottom phase and sampling was performed on the LHS ( $n=4$ ). Student's  $t$ -test showed no significant differences between spiked samples and controls ( $p > 0.05$ ). ATPS: A: 4/4; B: 4/5; C: 5/7 % (w/w) PEG 8,000/ dextran 500,000 in 0.11 M NaPi, pH 7.4. (d – f) Evaluation of mixing efficiency. (d – e) Dye distribution over shaking time.  $13 \mu\text{L}$  methyl violet stock solution was layered on top of ATPS B & C (see above), and the plate was shaken for 8 min on the integrated orbital shaker (shaking orbit: 3 mm, rotational speed: 1,300 rpm). Samples were taken every 60 s from the bottom of the well and 10-fold diluted with water, using the LHS. Dye concentrations were determined by absorbance measurement at 580 nm ( $n=4$ ). (f) Partitioning coefficients ( $K$ ) of methyl violet for different mixing modes. ATPS with different TLL were prepared on the LHS, methyl violet was added, and plates were mixed on an orbital shaker for 8 min or on an over-head shaker for 10 min (shaking radius: 100 mm, shaking speed: 40 rpm). Partitioning coefficients ( $K$ ) represent the ratio of dye concentrations between top and bottom phase. Variation coefficients of  $K$ -values were below 5%. Data show mean values + s.d. ( $n=8$ ). Student's  $t$ -test showed no significant differences between partitioning coefficients in dependence of the mixing mode ( $p > 0.05$ ). (g – h) Influence of cell number on multiplexed cell quantification & well-to-well carry-over during HT-flow cytometry. (g) Quantification of a mixture of HL-60 and L929 cells. HL-60 cells were stained with CellTracker™ Orange CMRA and mixed with L929 cells. A dilution series was prepared ( $1 \times 10^3$  -  $1 \times 10^6$  cells per mL) and quantified by HT-flow cytometry ( $n=3$ ). Statistical analysis (one-way ANOVA) of the ratio between HL-60 and L929 showed no significant changes over the entire calibration range ( $p > 0.05$ ).

---

**Figure 2:** (*continued*) (h) Well-to-well carry-over in HT-flow cytometry. Wells containing staining buffer were measured directly after wells containing  $10^5 - 10^6$  cells per mL ( $n=3$ ). (i) Influence of ATPS components on antibody staining using no-wash staining protocols for HT-flow cytometry. Robustness of antibody staining was investigated using an anti-CD11b-FITC antibody. After brief incubation in top (TP) and bottom phase (BP) of ATPS B (see above), the differentiated HL-60 cells were stained and the percentage of differentiated HL-60 cells was determined by flow cytometry ( $n=3$ ). Student's  $t$ -test showed no significant influence of the polymers on the detection of differentiated HL-60 cells ( $p>0.05$ ). Bars represent means. CV: coefficient of variation.

### 3.2 Implementation of no-wash staining protocols and high-throughput cell quantification

The easiest and most robust way to analyze and quantify cells after partitioning in ATPS is the use of no-wash staining protocols for flow cytometry. Since the polymer solutions have comparably high densities, cell sedimentation by centrifugation can be challenging. In order to keep the screening as robust and versatile as possible, we established no-wash staining protocols.

In previous work [25], we showed that flow cytometry is an excellent tool for cell quantification and shows high sensitivity, robustness, and a broad working range ( $>3$  orders of magnitude). Moreover, we showed that the presence of different salts and polymers ( $\leq 2\%$  (w/w)) did not significantly influence cell quantification. In the present work, we showed that the enumeration of a HL-60 and L929 cells in a mixture of both cell lines was not biased over the entire calibration range (**Fig. 2g**), and without significant well-to-well carry-over, which was determined by analyzing wells containing staining buffer directly after wells containing defined cell numbers. The number of counted events was well below the detection limit of 100 events, independent of the cell number (**Fig. 2h**). Likewise, we showed that antibody staining is not altered in the presence of low polymer concentrations when no-wash protocols are used (**Fig. 2i**). Overall pipetting accuracy was evaluated for each screening by including PBS controls that did not contain phase forming polymers. In average the variation coefficients of counted cell numbers were in the range of 5 to 6% ( $n=8$ ) demonstrating excellent overall pipetting accuracy, and cell viability was  $\geq 92\%$  in all experiments, which was determined by HT-flow cytometry at the end of each screening based on forward (FSC) and side scatter signal (SSC) analysis (**Fig.1**).

### 3.3 Characterization of PEG-dextran ATPS

The ATPS used in this work consisted of PEG 8,000 and dextran 500,000, buffered with isotonic concentrations of NaPi and NaCl. These conditions were chosen as they are well described in literature. Phase diagrams were determined using a HT-approach, to select suitable screening ranges. The binodal was determined by titration of the two polymers, since turbidity occurs when polymer concentrations are within the two-phase region (**Fig. 3a, top**). Tie-lines were determined from the volume ratio of top and bottom phase by applying the lever-arm rule (**Fig. 3a, bottom**). To validate the HTS-based method, the binodal of PEG 8,000 and dextran 500,000 was compared with a dataset determined manually by cloud-point titration [6], and data from literature [35].

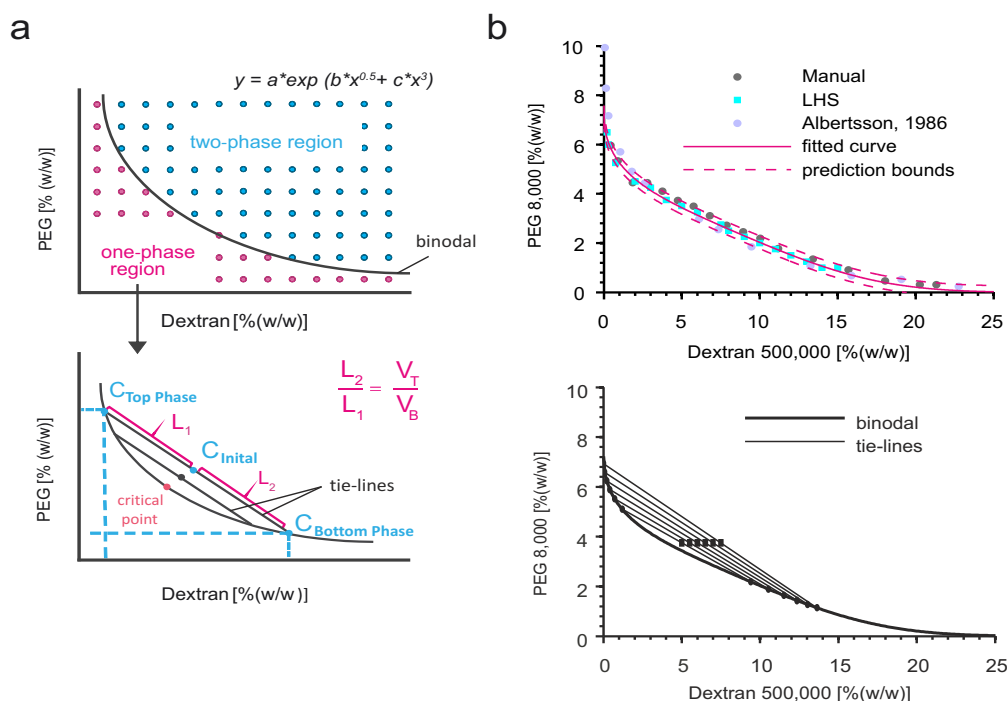


**Figure 3:** Determination of phase diagrams of polymer–polymer ATPS. (a) HT–method for determination of binodals. Binodals are constructed by preparing increasing concentrations of the phase forming polymers on the Tecan LHS. After shaking, the binodal can be determined by turbidity analysis. The binodal is then fitted to equation 1 using least–square regression. Tie–lines are determined using the lever–arm rule, which states that the volume ratio of top and bottom phase ( $V_T/V_B$ ) equals the distance ratio ( $L_2/L_1$ ) between the initial system point and the intersects between tie–line and binodal. ATPS are prepared at distinct points above the binodal and volume ratios of top and bottom phase are measured. (b) Binodal and tie–line data of PEG 8,000–dextran 500,000. Data sets determined by HTS and manual titration were compared to data published by Albertsson *et al.*, 1986 (top panel). The fitted curve was calculated based on HTS–data. Dashed lines represent 95% prediction bounds of the fit. The following coefficients of equation 1 were calculated: a: 7.23 (6.98, 7.48), b: -0.318 (-0.344, -0.292), c: -0.00027 (-0.00032, -0.00021), with a Pearson  $r^2$  of 0.996. 95% prediction bounds of the fit coefficients are shown in parentheses. Tie–lines are shown in the bottom panel.

The HTS–dataset was fitted to equation 1, as described by Merchuk [27].

$$y = a \times e^{(b \times x^{0.5} + c \times x^3)} \quad (1)$$

As shown in **Fig. 3b**, we found an excellent congruence between the three data sets. Both, the dataset determined by manual titration and the dataset from literature were found within the 95%–confidence interval of the HTS–dataset. We only observed slight deviations of the dataset determined by Albertsson, 1986, at very low dextran concentrations. This is due to missing data points in the HTS–dataset at very low concentrations. At very low concentration of either polymers, visual discrimination between one and two–phase region becomes increasingly difficult. Nonetheless, shape and location of the binodal could be determined with good accuracy. In addition TLL, tie–line slopes (STL), and phase compositions determined here, were in excellent agreement with literature data. As shown before [35–37], tie–line slope increased slightly with increasing TLL. Phase compositions of the ATPS used in this work are summarized in **Table 1**. In addition, the influence of physiological concentrations of phosphate and NaCl was investigated, since even low salt concentrations have been shown to alter shape and position of binodal and tie–lines. As described by Walter [21], the addition of physiological concentrations of phosphate results in a minor shift of the binodal towards lower polymer concentrations, while NaCl did not alter shape or location of the binodal (data not shown). The influence on TLL was however minimal which was in excellent agreement with literature data [21]. The physicochemical properties of ATPS are highly dependent on the TLL. With increasing TLL, the polymer concentration in the respective phase increases, along with the densities. At the same time, the concentration and density difference, as well as the interfacial tension between the phases increases [34]. Thus, determination of phase diagrams is essential to develop downstream processing strategies using ATPS.

**Table 1:** Summary of phase compositions, tie–line lengths (TLL), and slope of tie–line (STL) at RT.

Total system composition		Bottom phase composition		Top phase composition		TLL	STL
PEG	dextran	PEG	dextran	PEG	dextran		
[%(w/w)]	[%(w/w)]	[%(w/w)]	[%(w/w)]	[%(w/w)]	[%(w/w)]	[%(w/w)]	
4	4	2.3	8.8	4.7	1.9	7.3	–0.35
4	5	1.8	11.0	5.5	1.0	10.7	–0.37
5	7	0.5	17.8	7.9	0.00045	19.3	–0.41

### 3.4 Separation of HL-60 cells after partial granulocytic differentiation

The aim of this first case study was to investigate the influence of TLL, salt composition, and pH on the resolution of partially differentiated HL-60 cells, and we screened for ATPS compositions that are capable of separating undifferentiated and differentiated HL-60 cells. The promyelocytic cell line HL-60 can be differentiated towards granulocytes by DMSO treatment. The differentiation is accompanied by changes in cell morphology, growth rate, and cell-surface antigen expression [38,39]. As cells enter the granulocytic differentiation pathway, proliferation is dramatically decreased [38], which was shown by monitoring cell growth and viability over the differentiation period (**Fig. 4**). In addition, DMSO-mediated differentiation results in increased granularity and decreased cell size, which is represented by a decrease of forward and side scatter signal (**Fig. 4a**). In addition, we analyzed CD11b-expression, which is upregulated after the promyelocytic stage (**Fig. 4b**). The differentiation efficiency was typically between 40 and 60%, which is ideal for separation studies, as we have two distinct cell populations in similar quantities. In our screenings we analyzed CD11b-expression to discriminate between the two cell populations. It is well established that ATPS are an excellent tool to separate cells according to differences in physicochemical cell surface properties, i.e. cell surface charge and membrane lipid composition [21,35]. The multitude of morphological and functional changes during differentiation of HL-60 cells can thus be exploited for ATPS-mediated cell separation.

In contrast to smaller biomolecules such as proteins and nucleic acids, cells partition between one of the bulk phases, i.e. top or bottom phase, and the interface, depending on the ATPS composition. The interfacial tension, and thus the TLL, plays a major role in cell partitioning in ATPS, since the interfacial tension acts to minimize the interfacial area. The adsorption of cells and other particles to the interface reduces the interfacial area, and thus the total free energy of the system. As a consequence, partitioning into either phase can only take place when the interaction with the cell surface is strong enough to "pull" the cells out of the interface. The higher the interfacial tension, the stronger interactions are required to enable partitioning to either of the bulk phases [21,34]. To date, two main factors in ATPS-mediated cell separation have been identified: surface charge and membrane lipid composition, and cell separation based on these factors can be achieved in dependence of the salt composition. Salts with polyvalent anions, e.g. phosphate, have a higher affinity for the dextran-rich bottom phase, while salts of halides, for example NaCl, partition equally between the phases. Unequal partitioning of a salt results in an interfacial electrostatic potential difference (Donnan potential), and molecules partition according to their charge in such ATPS [21,40-42]. At moderate interfacial tensions cells can thus be separated based on differences in surface charge in PEG-dextran ATPS containing phosphate (charge-dependent partitioning). Since cells have a negative net surface charge, they partition into the top phase in ATPS containing phosphate [20,42]. Further, cell partitioning according to membrane lipid-composition can be achieved in ATPS with low interfacial tension, i.e. close to the critical point, containing salts that partition equally between the two phases (charge-independent partitioning) [43].

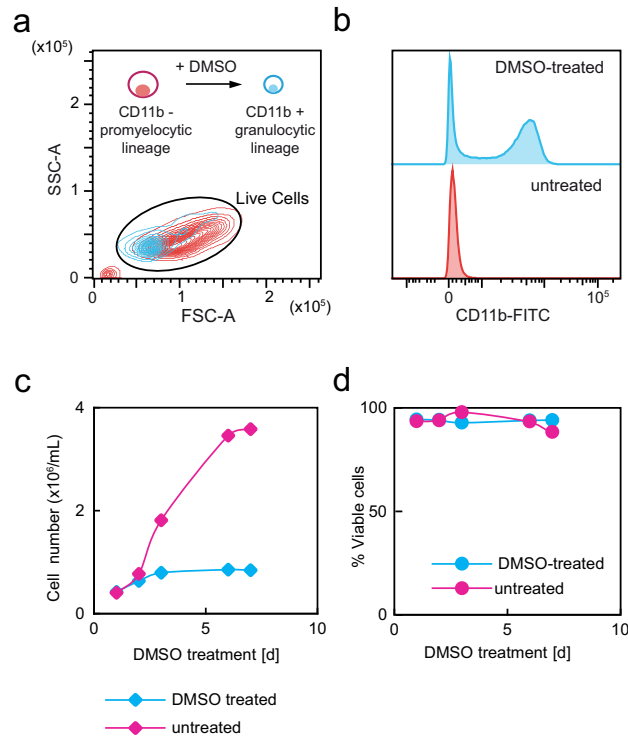


**Figure 4:** Granulocytic differentiation of the promyelocytic cell line HL-60. HL-60 cells were differentiated towards granulocytes by DMSO-treatment. Differentiation was assessed by flow cytometric analysis of cell morphology and cell-surface antigen expression after 7 days of DMSO-treatment. (a) DMSO-mediated differentiation towards cell types of the granulocytic lineage results in increased granularity and decreased cell size, represented by a decrease of forward (FSC) and side scatter (SSC) signal. (b) Discrimination between undifferentiated and differentiated HL-60 cells was performed by analysis of CD11b-expression which is up-regulated after the promyelocytic stage. (c – d) Proliferation and cell viability during DMSO-mediated granulocytic differentiation. (c) Growth curves and (d) viability of untreated and DMSO treated HL-60 cells over seven days. Cell numbers and viability were determined by trypan blue staining using a hemocytometer.

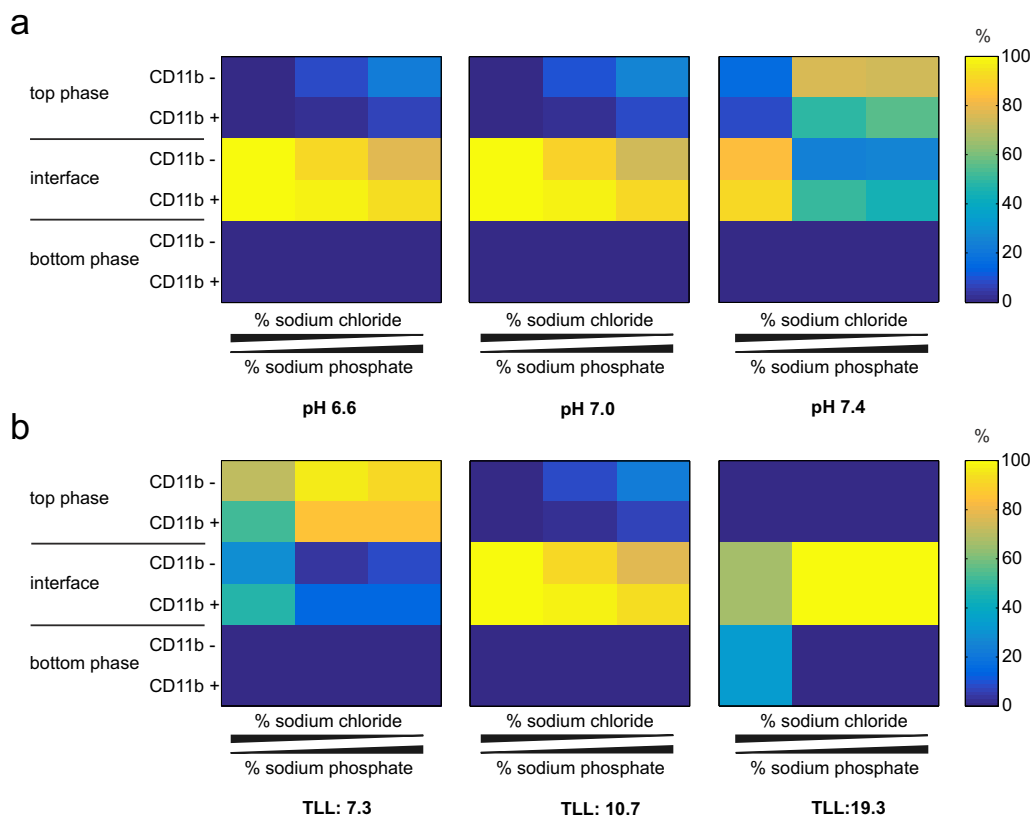


**Figure 5:** HT-partitioning analysis of CD11b-positive and CD11b-negative HL-60 cells in charge-sensitive ATPS in dependence of salt composition, pH and TLL, after DMSO-mediated differentiation. Cell partitioning was analyzed in PEG 8,000-dextran 500,000 ATPS with varying ratios of NaPi and NaCl. While the overall salt concentration was kept at isotonic concentrations, the molar ratio of NaPi and NaCl was varied (50%, 65%, 100% mM NaPi). (a) At an intermediate TLL of 10.7 (4% PEG, 5% dextran) at pH 6.6, 7.0, and 7.4, and (b) at three different TLL (4% PEG, 4% dextran; 4% PEG, 5% dextran; 5% PEG, 7% dextran) at pH 6.6. Heat maps represent the mean percentage of live cells in each phase (n=4).

Stendahl *et al.* investigated the changes in hydrophobic surface properties of HL-60 cells during DMSO-mediated differentiation [44]. They showed that DMSO-treated HL-60 cells have a higher affinity to the top phase in charge-insensitive PEG-dextran ATPS. In analogy to these studies we investigated charge-independent partitioning of differentiated HL-60 cells (4% PEG 8,000, 4% dextran 500,000, in 0.14 M NaCl) and detected 6.5% (2.6%) and 13.7% (4.9%) (mean (s.d.), n=4) of total CD11b-negative and CD11b-positive HL-60 cells in the top phase, respectively. In addition, we determined the fold change of the percentage of CD11b-positive HL-60 cells in the top phase (TP) compared to the PBS control (C) using equation 2.

$$fold\ change = \frac{\%CD11b - positive\ cells_{TP}}{\%CD11b - positive\ cells_C} \quad (2)$$

Fold enrichment of CD11b-positive HL-60 cells in the top phase (1.30 (0.03) (mean (s.d.), n=4)) was highly significant ( $p < 0.001$ ) and in excellent agreement with literature [44]. We further studied changes in charge-associated surface properties of HL-60 cells by investigating the resolution of CD11b-positive and CD11b-negative HL-60 cells after DMSO-mediated differentiation in charge-sensitive ATPS, in dependence of TLL, salt composition, and pH. We chose ATPS with varying ratios of phosphate and NaCl, at isotonic concentrations, at three different TLL and different pH-values. ATPS-compositions are summarized in **Table A4**, and the results of this study are summarized in **Fig. 5**. At intermediate TLL of 10.7% (w/w), the cells partitioned increasingly to the top phase with increasing phosphate concentration, and we observed resolution of the two cell populations according to their surface charge. We found that CD11b-negative HL-60 cells have lower net surface-charge than CD11b-positive HL-60 cells, and consequently lower partitioning ratios in charge-sensitive ATPS (**Fig. 5a**). We further observed a slight pH-dependence, with increasing cell partitioning to the top phase with increasing pH (**Fig. 5a**). This is most likely due to an increase in the ratio of di- to mono-basic phosphate [21,35]. Since the electrostatic potential difference increases with increasing TLL, we observed excellent resolution of CD11b-positive and CD11b-negative HL-60 cells at high phosphate concentrations at intermediate TLL (**Fig. 5b, middle**), but less close to the critical point (**Fig. 5b, right**). Even though the electrostatic potential difference increases with increasing TLL we observed no partitioning into the top phase at long TLL of 19.3% (w/w). This is due to the fact that at some distance from the critical point, the increase in interfacial tension offsets the increase in electrostatic potential difference [21]. At high phosphate concentrations both cell populations thus accumulated at the interface. With decreasing phosphate concentrations, however, we observed increased partitioning into the bottom phase and we did not observe differences in partitioning of CD11b-positive and CD11b-negative HL-60 cells at higher TLL (**Fig. 5b, left**). In summary, differences in partitioning varied with TLL and phosphate concentration, and can be selected accordingly for multi-step separations. The observed trends were in excellent agreement with literature data [21,35]. To select ATPS that enable maximal resolution in a multi-stage purification process, we calculated partitioning ratios (K), and the quotient of the partitioning ratios of CD11b-negative and CD11b-positive HL-60 cells (Q):

$$K = \frac{P}{I} \quad (3)$$

$$Q = \frac{K_{\text{CD11b-negative}}}{K_{\text{CD11b-positive}}} \quad (4)$$

where  $P$  represents the fraction of cells in the top phase and  $I$  the fraction of cells at the interface. We investigated  $Q$  in dependence of  $K$  to select ATPS that give maximal resolution (**Fig. 6a**). We were able to obtain partitioning ratios over more than two orders of magnitude and  $Q$ -values of up to 5. This type of plot provides a simple means to select systems with maximal differences in partitioning ratios at different  $K$ -values.

Countercurrent distribution (CCD) is a well-established method in liquid-liquid extraction and has been successfully used in cell separation [21,23]. In CCD the top phase is transferred stepwise, while the bottom phase is retained. After transfer of the top phase, the ATPS are mixed and allowed to separate by gravity. Depending on the application, the interface can either be transferred or retained. As cells partition between either of the bulk phases and the interface, the interface is retained when cells partition between top phase and interface, and transferred when the cells partition between interface and bottom phase. Cells that partition largely into the top phase, thus, move faster through the CCD-device than cells that partition largely to the interface, which enables separation (**Fig. 6b**). Based on the data shown in **Fig. 6a**, CCD-curves can be predicted by applying equation (5) [21]:

$$F(r) = \frac{n!}{r!(n-r)!} P^r (1-P)^{n-r} \quad (5)$$

where  $F$  represents the fraction of the total cell population appearing in each theoretical cavity ( $r$ ) of the CCD-apparatus, and  $n$  represents the total number of transfers. We chose four conditions with different  $K$ -values and the corresponding highest  $Q$ -value (**Fig. 6a**), and calculated theoretical CCD-experiments with 30 and 60 transfers, based on the respective  $P$ -values of CD11b-positive and CD11b-negative cells (**Fig. 6c**).

Our data show that  $K$ -values around 1 enable optimal resolution of CD11b-positive and CD11b-negative HL-60 cells by CCD. As described before, CCD-curves are skewed at very high and very low  $K$ -values, and resolution is decreased, with the exception of ATPS, where 100% of the target cell type and <100% of the contaminants are found in one of the phases [21]. In this case excellent purities and yields can be obtained, since contaminants can be washed out with minimal loss of target cells. Maximal resolution of CD11b-negative and CD11b-positive HL-60 cells can be obtained by using ATPS 3 in a CCD-experiment. The modeling data indicate that complete peak separation is possible when performing 60 transfers, and > 99.9% of CD11b-positive HL-60 cells can be recovered with > 99% purity. Even with 30 transfers, more than 93% yield at > 99% purity is possible, reducing the processing time by half. Further optimization of separation conditions at TLL between 7 and 11, at salt ratios between 70 and 100% sodium

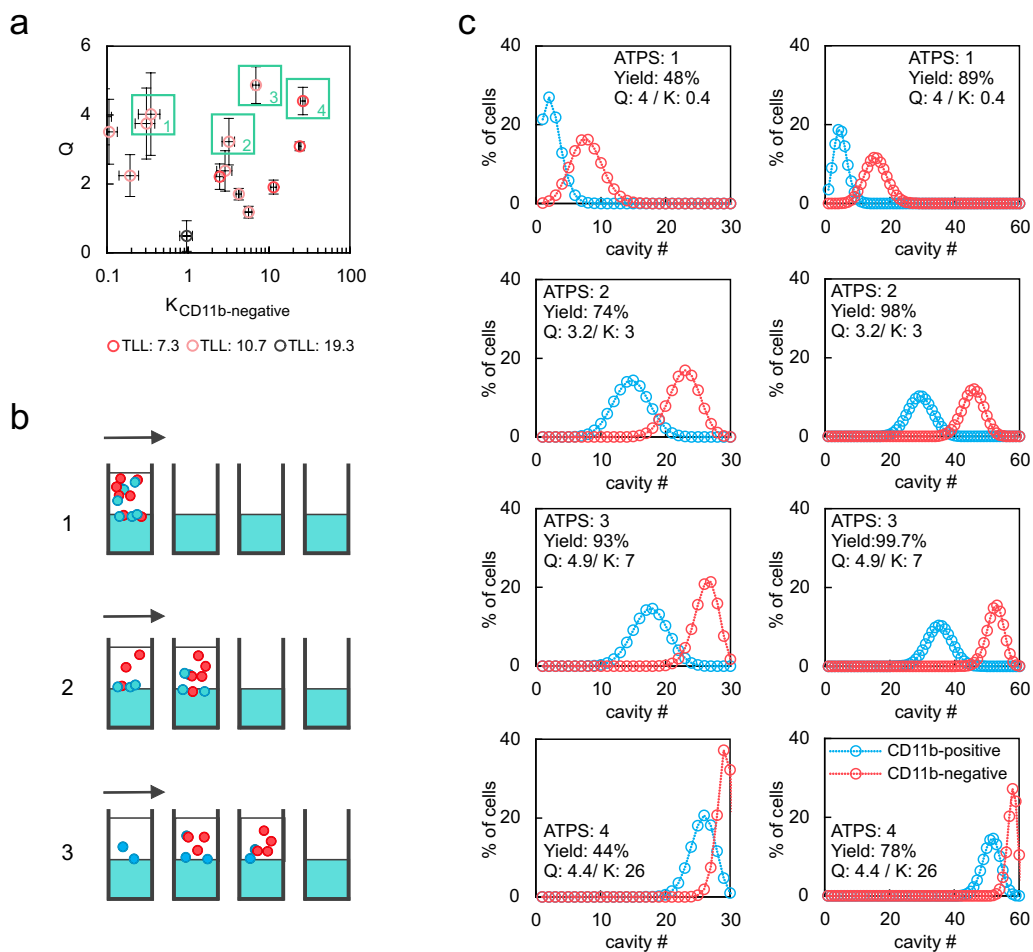


**Figure 6:** Selection of separation conditions for CD11b-negative and CD11b-positive HL-60 cells based on CCD-modeling. **(a)** The partitioning ratio of CD11b-negative cells ( $K_{CD11b\text{-negative}}$ ) was plotted against the quotient of the partitioning ratios of CD11b-negative and CD11b-positive HL-60 cells ( $Q$ ) obtained from the data shown in Fig. 4. Systems selected for the calculation of CCD-curves are indicated and numbered. ATPS 1-3: 4% PEG, 5% dextran, with ATPS 1: 70% NaPi, pH 7.0, ATPS 2: 70% NaPi, pH 7.4; ATPS 3: 100% NaPi, pH 7.4, and ATPS 4: 4% PEG, 4% dextran, 50% NaPi, pH 6.6. Data show mean values  $\pm$  s.d. ( $n=4$ ). **(b)** Scheme of the CCD-principle for ATPS in which cells partition between top phase and interface. The top phase is transferred stepwise. Between the transfers ATPS are mixed and phases are separated by gravity. Blue and red circles represent two cell types. The cell type represented by the blue circles has a higher partitioning ratio than the cell type represented by the red circles. **(c)** CCD-model with 30 (left panel) and 60 (right panel) theoretical transfers for the four ATPS indicated in (a). Theoretical yields of CD11b-positive HL-60 cells were calculated for a target purity of  $> 99\%$ .

phosphate and at pH-values between 7.0 and 7.5, could result in separation conditions where complete separation can be obtained with even fewer number of transfers.

After identifying ATPS with maximal possible resolution at a given number of transfers, resolution vs. processing time can be modeled and final purification conditions can be chosen for a specific purification task. It should be noted that partitioning ratios of cells are highly dependent on vessel geometry, fill volume, mixing efficiency, and phase separation time. Thus, these conditions need to be identical in batch- and CCD-experiments, otherwise predicted CCD-curves will not be accurate [21]. The strength of the here described HTS-platform is that it is extremely versatile and applicable for most labware types, which enables direct optimization of all these parameters in high-throughput.

Depending on target yield and purity, as well as maximal processing time for a specific application, separation conditions can be further optimized by varying salt concentrations, pH, and TLL. The analysis of additional factors such as polymer molecular weight and the investigation of a variety of salts, additives, and polymers, will enable us to identify the main factors influencing cell separation in ATPS. Such large and systematic screenings combined with CCD-modeling will enable fast and directed development of purification strategies for cell based-products.

### 3.5 Influence of polymers on viability and functionality

PEG-dextran ATPS are generally regarded to offer physiological conditions for cell purification [21], and both polymers are used in many medical applications. However, PEG and dextran have also been associated with cell fusion, and effects on live cells are not fully characterized [21,45,46]. Therefore, the polymers might have adverse effects on certain cell types or under certain conditions, which needs to be evaluated, respectively.

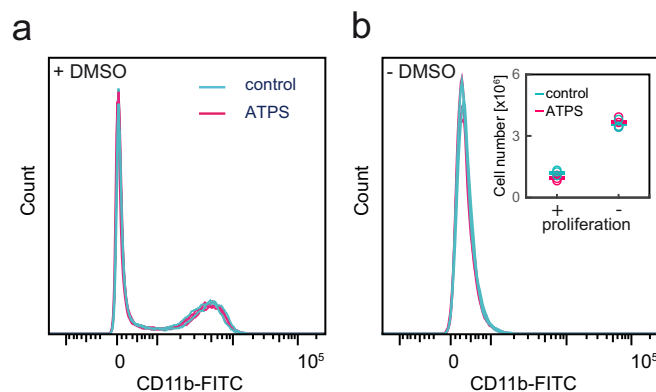


**Figure 7:** Influence of PEG and dextran on cell proliferation and granulocytic differentiation. HL-60 cells were added to an ATPS containing 5% dextran 500,000, 4% PEG 8,000, and 0.14 M NaCl, and incubated for 30 min at room temperature (red). Control cells (blue) were untreated. After washing the cells with PBS, 50% of the cells were resuspended in differentiation medium (a) and 50% in culture medium (b). After culturing the cells for seven days, flow cytometric analysis of CD11b-expression was performed as described. The histograms show overlays of treated samples and controls. The experiment was performed in biological triplicates. Proliferation was analyzed by determining the number of viable cells after the culture period. Bars represent mean values (n=3 biological replicates). Statistical analysis (Student's *t*-test) of viable cell numbers and percentage of CD11b-positive cells showed no significant differences between cells incubated in ATPS and PBS controls ( $p > 0.05$ ).

---

Since differentiation of HL-60 cells is triggered by relatively unspecific factors, such as the presence of polar solvents, they are an excellent model to evaluate potential adverse effect of PEG-dextran ATPS on functionality and viability. Changes in membrane permeability, caused by the presence of the polymers is likely to induce differentiation or cell death. We thus evaluated if viability and differentiability of HL-60 cells is influenced after ATPS-treatment, or if differentiation is induced. Investigation of cell growth, differentiability and differentiation stage was not significantly ( $p > 0.05$ ) altered compared to untreated cells (**Fig. 7**). These results indicate that cell purification in ATPS does not interfere with cell viability and functionality. However, more comprehensive studies will have to be performed to confirm this assumption.

## 4 Conclusion & Outlook

We have developed and validated an automated robotic screening that enables HT-cell partitioning analysis in ATPS. We demonstrated that this setup enables fast and systematic investigation of factors influencing cell partitioning. We further showed that CCD-models can be used to design purification processes based on screening data, and we successfully designed a purification process for CD11b-positive HL-60 cells. Due to the versatility of Tecan LHS, the screening platform can easily be adapted to countless applications. Up- and downscaling can be performed by simply changing the labware type, and the influence of settling time, mixing intensity, fill volume, and vessel geometry can be studied. This enables the simultaneous optimization of multiple parameters for purification in a CCD-device. Likewise, numerous analytical methods, such as various PCR-techniques, ELISAs, and high-content screening can be directly integrated in the screening process. The use of design of experiments (DoE) will enable us to simultaneously investigate the effects of numerous parameters, and optimize separation conditions for various applications. Future exploitation of this platform will, thus, enable us to gain a more detailed understanding of the mechanisms underlying cell partitioning in ATPS. We expect that this technology will facilitate faster, cheaper, and more directed downstream process development for cell-based therapeutics.

## 5 References

- [1] R.P. Hertzberg, A.J. Pope, High-throughput screening: new technology for the 21st century., *Curr. Opin. Chem. Biol.* 4 (2000) 445–51.
- [2] R. Macarron, M.N. Banks, D. Bojanic, D.J. Burns, D.A. Cirovic, T. Garyantes, et al., Impact of high-throughput screening in biomedical research., *Nat. Rev. Drug Discov.* 10 (2011) 188–95.
- [3] L.M. Mayr, D. Bojanic, Novel trends in high-throughput screening, *Curr. Opin. Pharmacol.* 9 (2009) 580–588.
- [4] K.M. Łacki, High throughput process development in biomanufacturing, *Curr. Opin. Chem. Eng.* 6 (2014) 25–32.
- [5] M. Wiendahl, S.A. Oelmeier, F. Dimer, J. Hubbuch, High-throughput screening-based selection and scale-up of aqueous two-phase systems for pDNA purification., *J. Sep. Sci.* 35 (2012) 3197–207.
- [6] S.A. Oelmeier, F. Dimer, J. Hubbuch, Application of an aqueous two-phase systems high-throughput screening method to evaluate mAb HCP separation., *Biotechnol. Bioeng.* 108 (2011) 69–81.
- [7] S.A. Oelmeier, C. Ladd Effio, J. Hubbuch, High throughput screening based selection of phases for aqueous two-phase system-centrifugal partitioning chromatography of monoclonal antibodies., *J. Chromatogr. A.* 1252 (2012) 104–14.
- [8] Y. Zang, B. Kammerer, M. Eisenkolb, K. Lohr, H. Kiefer, Towards protein crystallization as a process step in downstream processing of therapeutic antibodies: screening and optimization at microbatch scale., *PLoS One.* 6 (2011) e25282.
- [9] J. Welsh, Pushing the limits of high-throughput chromatography process development: current state and future directions, *Biopharmaceutical Bioprocess.* 3 (2015) 1–3.
- [10] K.M. Łacki, High-throughput process development of chromatography steps: advantages and limitations of different formats used, *Biotechnol. J.* 70 (2012) 1192–1202.
- [11] K. Baumgartner, L. Galm, J. Nötzold, H. Sigloch, J. Morgenstern, K. Schleining, et al., Determination of protein phase diagrams by microbatch experiments: Exploring the influence of precipitants and pH, *Int. J. Pharm.* 479 (2015) 28–40.
- [12] M. Al-Rubeai, M. Naciri, *Stem Cells and Cell Therapy*, Springer Netherlands, 2014.
- [13] A. Trounson, C. McDonald, *Stem Cell Therapies in Clinical Trials: Progress and Challenges*, *Cell Stem Cell.* 17 (2015) 11–22.

- 
- [14] M.A. Fischbach, J.A. Bluestone, W.A. Lim, Cell-Based Therapeutics: The Next Pillar of Medicine, *Sci. Transl. Med.* 5 (2013) ps7.
- [15] P.J. Amos, E. Cagavi Bozkulak, Y. Qyang, Methods of cell purification: a critical juncture for laboratory research and translational science., *Cells. Tissues. Organs.* 195 (2012) 26–40.
- [16] G.M.C. Rodrigues, C.A.V. Rodrigues, T.G. Fernandes, M.M. Diogo, J.M.S. Cabral, Clinical-scale purification of pluripotent stem cell derivatives for cell-based therapies, *Biotechnol. J.* 10 (2015) 1103–1114.
- [17] C. Stemberger, S. Dreher, C. Tschulik, C. Piossek, J. Bet, T.N. Yamamoto, et al., Novel serial positive enrichment technology enables clinical multiparameter cell sorting., *PLoS One.* 7 (2012) e35798.
- [18] T.G. Fernandes, C.A. V. Rodrigues, M.M. Diogo, J.M.S. Cabral, Stem cell bioprocessing for regenerative medicine, *J. Chem. Technol. Biotechnol.* 89 (2014) 34–47.
- [19] A. Chen, S. Ting, J. Seow, S. Reuveny, S. Oh, Considerations in designing systems for large scale production of human cardiomyocytes from pluripotent stem cells., *Stem Cell Res. Ther.* 5 (2014) 12.
- [20] J.M.S. Cabral, Cell Partitioning in Aqueous Two-Phase Polymer Systems, *Adv. Biochem. Eng. Biotechnol.* 106 (2007) 151–171.
- [21] H. Walter, D.E. Brooks, D. Fisher, Partitioning in Aqueous Two-Phase Systems - Theory, Methods, Uses, and Applications to Biotechnology, Academic Press, Inc., 1985.
- [22] R.R.G. Soares, A.M. Azevedo, J.M. van Alstine, M.R. Aires-Barros, Partitioning in aqueous two-phase systems: Analysis of strengths, weaknesses, opportunities and threats, *Biotechnol. J.* 10 (2015) 1158–1169.
- [23] P.A. Albertsson, G.D. Barid, Counter-Current Distribution of Cells, *Exp. Cell Res.* 28 (1962) 296–322.
- [24] K.T. Tran, D.M. Fishwild, Hematopoietic Cell Differentiation and Activation in Primary and Cultured Leukocytes, *Present. ASCB Meet.* (2006).
- [25] S. Zimmermann, S. Gretzinger, M.-L. Schwab, C. Scheeder, S.A. Oelmeier, A. Osberhaus, et al., High-throughput cell quantification assays for use in cell purification development – Enabling technologies for cell production, *Biotechnol. J.* 11 (2016) 676–686.
- [26] M. Bensch, B. Selbach, J. Hubbuch, High throughput screening techniques in downstream processing: Preparation, characterization and optimization of aqueous two-phase systems, *Chem. Eng. Sci.* 62 (2007) 2011–2021.

- [27] J.C. Merchuk, B.A. Andrews, J.A. Asenjo, Aqueous two-phase systems for protein separation Studies on phase inversion, *J. Chromatogr. B.* 711 (1998) 285–293.
- [28] D.F.C. Silva, A.M. Azevedo, P. Fernandes, V. Chu, J.P. Conde, M.R. Aires-Barros, Determination of aqueous two phase system binodal curves using a microfluidic device, *J. Chromatogr. A.* 1370 (2014) 115–120.
- [29] I. Coma, L. Clark, E. Diez, G. Harper, J. Herranz, G. Hofmann, et al., Process validation and screen reproducibility in high-throughput screening., *J. Biomol. Screen.* 14 (2009) 66–76.
- [30] P.J. Rousseeuw, M. Hubert, Robust statistics for outlier detection, *Wiley Interdiscip. Rev. Data Min. Knowl. Discov.* 1 (2011) 73–79.
- [31] P. Bevington, D.K. Robinson, Data reduction and error analysis for the physical sciences, 3rd ed., McGraw Hill, 2003.
- [32] R. Hatti-Kaul, Aqueous Two-Phase Systems, Humana Press, New Jersey, 2000.
- [33] E. Atefi, J.A. Mann, H. Tavana, Ultralow Interfacial Tensions of Aqueous Two-Phase Systems Measured Using Drop Shape, *Langmuir.* 30 (2014) 9691–9699.
- [34] D. Forciniti, C.K. Hall, M.R. Kula, Interfacial tension of polyethyleneglycol-dextran-water systems: influence of temperature and polymer molecular weight, *J. Biotechnol.* 16 (1990) 279–296.
- [35] P.A. Albertsson, Partition of Cell Particles and Macromolecules, 3rd ed., John Wiley & Sons, New York, 1986.
- [36] R.S. King, H.W. Blanch, J.M. Prausnitz, Molecular thermodynamics of aqueous two-phase systems for bioseparations, *AIChE J.* 34 (1988) 1585–1594.
- [37] A.D. Diamond, J.T. Hsu, Fundamental studies of biomolecule partitioning in aqueous two-phase systems., *Biotechnol. Bioeng.* 34 (1989) 1000–1014.
- [38] D. Brackman, F. Lund-Johansen, D. Aarskog, Expression of Cell Surface Antigens During the Differentiation of HL-60 Cells induced by 1,25-Dihydroxyvitamin D<sub>3</sub>, Retionic Acid and DMSO, *Leuk. Res.* 19 (1995) 57–64.
- [39] I.D. Trayner, T. Bustorff, A.E. Etches, G.J. Mufti, Y. Foss, F. Farzaneh, Changes in antigen expression on differentiating HL-60 cells treated with dimethylsulphoxide, all-trans retinoic acid,  $\alpha$ -1,25-dihydroxyvitamin D<sub>3</sub> or 12-O-tetradecanoyl phorbol-13-acetate, *Leuk. Res.* 22 (1998) 537–547.
- [40] P.S. Gascoine, D. Fisher, The dependence of cell partition in two-polymer aqueous phase systems on the electrostatic potential between the phases, *Biochem. Soc. Trans.* 12 (1984) 1085–1086.
- [41] M. Vis, V.F.D. Peters, R.H. Tromp, B.H. Ern e, Donnan Potentials in Aqueous Phase Separated Polymer Mixtures., *Langmuir.* 30 (2014) 5755–5762.

- 
- [42] R. Reitherman, D. Flanagan, H. Barondes, Electromotive Phenomena in Partition of Erythrocytes in Aqueous Polymer Two Phase Systems, *Biochim. Biophys. Acta.* 297 (1973) 193–202.
- [43] H. Walter, E.J. Krob, A. Pedram, Subfractionation of cell populations by partitioning in dextran–poly (ethylene glycol) aqueous phases. "Discriminating" and "nondiscriminating" systems., *Cell Biophys.* 4 (1982) 273–284.
- [44] O. Stendahl, C. Dahlgren, J. Hed, Physicochemical and Functional Changes in Human Leukemic Cell Line HL-60, *J. Cell. Physiol.* 112 (1982) 217–221.
- [45] S.W. Hui, T. Isac, L.T. Boni, A. Sen, Action of polyethylene glycol on the fusion of human erythrocyte membranes., *J. Membr. Biol.* 84 (1985) 137–46.
- [46] C. Fruijtier-Pöllöth, Safety assessment on polyethylene glycols (PEGs) and their derivatives as used in cosmetic products, *Toxicology.* 214 (2005) 1–38.

**Table A1:** Pipetting parameters and calibration functions of stock solutions. <sup>1</sup>STAG: System trailing airgap; <sup>2</sup>LAG: leading airgap; <sup>3</sup>TAG: trailing airgap. All aqueous solutions were dispensed without immersion, polymers and cell suspensions were dispensed with immersion.

Liquid	Volume [ $\mu\text{L}$ ]	Asp. speed [ $\mu\text{L}\cdot\text{s}^{-1}$ ]	Asp. De-lay [ $\mu\text{L}\cdot\text{s}^{-1}$ ]	Disp. speed [ $\mu\text{L}\cdot\text{s}^{-1}$ ]	Disp. De-lay [ms]	STAG <sup>1</sup> [ $\mu\text{L}$ ]	LAG <sup>2</sup> [ $\mu\text{L}$ ]	TAG <sup>3</sup> [ $\mu\text{L}$ ]	Calibration
Water	20-50	30	500	300	300	20	10	10	$1.0138x + 1.3354$
	50-200	70	500	200	300	20	10	10	$1.0024x + 1.5773$
30% (w/w) PEG 8,000	200-1,000	125	500	200	300	20	10	10	$0.9942x + 4.7948$
	20-50	5	1,000	5	1,000	20	30	10	$1.0774x + 0.4086$
	50-200	10	1,500	10	1,500	20	30	10	$1.1156x - 1.5263$
20% (w/w) dextran 500,000	200-1,000	30	1,500	20	1,500	20	30	10	$1.0021x + 18.671$
	20-50	5	1,000	5	1,000	20	30	10	$1.1307x - 0.8459$
	50-200	10	1,500	10	1,500	20	30	10	$1.11x + 1.1752$
2% (w/w) dextran 500,000	200-1,000	30	1,500	20	1,500	20	30	10	$1.0144x + 16.928$
	20-50	25	750	50	1,000	20	30	10	$1.0041x + 0.3637$
	50-200	75	750	50	1,000	20	30	10	$1.0002x + 0.6364$
1M NaPi	200-1,000	100	750	50	1,000	20	30	10	$1.0026x + 0.1384$
	20-50	30	500	300	300	20	10	10	$1.021x + 1.7995$
	50-200	70	500	200	300	20	10	10	$1.0098x + 2.0507$
1M NaCl	200-1,000	125	500	200	300	20	10	10	$1.0071x + 3.286$
	15-50	30	500	300	300	20	10	10	$1.0332x + 1.1967$
	50-200	70	500	200	300	20	10	10	$1.0163x + 1.6911$
0.5M NaPi	200-1,000	125	500	200	300	20	10	10	$1.0059x + 5.6541$
	20-50	30	500	300	300	20	10	10	$1.0212x + 1.0139$
	50-200	70	500	200	300	20	10	10	$1.0513x + 1.4015$
0.5M NaCl	200-1,000	125	500	200	300	20	10	10	$1.0087x + 2.2871$
	15-50	30	500	300	300	20	10	10	$1.0052x + 1.1549$
	50-200	70	500	200	300	20	10	10	$1.0069x + 1.2798$
PBS	200-1,000	125	500	200	300	20	10	10	$1.0041x + 1.0152$
	10-50	30	500	300	300	20	10	10	$1.0136x + 1.357$
	50-200	70	500	200	300	20	10	10	$1.0011x + 1.6279$
Staining buffer	200-1,000	125	500	200	300	20	10	10	$1.0023x + 1.5476$
	10-50	30	500	300	300	20	10	10	$1.0136x + 1.357$
	50-200	70	500	200	300	20	10	10	$1.0011x + 1.6279$
Cell suspension	200-1,000	125	500	200	300	20	10	10	$1.0023x + 1.5476$
	10-15	20	250	20	200	20	10	10	$0.9914x + 0.358$

**Table A2:** Pipetting parameters for top and bottom phase sampling. Parameters for bottom phase sampling are stated in parentheses if differing from top phase sampling. STAG: System trailing airgap; TAG: trailing airgap; AG: Airgap which is dispensed before sample aspiration; WP: volume pipetted into wash plate before sample is dispensed, to reduce carry-over. <sup>1</sup>Sample+LAG & TAG.

	No of Plunger steps [-]	Speed [ $\mu\text{Ls}^{-1}$ ]
Aspiration (incl. excess volume)	90 (149)	5
Dispense (WP)	0 (32)	5
Dispense	149 <sup>1</sup> (88)	5
STAG	150 (150)	70
TAG	30 (0)	70
AG	0 (32)	70

**Table A3:** Summary of pipetting accuracy and precision for different TLL determined by petting on an analytical balance. Std: standard deviation (n=8); CV: coefficient of variation. Mean volumes were calculated by multiplying the pipetted masses with the phase densities.

ATPS	4% (w/w) PEG 8,000/ 4% (w/w) dextran 500,000		4% (w/w) PEG 8,000/ 5% (w/w) dextran 500,000		5% (w/w) PEG 8,000/ 7% (w/w) dextran 500,000	
TLL	7.3		10.8		19.3	
Phase	<i>top</i>	<i>bottom</i>	<i>top</i>	<i>bottom</i>	<i>top</i>	<i>bottom</i>
Mean volume [ $\mu\text{L}$ ]	29.98	29.29	30.22	29.48	30.24	29.45
Std [ $\mu\text{L}$ ]	0.40	0.46	0.64	0.46	0.68	0.48
CV [%]	1.35	1.57	2.11	1.57	2.24	1.63

**Table A4:** Summary of ATPS-compositions.

ATPS #	PEG 8,000 [% (w/w)]	dextran 500,000 [% (w/w)]	sodium phosphate [mM]	sodium chloride [mM]	pH [-]	sodium chloride [%]
1	4	4	110	0	6.6	0
2	4	4	90	50	6.6	35
3	4	4	70	70	6.6	50
4	4	5	110	0	6.6	0
5	4	5	90	50	6.6	35
6	4	5	70	70	6.6	50
7	4	5	110	0	7.0	0
8	4	5	90	50	7.0	35
9	4	5	70	70	7.0	50
10	4	5	110	0	7.4	0
11	4	5	90	50	7.4	35
12	4	5	70	70	7.4	50
13	5	7	110	0	6.6	0
14	5	7	90	50	6.6	35
15	5	7	70	70	6.6	50



---

Cell separation in aqueous two-phase systems - Influence of  
polymer molecular weight and tie-line length on the resolution  
of five model cell lines

**Sarah Zimmermann<sup>a,†</sup>, Sarah Gretzinger<sup>a,b,†</sup>, Philipp K. Zimmermann<sup>a</sup>, Are  
Bogsnes<sup>c</sup>, Mattias Hansson<sup>d</sup> & Jürgen Hubbuch<sup>a,\*</sup>**

<sup>a</sup> Karlsruhe Institute of Technology (KIT), Institute of Process Engineering in Life Science, Section IV: Biomolecular Separation Engineering (MAB), Engler-Bunte-Ring 3, 76131 Karlsruhe, Germany

<sup>b</sup> Karlsruhe Institute of Technology (KIT), Institute of Functional Interfaces (IFG), Hermann-von-Helmholtz-Platz 1, 76344 Eggenstein-Leopoldshafen, Germany

<sup>c</sup> Novo Nordisk A/S, Biopharm Purification Development & Virology, Hagedornsvej 1, 2820 Gentofte, Denmark

<sup>d</sup> Novo Nordisk A/S, Diabetes Research, Novo Nordisk Park, 2760 Måløv, Denmark

\* *Correspondence to Prof. Dr. Jürgen Hubbuch, telephone: +49 721 608 47526; fax: + 49 721 608 46240; e-mail: juergen.hubbuch@kit.edu*

† Authors contributed equally

## Abstract

The availability of clinical-scale downstream processing strategies for cell-based products presents a critical juncture between basic research and clinical development. Aqueous two-phase systems (ATPS) facilitate the label-free, scalable, and cost-effective separation of cells, and are a versatile tool for downstream processing of cell-based therapeutics. Here, we report the application of a robotic screening platform that enables high-throughput cell partitioning analysis in ATPS. We investigated the influence of polymer molecular weight and tie-line length on the resolution of five model cell lines in charge-sensitive PEG-dextran ATPS. We show, how these factors influence cell partitioning, and that the combination of low molecular weight PEGs and high molecular weight dextrans enable the highest resolution of the five cell lines. Furthermore, we demonstrate that the separability of each cell line from the mixture is highly dependent on the polymer molecular weight composition and tie-line length. Using a countercurrent distribution model we demonstrate that our screenings yielded conditions that enable the isolation of four of the five cell lines with high purity (>99.9%) and yield.

**Keywords:** high-throughput screening, cell separation, aqueous two-phase systems (ATPS), charge-dependent partitioning, tie-line length, polymer molecular weight

---

# 1 Introduction

Cell-based therapeutics for a variety of diseases and from a variety of cell sources have made their way to clinical trials. The availability of clinical-scale downstream processing strategies for cell-based products represents a crucial juncture between basic research and clinical development. For clinical applications, cell-based products often need to be enriched to high purities, since certain contaminants can cause severe side effects, such as teratoma formation or graft-versus-host-disease (GvHD) [1–6]. The most widely applied cell purification methods are based on affinity-purification. These methods, however, require large amounts of clinical-grade antibodies, presenting a significant cost-factor [5,7,8]. Likewise, antibody-labels remaining on the cell surface, pose considerable regulatory obstacles for the treatment of patients, as they may cause adverse reactions [4,5]. Aqueous two-phase systems (ATPS) present a gentle, cost-effective, scalable, and label-free method for cell purification. ATPS are aqueous solutions consisting of one or more compounds, e.g. different polymers, which form two immiscible phases above a certain threshold (e.g. concentration, temperature). The two phases have distinct physicochemical properties, consequently, biomolecules partition between them according to their respective physicochemical properties. By now, they are well established in downstream processing of biopharmaceuticals, such as protein- and DNA-based pharmaceuticals [9–11]. Polyethylene-glycol (PEG)-dextran ATPS have been successfully used to separate cells according to their surface properties, and it is well established that ATPS facilitate the separation of different cell types with high selectivity and resolution [10,12]. In multi-stage experiments, e.g. countercurrent distribution (CCD), even complex cell mixtures were effectively separated [10,13]. While the mechanisms underlying cell partitioning in ATPS are not fully understood, two main factors in cell separation have been identified: surface charge and membrane lipid composition. Surface charge-dependent cell separation is possible in ATPS containing isotonic concentrations of phosphate (charge-sensitive ATPS), and partitioning coefficients could be correlated to the cells electrophoretic mobility. Charge-independent cell separation can be achieved in ATPS containing isotonic concentrations of NaCl (charge-insensitive ATPS), and partitioning coefficients have been correlated with the cells membrane lipid composition, i.e. membrane hydrophobicity [10,12,14,15]. These phenomena are based on different partitioning properties of the respective salts. While sodium chloride partitions almost equally between the phases, sodium phosphate has a stronger affinity to the dextran-rich bottom phase, resulting in an interfacial electrostatic potential difference (Donnan potential) [16,17]. The Donnan potential is highly dependent on salt-composition, tie-line length (TLL), polymer type and molecular weight [10,12,18]. At the same time, TLL and polymer molecular weight significantly influence cell partitioning in the absence of a Donnan potential [10,12]. A key factor in cell partitioning is the interfacial tension [19], which is directly correlated with TLL and polymer molecular weight [20]. The interaction of all these parameters in respect to cell partitioning and the resolution of different cell populations is however unclear. In previous work, we developed an integrated high-throughput screening (HTS)-platform for the analysis of cell partitioning in ATPS. We investigated the influence of TLL, salt composition, and pH on the resolution of several model cell lines and described strategies for fast and directed HT-downstream process development [21]. In this work, we used this HTS-platform to investigate the influence of the PEG

and dextran molecular weights in dependence of the TLL on cell partitioning in ATPS. Using different CellTracker<sup>TM</sup> dyes in a combinatorial fashion for cell barcoding, enables multiplexing of several cell lines in a single experiment, and results in a substantial decrease in time and material consumption. Moreover, batch variability can be eliminated by analyzing numerous cell lines in the same experiment. The present work describes how TLL in dependence of the polymer molecular weight influence the resolution of five bar-coded model cell lines in charge-sensitive ATPS, characterizes suitable screening ranges and shows how these data can be used to design purification strategies for the various cell populations.

---

## 2 Materials & Methods

### 2.1 Disposables

For ATPS preparation, 1.3 mL deep well plates (Nalgene Nunc, Rochester, NY, cat. 260252) and for flow cytometry, 96-well U-bottom plates (BD Falcon<sup>TM</sup>, Franklin Lakes, NJ, cat. 353910) were used. Polypropylene flat-bottom microplates (Greiner Bio-One, Kremsmünster, Austria, cat. 655261) were used for all other purposes.

### 2.2 Software and data processing

Evoware 2.5 SP2 standard (Tecan, Crailsheim, Germany) was used to control the Tecan Freedom Evo 200 liquid handling station. Advanced applications such as sampling and cell resuspension were realized via visual basic scripts that were directly fed into Evoware. For data storage Excel 2013 (Microsoft, Redmond, WA, USA) was used. Matlab R2014a (The MathWorks, Natick, ME, USA) and Excel 2013 were used for data evaluation and visualization. Statistical data analysis was performed with Matlab R2014a. The BD LSR Fortessa Cell Analyzer was controlled using BD FACSDiva 8.0 (BD Biosciences, San Jose, CA, USA). In addition, BD FACSDiva 8.0 was used to calculate the compensation of spectral overlap and for raw data analysis. Flow cytometry data visualization was performed with Flow Jo V10 (Tree Star, Ashland, OR, USA).

### 2.3 Preparation of buffers and stock solutions

For the preparation of buffers and stock solutions ultra-pure water ( $0.55 \mu\text{S}/\text{cm}$ ) obtained from an Arium<sup>®</sup> proUV water system (Sartorius Stedim Biotech, Goettingen, Germany) was used. Stock solutions of 2% and 20% dextran 70,000 (Carl Roth Karlsruhe, Germany, cat. 9228.2, Batch No.: 215229323), 2% and 20% dextran 500,000 (Pharmacosmos A/S, Holbæk, Denmark, cat. 5510 0500 9007, Batch No.: HT3229), 40% PEG 4,000 (Merck Millipore, Billerica, MA, USA, cat. 8.17066.5000, Batch No.: K46660006524), 30% PEG 8,000 (Sigma Aldrich, St. Louis, MO, USA, cat. P2139, Batch No.: 059Ko121), and 20% PEG 20,000 (Sigma Aldrich, cat. 95172-250G-F, Batch No.: BCBP5677V) were prepared in ultra-pure water and dissolved on a magnetic stirrer overnight. 500 mM sodium phosphate (NaPi) buffer stock solutions with pH 6.6, and 7.4 were prepared as described before [21]. Sodium chloride (NaCl) (Merck Millipore) was prepared as a 500 mM stock solution. Sterile filtration ( $\varnothing 0.22 \mu\text{m}$ ) was performed for all buffers and stock solutions. Polymer solutions were stored at 4°C whereas buffers were stored at room temperature. The flow cytometry staining buffer was prepared directly before use and consisted of phosphate buffered saline (PBS) (Life Technologies<sup>TM</sup>, Carlsbad, CA, USA) supplemented with 2 mM EDTA (Life Technologies<sup>TM</sup>) and 0.5% bovine serum albumin (BSA) (Miltenyi Biotech, Bergisch Gladbach, Germany).

### 2.4 Cell culture

Unless otherwise stated cell culture reagents were purchased from Life Technologies<sup>TM</sup>. The murine fibroblast cell line L929 was purchased from CLS (Cell lines Service Eppelheim, Germany, cat. 400260), and the rat ileum cell line IEC-18 was purchased from

ATCC (cat. CRL-1589). The human lung carcinoma cell line A549 (ATCC, cat. CCL-185) and the human colorectal carcinoma cell line HCT 116 (ATCC, cat. CCL-247) were a gift from Prof. Hartwig's lab. The rat beta-cell line INS-1E [22] was kindly provided by Prof. Maechler from the Department of Cell Physiology and Metabolism at the University of Geneva Medical Centre, Switzerland. All cell lines were propagated at 37°C in a humidified 5% CO<sub>2</sub> incubator. L929, A549 and HCT 116 cells were grown in DMEM with GlutaMAX supplemented with 10% FBS and 1% Penicillin/ Streptomycin. IEC-18 cells were cultivated in DMEM with GlutaMAX supplemented with 5% FBS, 1% NEAA, 1% Penicillin/ Streptomycin and 0.1 U per mL bovine insulin (Sigma Aldrich, cat. I1882). INS-1E cells were cultivated in RPMI 1640 with GlutaMAX supplemented with 10% FBS, 1% sodium pyruvate, 1% Penicillin/ Streptomycin, 10 mM HEPES and 50 μM beta mercaptoethanol (Sigma Aldrich). All cell lines were split every 3–4 days to a concentration of 2 x 10<sup>4</sup> cells per cm<sup>2</sup> for a maximum of 20 passages, with the exception of INS-1E which were seeded at a concentration of 7 x 10<sup>4</sup> cells per cm<sup>2</sup>. In order to obtain maximal reproducibility between different screenings, all cell lines were seeded at a density of 2.7 x 10<sup>5</sup>, 48 hours prior to the screening.

## 2.5 Cell barcoding and viability staining

In order to enable multiplexing of several cell lines and eliminate inter-experimental variability, the five cell lines were stained with different CellTracker™ dyes (Life Technologies™) in a combinatorial fashion. For staining, cells were trypsinized and resuspended in serum-free medium to a final concentration of 2 x 10<sup>6</sup> cells per mL. The CellTracker™ dyes were added to a final concentration of 3 μM for CellTracker™ Violet BMQC, 0.2 μM for CellTracker™ Green CMFDA, and 0.05 μM for CellTracker™ Deep Red, respectively. The cells were stained at 37°C for 30 minutes and subsequently resuspended in culture medium and incubated at 37°C for 20 minutes to inactivate unbound dye molecules. Prior to flow cytometric analysis, cells were stained with the viability dye 7-AAD (Biolegend, San Diego, CA, USA), according to the manufacturer's instructions. Dead cells were gated using heat inactivated controls (70°C, 10 minutes).

## 2.6 Cell quantification using high-throughput flow cytometry

Flow cytometric cell quantification was performed as previously described [21].

## 2.7 Liquid-handling calibration

Liquid handling calibration was performed for all buffers and stock solutions as described previously [21]. Calibration was performed in the range of 50–1,000 μL. Variation coefficients were below 1.6% for all aqueous solutions and below 3% for the more viscous polymer solutions.

---

## 2.8 HT–binodal and tie–line determination

A HTS–method for binodal determination based on cloud–point titration has previously been established in our group and was performed as described [21].

## 2.9 Automated high–throughput screening of cell partitioning in aqueous two–phase systems

The automated HTS–method was used as described in a previous publication [21]. The entire HTS was performed on a Tecan Freedom Evo<sup>®</sup> 200 liquid–handling station (LHS). Subsequently, the sample plates were transferred to the high–throughput sampler of the BD LSR Fortessa for cell quantification and analysis. ATPS were prepared in a 1.3 mL 96–well plate with a final volume of 637  $\mu\text{L}$ . After mixing and addition of cells ( $1 \times 10^6$  cells per well), phases were allowed to settle by gravity (20 minutes, RT) and sampling was performed as previously described. During the sampling procedure samples were 5–fold diluted in staining buffer. After adding an equal volume of staining buffer containing 7–AAD for viability staining and incubation for 10 minutes at RT in the dark, flow cytometric analysis was performed.

## 2.10 Statistical data analysis

Pre–processing of screening data was performed as described in previous work [21]. A two–sided Student’s  $t$ –test was performed to determine differences in means, provided that equal variances were asserted by an F–test. Error propagation was considered throughout our analyses [23].

### 3 Results

We previously developed a fully automated screening set-up that integrates cell partitioning in ATPS on a Tecan liquid-handling station and cell quantification and analysis at the single cell level using high-throughput flow cytometry [21]. In the present study we investigated the influence of PEG and dextran molecular weight and TLL on the resolution of five cell lines in charge-sensitive ATPS. The following cell lines were chosen for this study: the murine fibroblast cell line L929, the rat ileum cell line IEC-18, the human lung carcinoma cell line A549, the human colorectal carcinoma cell line HCT 116, and the rat beta-cell line INS-1E. Due to their different origins, we expected these cell lines to differ significantly in their cell surface properties. We used a barcoding strategy that enabled multiplexing of several cell lines in a single experiment (**Figure 1a**). By using three different CellTracker™ dyes in a combinatorial fashion, the cell lines were successfully barcoded (**Figure 1b**).

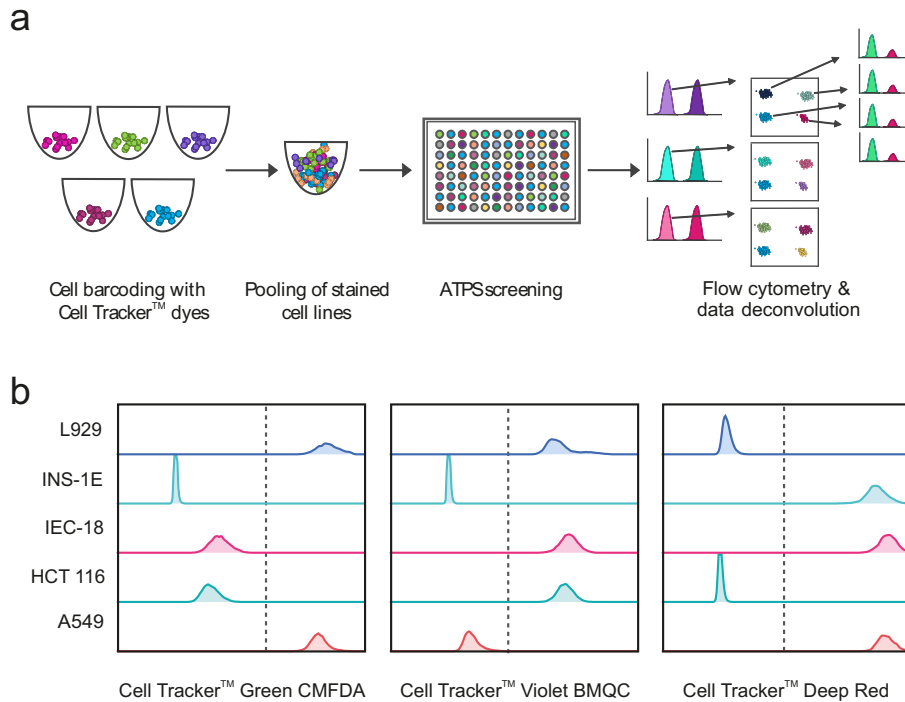


**Figure 1:** Cell barcoding for multiplexing of partitioning analysis in ATPS. (a) Scheme of the barcoding strategy. Several cell lines are stained with CellTracker™ dyes in a combinatorial fashion and pooled, before HT-partitioning analysis in ATPS. Cell quantification and analysis is performed by HT-flow cytometry. After data deconvolution, the partitioning coefficients of each cell type can be determined. (b) Efficient labelling of five cell lines with three CellTracker™ dyes. A549 cells were stained with CellTracker™ Green CMFDA and CellTracker™ Deep Red, INS-1E cell were stained with CellTracker™ Deep Red, IEC-18 cells were stained with CellTracker™ Deep Red and CellTracker™ Violet BMQC, HCT 116 cells were stained with CellTracker™ Violet BMQC, and L929 cells were stained with CellTracker™ Green CMFDA and CellTracker™ Violet BMQC.

Spill-over between barcoded cell lines can result in inaccurate analysis of cell partitioning, however, this was not observed here. We determined that spill-over was  $< 0.1\%$  in all experiments. The gating-strategy used for data deconvolution is shown in **Figure 2**. Partitioning coefficients were calculated based on the live cell counts of each cell line. Cell viability was high throughout the screening ( $> 98\%$  viable cells), and comparable between the cell lines.

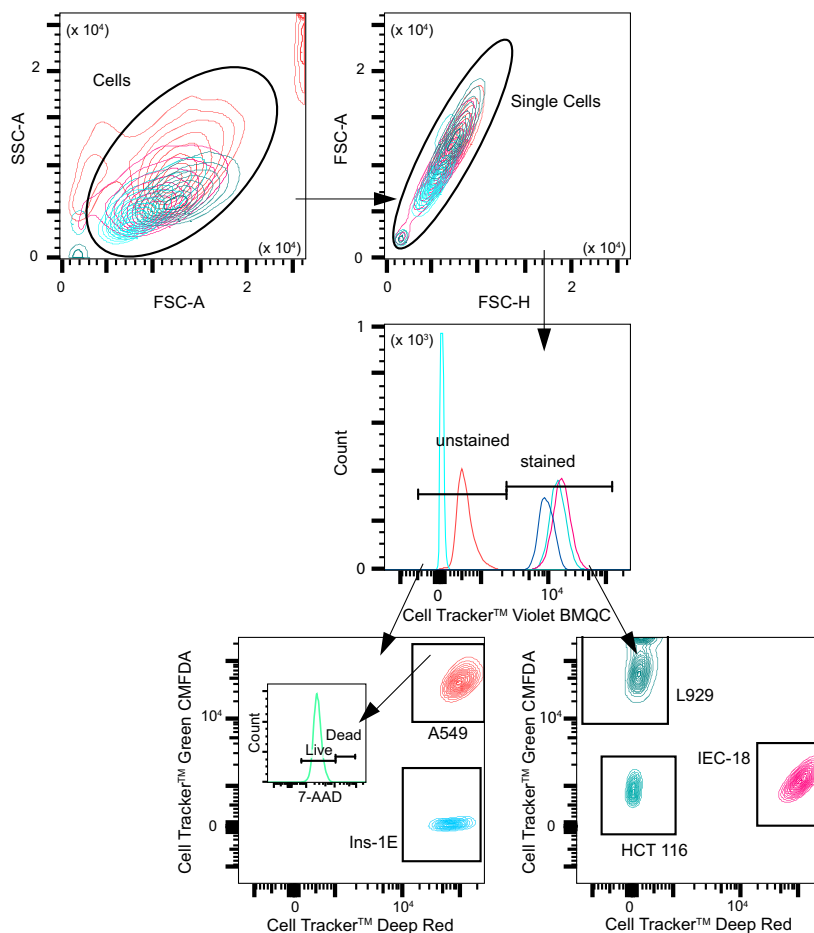


**Figure 2:** Deconvolution method for barcoded cell lines. Single cells are gated for CellTracker<sup>™</sup> Violet BMQC staining and then further gated into single cell lines based on CellTracker<sup>™</sup> Green CMFDA and CellTracker<sup>™</sup> Deep Red staining. The live cell population of each cell line was the gated based on 7-AAD staining. FSC-A: forward scatter peak area, SSC-A: side scatter peak area, FSC-H: forward scatter peak height.

### 3.1 Characterization of PEG-dextran ATPS

Phase diagrams are essential to determine suitable screening ranges in ATPS research, since they enable the selection of suitable volume ratios and TLL. The ATPS used in this work consisted of different combinations of PEG 4,000, 8,000, and 20,000, and dextran 70,000 and 500,000, buffered with isotonic concentrations of sodium phosphate. Phase diagrams were determined using a HTS-method described in previous studies [24](**Figure 3 & Table 1**). Binodal curves were fitted to equation 1 using least square regression.

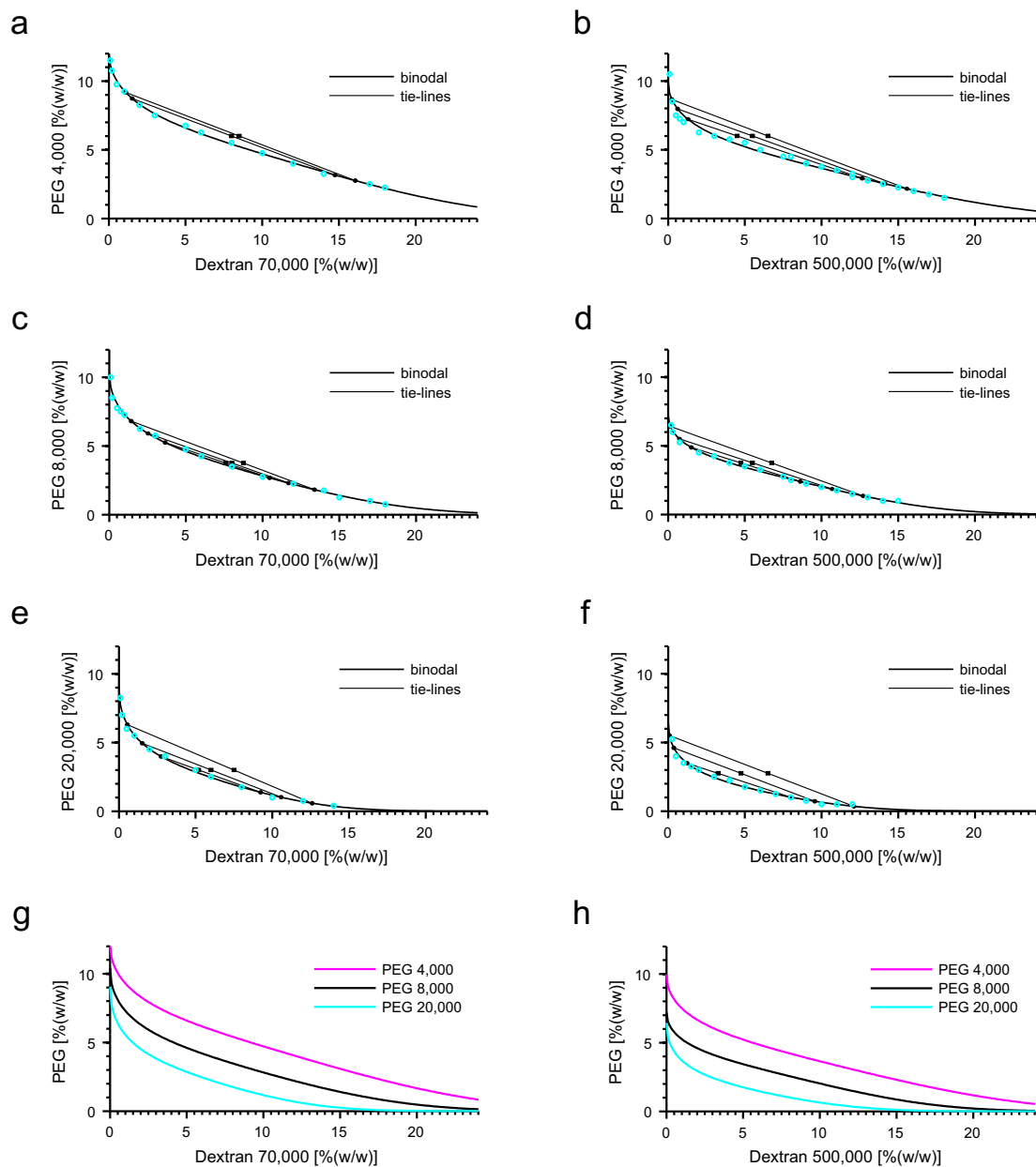


**Figure 3:** Phase diagrams of different PEG and dextran molecular weights. Blue circles represent binodal data points determined by HTS cloud point titration. Fit parameters of equation 1 with 95% prediction bounds and Pearson's  $r^2$  are shown in parentheses. (a) PEG 4,000 and dextran 70,000 (fit parameters: a: 12.17 (11.88 / 12.46), b:  $-0.27$  ( $-0.29$  /  $-0.25$ ), c:  $-0.00010$  ( $-0.00012$  /  $-0.000075$ ),  $r^2$  of 0.998), (b) PEG 4,000 and dextran 500,000 (fit parameters: a: 9.96 (9.3 / 10.62), b:  $-0.28$  ( $-0.33$  /  $-0.24$ ), c:  $-0.00011$  ( $-0.00017$  /  $-0.00005$ ),  $r^2$  of 0.972), (c) PEG 8,000 and dextran 70,000 (fit parameters: a: 10.41 (9.92 / 10.89), b:  $-0.35$  ( $-0.40$  /  $-0.31$ ), c:  $-0.00019$  ( $-0.00026$  /  $-0.00012$ ),  $r^2$  of 0.993), (d) PEG 8,000 and dextran 500,000 (fit parameters: a: 7.23 (6.98 / 7.48), b:  $-0.32$  ( $-0.34$  /  $-0.29$ ), c:  $-0.00027$  ( $-0.00032$  /  $-0.00021$ ),  $r^2$  of 0.996), (e) PEG 20,000 and dextran 70,000 (fit parameters: a: 9.04 (8.43 / 9.65), b:  $-0.49$  ( $-0.56$  /  $-0.42$ ), c:  $-0.00051$  ( $-0.00084$  /  $-0.00018$ ),  $r^2$  of 0.992), (f) PEG 20,000 and dextran 500,000 (fit parameters: a: 6.44 (5.82 / 7.05), b:  $-0.55$  ( $-0.64$  /  $-0.46$ ), c:  $-0.00057$  ( $-0.00094$  /  $-0.00019$ ),  $r^2$  of 0.987). 95% prediction bounds of the fit parameters are shown in parentheses. (g-h) Overlay of binodal fits.

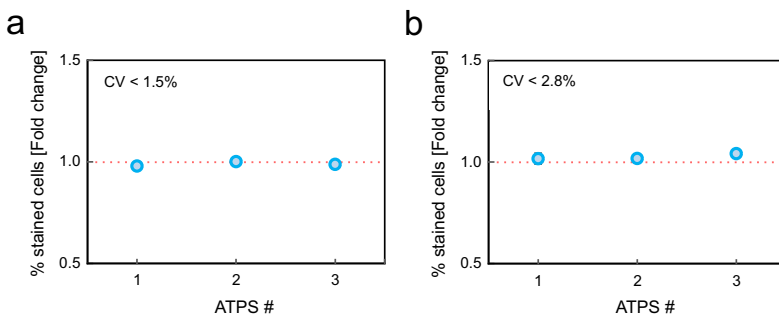


**Figure 4:** Influence of cell barcoding on partitioning in charge-sensitive and charge-insensitive ATPS at different TLL (# 1: 4% PEG 8,000, 4% dextran 500,000, 0.01 M NaPi, 0.138 M NaCl, pH 6.6, TLL: 6.9; # 2: 4% PEG 8,000, 4% dextran 500,000, 0.11 M NaPi, pH 7.4, TLL: 6.9; # 3: 4% PEG 8,000, 5% dextran 500,000, 0.11 M NaPi, pH 7.4, TLL: 10.4). Two of the cell lines were barcoded with different CellTracker<sup>TM</sup> dyes and mixed with an equal number of unstained cells of the same cell line. HCT 116 (a) was stained with Cell Tracker<sup>TM</sup> Violet BMQC and INS-1E (b) was stained with CellTracker<sup>TM</sup> Deep Red. Partitioning analysis was performed in HTS and the fold change of the percentage of stained cells was calculated compared to a PBS control. Error bars represent 1 s.d. of 4 technical replicates. Pairwise *t*-test showed no significant changes of partitioning due to CellTracker<sup>TM</sup> staining ( $p > 0.05$ ). Error bars are within symbol size.

$$y = a \times e^{(b \times x^{0.5} + c \times x^3)} \quad (1)$$

All binodal curves could be fitted with a Pearson's  $r^2$  of at least 0.99. A change in shape and location of the binodal in dependence of the polymer molecular weight was observed. With increasing PEG molecular weight, the binodal shifts towards lower PEG and dextran concentrations. This trend was observed for both dextran molecular weights (**Figure 3 g & h**). The same effect was observed when increasing the dextran molecular weight. At a given PEG molecular weight, the increase of the dextran molecular weight results in a shift of the binodal towards lower PEG and dextran concentrations. In addition, changes in binodal asymmetry could be observed in all phase diagrams. The higher the difference in the molecular weight of PEG and dextran, the stronger the observed asymmetry. Tie-line slopes increased slightly with increasing TLL, and the increase was very comparable for different PEG and dextran molecular weights. We chose three screening points from each phase diagram, with TLL of 7, 10 and 13 % (w/w), with the exception of the phase diagrams of PEG 4,000. Due to the flatness of the binodals, even systems close to the critical point had TLL of  $\geq 12$  % (w/w). Thus, we chose TLL of 12, 14 and 16% (w/w) for PEG 4,000 – dextran 500,000 and 14 & 16% (w/w) for PEG 4,000 – dextran 70,000.

### 3.2 Influence of cell barcoding on their partitioning in PEG-Dextran ATPS

Cell barcoding enables the evaluation of numerous cell lines in a single experiment. As cell partitioning in ATPS is primarily dependent on cell surface properties, we chose a barcoding reagent that does not bind to the cell surface, as for example described by [25]. Instead, we chose the CellTracker<sup>TM</sup> dyes, which are cell permeant fluorescent

probes that are retained inside living cells after a glutathione S-transferase-mediated reaction, with the exception of CellTracker<sup>TM</sup> Deep Red, which is an amine-reactive dye. Even though amine reactive dyes do not exclusively bind to proteins inside the cell, CellTracker<sup>TM</sup> Deep Red was used at very low concentrations (50 nM). Thus, we expected that the CellTracker<sup>TM</sup> dyes can be used for cell barcoding without significantly altering their partitioning behavior. To confirm this assumption, we mixed CellTracker<sup>TM</sup> Violet BMQC stained and unstained HCT 116 cells and CellTracker<sup>TM</sup> Deep Red stained and unstained INS-1E cells, and studied their partitioning in a number of ATPS. We chose ATPS composed of 4% PEG 8,000, 5% dextran 500,000, 0.11 M NaPi, pH 7.4, with a TLL of 10.4 and of 4% PEG 8,000, 4% dextran 500,000, 0.11 M NaPi, pH 7.4, with a TLL of 6.9, which were previously shown to enable cell separation based on surface charge [10]. In addition, we chose a ATPS consisting of 4% PEG 8,000, 4% dextran 500,000, 0.01 M NaPi, 0.138 M NaCl, pH 6.6, with a TLL of 6.9 which was previously shown to enable cell separation based on their membrane lipid composition [10]. In **Figure 4**, the fold change of the percentage of stained HCT 116 and INS-1E cells after partitioning is shown. No significant enrichment or depletion of the CellTracker<sup>TM</sup> stained cell populations was observed ( $p > 0.05$ ).

### 3.3 Resolution of five model cell lines in charge-sensitive ATPS in dependence of TLL and polymer molecular weight

The aim of this case study was to investigate the influence of TLL and polymer molecular weight on the resolution of different cell lines. To do so, the partitioning of five cell lines that differ in species and tissue type was investigated in charge-sensitive ATPS at different TLL and different combinations of PEG and dextran molecular weights. The partitioning coefficient  $P$  of each cell line was defined as the ratio of cells in the top phase (equation 2). The partitioning coefficient for the bottom phase was determined accordingly.

$$P = \frac{Count_{TP} \times V_{TP}}{Count_C \times V_C} \quad (2)$$

*TP: top phase, C: PBS control, V: volume*

In **Figure 5** the partitioning coefficients of each cell line in dependence of TLL and polymer molecular weight in charge-sensitive ATPS is summarized. The screenings revealed a number of trends. Firstly, in the presence of NaPi, cells generally partitioned between top phase and interface, which is well described for charge-dependent cell partitioning. Further, partitioning coefficients decrease with increasing PEG molecular weight, while an increase in dextran molecular weight results in an increase of cell recovery in the top phase. Even though ATPS consisting of PEG 4,000 and either dextran 70,000 or 500,000 had considerably higher TLL very high partitioning coefficients were observed. Secondly, when comparing the partitioning coefficients for a given molecular weight combination, partitioning coefficients decrease with increasing TLL. This trend is more pronounced for ATPS consisting of PEG 8,000 than PEG 4,000 and either dextran 70,000 or 500,000. In ATPS consisting of PEG 20,000 and either dextran 70,000 or 500,000 less than 7%

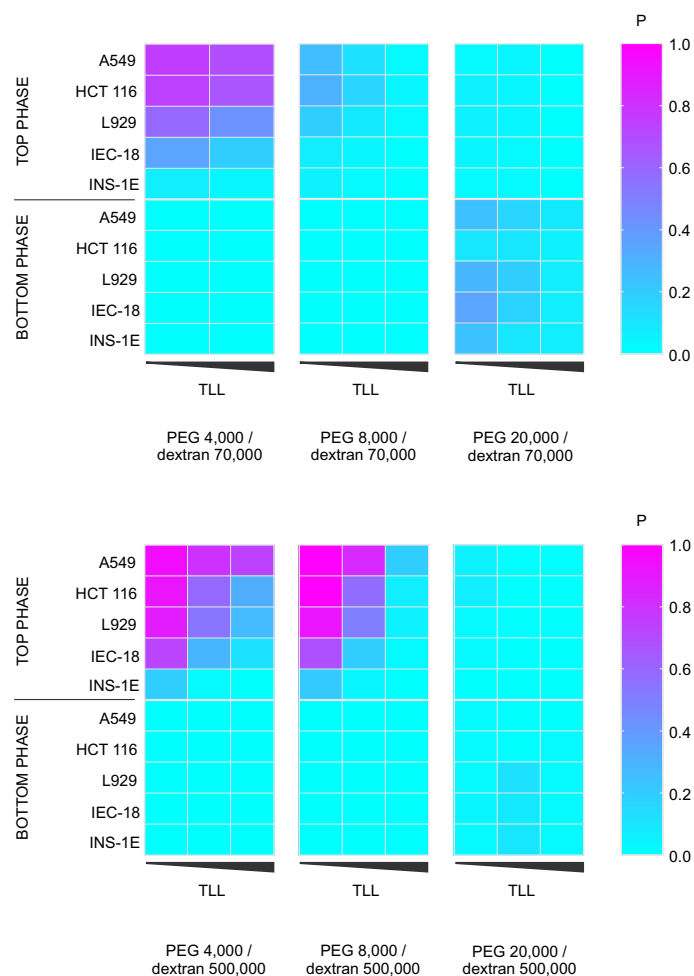


**Figure 5:** Partitioning coefficients of five model cell lines in ATPS containing 0.11 M NaPi, pH 7.4, in dependence of PEG and dextran molecular weight and TLL. ATPS compositions are summarized in **Table 1**. Heat maps represent the mean percentage of live cells in each phase (3 technical replicates). TLL: tie-line length.

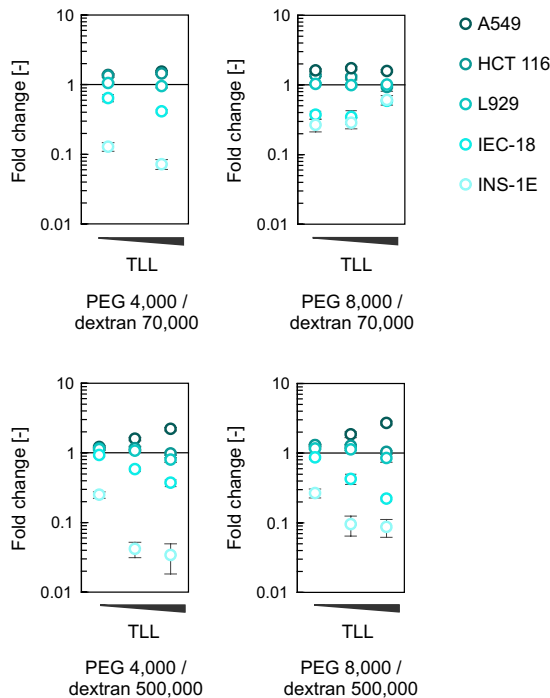


**Figure 6:** Fold change of the percentage of five model cell lines compared to a PBS control in the top phase of charge-sensitive ATPS in dependence of polymer molecular weight and TLL. ATPS compositions are summarized in Table 1. Error bars represent 1 s.d. of 3 technical replicates. TLL: tie-line length.

of either cell line was recovered in the top phase, thus, cells were almost completely adsorbed to the interface. In ATPS consisting of PEG 4,000 and dextran 70,000 approximately 25% of the cells partitioned to the bottom phase, which is not consistent with charge-dependent cell partitioning. These ATPS were thus not included in further analyses. Thirdly, the same overall trends were observed when comparing the partitioning coefficients of the five cell lines in a given ATPS. The cell line A549 has the strongest affinity for the top phase, followed by HCT 116, L929, IEC-18, and INS-1E. However, absolute partitioning coefficients as well as differences between partitioning coefficients change in dependence of TLL and molecular weight of the polymers. This means that the resolution, i.e. separability, between the cell lines changes. Next, we determined enrichment/depletion factors for each cell line. In **Figure 6** the fold change of the percentage of each cell line in dependence of TLL and polymer molecular weight is summarized. The fold change of each cell line was determined using equation 3.

$$fold\ change = \frac{\%cell\ line X_{TP}}{\%cell\ line X_C} \quad (3)$$

We observed up to 3-fold enrichment of A549 cells in the top phase and > 30 fold depletion of INS-1E cells from the top phase. Moreover, the resolution of the five cell lines changes in dependence of TLL and polymer molecular weight. For example, in ATPS consisting of PEG 4,000 dextran 70,000 large differences exist between the fold change-values of IEC-18 and INS-1E, while those values are close to identical in ATPS consisting of PEG 8,000 and dextran 70,000. This indicates that by changing the polymer molec-

---

ular weight and TLL of charge-sensitive ATPS, the separation of two cell types might be possible even if initial screenings indicate that they are not. In order to evaluate the separability of the five cell lines in more detail, CCD-curves were calculated. CCD is a well-established technique in liquid-liquid extraction, and has successfully been applied in cell separation [10,13]. In CCD, the top phase is sequentially transferred, while the bottom phase is retained. Between transfers, the ATPS are mixed and allowed to settle, to achieve phase separation. Dependent on the application, the interface is either transferred or retained. Since cells partition between one of the bulk phases and the interface, the interface is retained when cells partition between top phase and interface, and transferred when the cells partition between interface and bottom phase. As a consequence, cells that partition mainly into the top phase move faster through the CCD-apparatus than cells that partition mostly to the interface. As a result, the two cell types are separated.

Based on the data shown in **Figure 5**, CCD-curves were calculated by applying equation 4 [10]:

$$F(r) = \frac{n!}{r!(n-r)!} P^r (1-P)^{n-r} \quad (4)$$

where F represents the fraction of the total cell population appearing in each theoretical cavity (r) of the CCD-apparatus, and n the total number of transfers. We calculated CCD-curves with 60 transfers for each cell line. The results are shown in **Figure 7**. The distribution between the 60 theoretical cavities is strongly dependent on the partitioning coefficients, and thus directly influences the resolution of the five cell lines [10,12]. In ATPS in which high partitioning coefficients were obtained, e.g. ATPS # 3 and # 9 the calculated CCD-curves are skewed towards the right, and only cell lines with the lowest partitioning coefficients, i.e. IEC-18 and INS-1E can be separated from the mixture. In ATPS # 9 A549 and HCT 116 have partitioning coefficients of 1 and thus do not distribute in CCD. In ATPS in which very low partitioning coefficients were obtained, e.g. ATPS # 7 and # 8 the calculated CCD-curves are skewed towards the left and very little resolution can be obtained, whereas in ATPS in which intermediate partitioning (0.5) coefficients were obtained, e.g. ATPS # 1 and # 4 the calculated CCD-curves are symmetrical and distribute evenly. Moreover, we observed that the resolution varies with TLL and polymer molecular weight at comparable partitioning coefficients. In ATPS # 1 and # 4 for example, intermediate partitioning coefficients were obtained, however, in ATPS # 4 A549 and HCT 116 cell can be separated but not in ATPS # 1. This demonstrates that the combination of PEG and dextran molecular weights can influence the separability of different cell types. Finally, the calculated CCD-curves indicate that we identified conditions that enable peak separation of four of the five cell lines from the mixture, indicating that very high purities and yields can be obtain with 60 transfers. ATPS # 5 enables the isolation of A549 with > 99.9% purity and yield, and ATPS # 2 enables the separation of L929 cells with > 99.9% purity and > 45% yield. Moreover, ATPS # 9 enables the isolation of IEC-18 with > 99.9% purity and > 95% yield and ATPS # 3 enables the isolation of INS-1E with > 99.9% purity and yield.

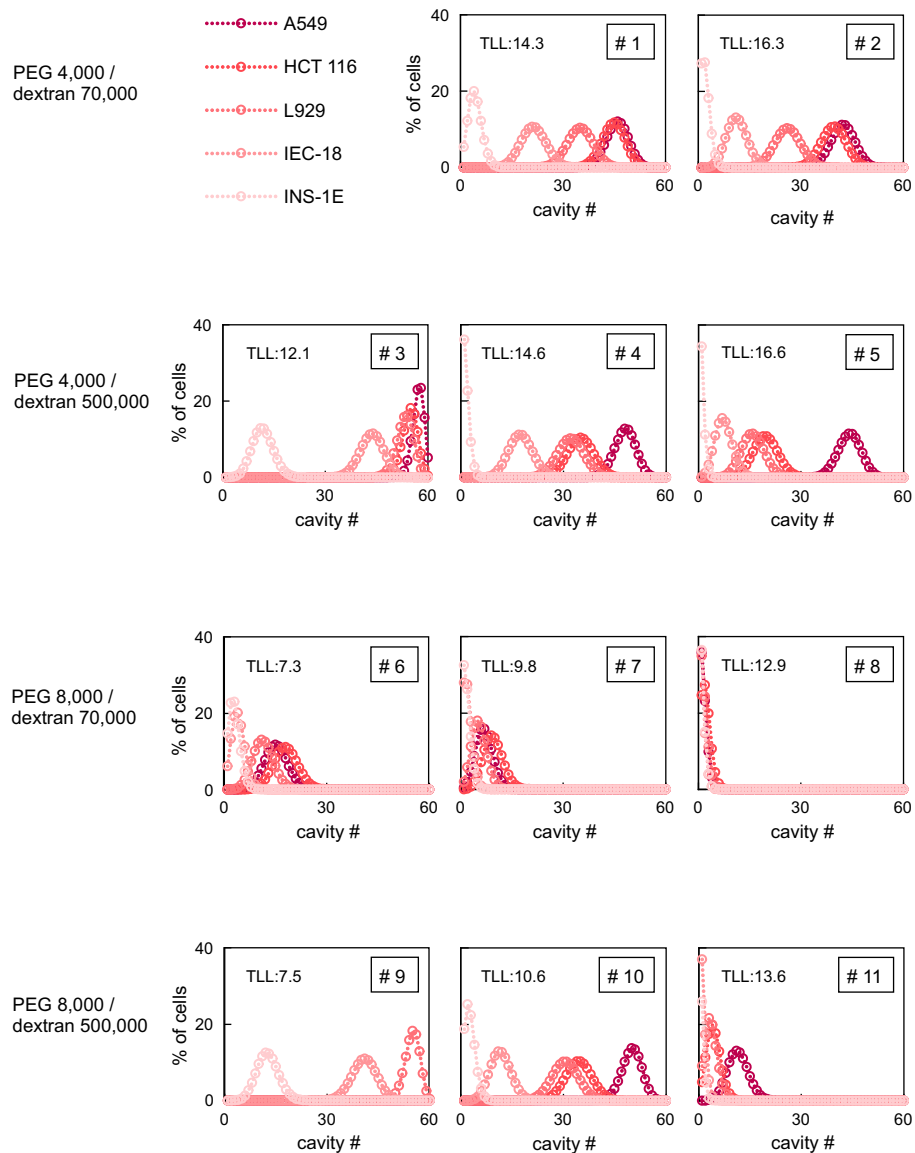


**Figure 7:** CCD-curves. CCD-curves were calculated for each cell line based on the partitioning coefficients determined by HTS, with 60 theoretical transfers for ATPS # 1–11. The corresponding ATPS composition and TLL are summarized in Table 1. TLL: tie-line length in % (w/w).

---

## 4 Discussion

The aim of the present work was to investigate the influence of polymer molecular weight and TLL on the resolution of five model cell lines in charge-sensitive ATPS. Prior to the screenings, phase diagrams for all PEG and dextran molecular weight combinations were determined. We chose charge-sensitive ATPS consisting of different combinations of PEG 4,000, 8,000, and 20,000, and dextran 70,000 and 500,000, with three TLL per combination. Trends in location and shape on the binodals are in good agreement with literature [12]. Higher polymer molecular weights result in a shift of the binodal towards lower concentrations of PEG and dextran, and the larger the difference in the molecular weights of PEG and dextran, the more asymmetric is the binodal curve [12]. Further, the influence of the barcoding strategy on the cell partitioning was evaluated prior to the screenings. We expected that staining with CellTracker<sup>TM</sup> dyes has no significant effect on the partitioning behavior, since CellTracker<sup>TM</sup> Green CMFDA und CellTracker<sup>TM</sup> Violet BMQC are cell permeant fluorescent probes that are retained inside living cells after a glutathione S-transferase mediated reaction, thus, the cell surface remains unaltered. As cell partitioning is largely dependent on cell surface properties, these dyes should not influence cell partitioning. CellTracker<sup>TM</sup> Deep Red, however, is an amine reactive dye and, thus, binds to cell surface proteins, which might influence cell partitioning by altering cell surface properties. It was thus to evaluate, whether significant effects are observed at the concentration used in this study. Partitioning studies showed no significant changes in partitioning coefficients due to CellTracker<sup>TM</sup> staining. Consequently, CellTracker<sup>TM</sup> dyes are an excellent tool for multiplexing in screenings investigating cell surface properties and enable a substantial decrease in time and material consumption. Moreover, batch variability can be eliminated by analyzing numerous cell lines in the same experiment, and the longevity (>72 h) and nontoxicity of the dyes enables prolonged screening times. Since our data indicate that low concentrations of amine-reactive dyes do not significantly alter cell partitioning in ATPS, it might be feasible to apply more complex barcoding strategies, as for example described by Krutzik *et al.* [25], which enables a further increase in throughput. Subsequently, we investigated the influence of polymer molecular weight and TLL on the resolution of five model cell lines in charge-sensitive ATPS. In contrast to smaller biomolecules, such as proteins and nucleic acids, cells partition between either top or bottom phase and the interface, depending on the ATPS composition. In general, partitioning in ATPS is driven by Brownian motion and interfacial forces. While the Brownian motion distributes the molecule or particle randomly within the ATPS, the interfacial tension acts to minimize the interfacial area. Accordingly, the interfacial tension and consequently TLL and polymer molecular weight, play a major role cell partitioning in ATPS [20]. The adsorption of cells and other particles to the interface reduces the interfacial area, and consequently the total free energy of the system. Thus, partitioning into either phase can only take place if the interaction with the cell surface is strong enough to "pull" the cells out of the interface. The higher the interfacial tension, the stronger the required interactions to enable partitioning to either bulk phase [10,12,20]. In addition, salts with polyvalent anions, e.g. phosphate have a higher affinity for the dextran-rich bottom phase than the PEG-rich top phase, while salts of halides, for example NaCl, partition almost equally between the phases. Unequal partitioning of a salt leads to the generation of an interfacial electrostatic potential difference (Donnan potential), and

molecules and particles partition in such ATPS according to their charge [10,15,26,17]. In PEG–dextran ATPS containing phosphate with moderate interfacial tensions cells can therefore be separated based on surface charge differences (charge–dependent partitioning). Cells have a negative net surface charge and consequently partition into the top phase in ATPS containing phosphate [9,17]. These phenomena were observed throughout the screening.

Both interfacial tension and Donnan potential increase with increasing TLL, but have opposite effects on cell partitioning [18,20,27]. While the Donnan potential "pulls" the cells into the top phase, the interfacial tension promotes cell adsorption at the interface. However, the increase of interfacial tension with TLL is stronger than the increase of the potential difference between the phases. Thus, at some distance from the critical point, the increase in interfacial tension offsets the increase in electrostatic potential difference [10]. Forciniti and several others [12,20,27] described a logarithmic increase of the interfacial tension with increasing TLL, and an increase in interfacial tension with polymer molecular weight at a given TLL, while a linear correlation between Donnan potential and TLL has been described in several publications [18,28,29]. These findings correlate well with the data presented in this work. With increasing TLL and polymer molecular weight, cell adsorption to the interface increased. At a PEG molecular weight of 20,000 Da no partitioning into the top phase was observed, even at low TLL. This indicates that the interfacial tension was too high for specific cell partitioning. Interestingly, the change of dextran molecular weight from 500,000 to 70,000 Da, at a given PEG molecular weight, did not result in an increase of partitioning coefficients, as assumed due to a decrease in interfacial tension, but a decrease. We assume that the partitioning coefficient of phosphate is closer to 1 in these ATPS, resulting in lower Donnan potentials. This assumption, however, will require further experimental validation. Our data showed that combinations of low PEG molecular weights, i.e.  $\leq 8,000$  Da, and high dextran molecular weights, i.e. 500,000 Da, at TLL between 10 and 15 % (w/w) enable high resolution of the five model cell lines. This is in good agreement with the findings of Albertsson [12], who describe an increase in partitioning coefficients when decreasing the PEG molecular weight. We assume that a further decrease in PEG molecular weight or an increase in dextran molecular weight might result in higher partitioning coefficients and in changes in resolutions. This however, needs to be validated in future work. Furthermore, our data indicate that charge–dependent cell separation is the major driving force, independent of TLL and polymer molecular weight, since the order of the affinity the five model cell lines exhibited to the top phase is independent of TLL and polymer molecular weight. However, the resolution between the five cell lines, which was evaluated by the calculation of CCD–curves, changes with TLL and polymer molecular weight. Thus, comprehensive screenings are necessary to investigate the separability of two cell populations. As hypothesized by Walter et al. [10], factors other than surface charge may play a minor role in charge–sensitive ATPS, and we assume that their contribution is dependent on TLL and polymer molecular weight. In addition, the strength of the Donnan potential might influence the resolution of cell lines in dependence of their net surface charge. This is supported by the fact that A549 and HCT 116, which show the highest affinity for the top phase, can be separated in ATPS with moderate mean partitioning coefficients, e.g. ATPS # 3 but not in ATPS with high mean partitioning coefficients, e.g. ATPS # 4. & 5. In addition, a number of other factors, such as phase densities and viscosities, and

---

cell size and density may play a role [12]. However, the exact role and interaction of all of these factors needs to be further investigated. In addition, the calculated CCD-curves indicate that the differences in partitioning coefficients can be used for cell separation. Our data show that we identified conditions that enable peak separation of each of the five cell lines from the mixture in a single CCD-run, with the exception of HCT 116 where two consecutive CCD-runs are necessary. However, further experimental validation of the CCD-curves is required, since they are based on an ideal model. Likewise, it should be noted that partitioning ratios of cells are highly dependent on vessel geometry, fill volume, mixing efficiency, and phase separation time. Thus, these conditions need to be identical in batch- and CCD- experiments, otherwise predicted CCD-curves will not be accurate [10]. While the calculation of fold-change values are an excellent means to evaluate separability of certain cell populations, CCD-models enable the estimation of obtainable purities, yields and overall processing time, and are thus an excellent tool for downstream process development of cell-based products. Finally, it should be noted that Walter et al. showed that cell age, cell cycle stage, and the use of enzymes for cell dissociation can influence cell partitioning [30–32]. Therefore, the effect of these parameters on cell partitioning needs to be considered when designing a purification process.

## 5 Conclusion

We investigated the influence of TLL and polymer molecular weight on cell partitioning in charge-sensitive ATPS. We showed that the interfacial tension, which is directly dependent on TLL and polymer molecular weight, is a main factor in cell partitioning. The present study showed that combinations of low PEG molecular weights and high dextran molecular weights enable high resolution of different cell lines. Moreover, we showed that the order of the affinity the five model cell lines exhibited to the top phase is independent of TLL and polymer molecular weight, indicating that cell surface charge-dependent cell partitioning due to an interfacial Donnan potential is the major driving force in ATPS containing phosphate. However, the separability of the cell lines strongly depends on TLL and polymer molecular weight. Thus, comprehensive screenings are necessary to investigate the separability of specific cell populations. Finally, we demonstrated that the combination of a HTS-platform for the investigation of cell partitioning in ATPS with the here described barcoding strategy and the application of CCD-modelling, is a powerful tool to study factors in cell separation and enables fast and directed downstream process development for cell-based products.

## 6 References

- [1] M. Al-Rubeai, M. Naciri, *Stem Cells and Cell Therapy*, Springer Netherlands, 2014.
- [2] A. Trounson, C. McDonald, *Stem Cell Therapies in Clinical Trials: Progress and Challenges*, *Cell Stem Cell*. 17 (2015) 11–22.
- [3] M.A. Fischbach, J.A. Bluestone, W.A. Lim, *Cell-Based Therapeutics: The Next Pillar of Medicine*, *Sci. Transl. Med.* 5 (2013) ps7.
- [4] P.J. Amos, E. Cagavi Bozkulak, Y. Qyang, *Methods of cell purification: a critical juncture for laboratory research and translational science*, *Cells. Tissues. Organs*. 195 (2012) 26–40.
- [5] G.M.C. Rodrigues, C.A.V. Rodrigues, T.G. Fernandes, M.M. Diogo, J.M.S. Cabral, *Clinical-scale purification of pluripotent stem cell derivatives for cell-based therapies*, *Biotechnol. J.* 10 (2015) 1103–1114.
- [6] C. Stemberger, S. Dreher, C. Tschulik, C. Piossek, J. Bet, T.N. Yamamoto, et al., *Novel serial positive enrichment technology enables clinical multiparameter cell sorting*, *PLoS One*. 7 (2012) e35798.
- [7] T.G. Fernandes, C.A.V. Rodrigues, M.M. Diogo, J.M.S. Cabral, *Stem cell bioprocessing for regenerative medicine*, *J. Chem. Technol. Biotechnol.* 89 (2014) 34–47.
- [8] A. Chen, S. Ting, J. Seow, S. Reuveny, S. Oh, *Considerations in designing systems for large scale production of human cardiomyocytes from pluripotent stem cells*, *Stem Cell Res. Ther.* 5 (2014) 12.
- [9] J.M.S. Cabral, *Cell Partitioning in Aqueous Two-Phase Polymer Systems*, *Adv. Biochem. Eng. Biotechnol.* 106 (2007) 151–171.
- [10] H. Walter, D.E. Brooks, D. Fisher, *Partitioning in Aqueous Two-Phase Systems - Theory, Methods, Uses, and Applications to Biotechnology*, Academic Press, Inc., 1985.
- [11] R.R.G. Soares, A.M. Azevedo, J.M. van Alstine, M.R. Aires-Barros, *Partitioning in aqueous two-phase systems: Analysis of strengths, weaknesses, opportunities and threats*, *Biotechnol. J.* 10 (2015) 1158–1169.
- [12] P.A. Albertsson, *Partition of Cell Particles and Macromolecules*, John Wiley & Sons, New York, 1986.
- [13] P.A. Albertsson, G.D. Barid, *Counter-Current Distribution of Cells*, *Exp. Cell Res.* 28 (1962) 296–322.
- [14] H. Walter, *Cell partitioning in two-polymer aqueous phase systems*, *TIBS*. 3.2 (1978) 97–100.

- 
- [15] P.S. Gascoine, D. Fisher, The dependence of cell partition in two-polymer aqueous phase systems on the electrostatic potential between the phases, *Biochem. Soc. Trans.* 12 (1984) 1085–1086.
- [16] G. Johansson, Partition of salts and their effects on partition of proteins in a dextran-poly(ethylene glycol)-water two-phase system, *BBA - Protein Struct.* 221 (1970) 387–390.
- [17] R. Reitherman, D. Flanagan, H. Barondes, Electromotive Phenomena in Partition of Erythrocytes in Aqueous Polymer Two Phase Systems, *Biochim. Biophys. Acta.* 297 (1973) 193–202.
- [18] W. Fan, U. Bakir, C.E. Glatz, Contribution of Protein Charge to Two-Phase Systems, *Biotechnol. Bioeng.* 59 (1998) 461–470.
- [19] H. Walter, E.J. Krob, A. Pedram, Subfractionation of cell populations by partitioning in dextran-poly (ethylene glycol) aqueous phases. "Discriminating" and "nondiscriminating" systems, *Cell Biophys.* 4 (1982) 273–284.
- [20] D. Forciniti, C.K. Hall, M.R. Kula, Interfacial tension of polyethyleneglycol-dextran-water systems: influence of temperature and polymer molecular weight, *J. Biotechnol.* 16 (1990) 279–296.
- [21] S. Zimmermann, S. Gretzinger, M.-L. Schwab, C. Scheeder, P.K. Zimmermann, S.A. Oelmeier, et al., High-throughput downstream process development for cell-based products using aqueous two-phase systems, *J. Chromatogr. A.* 1464 (2016) 1–11.
- [22] A. Merglen, S. Theander, B. Rubi, G. Chaffard, C.B. Wollheim, P. Maechler, Glucose Sensitivity and Metabolism-Secretion Coupling Studied during Two-Year Continuous Culture in INS-1E Insulinoma Cells, *Endocrinology.* 145 (2004) 667–678.
- [23] P. Bevington, D.K. Robinson, *Data reduction and error analysis for the physical sciences*, 3rd ed., McGraw Hill, 2003.
- [24] S. Zimmermann, S. Gretzinger, M.-L. Schwab, C. Scheeder, S.A. Oelmeier, A. Osberhaus, et al., High-throughput cell quantification assays for use in cell purification development – Enabling technologies for cell production, *Biotechnol. J.* 11 (2016) 676–686.
- [25] P.O. Krutzik, G.P. Nolan, Fluorescent cell barcoding in flow cytometry allows high-throughput drug screening and signaling profiling, *Nat. Methods.* 3 (2006) 361–368.
- [26] M. Vis, V.F.D. Peters, R.H. Tromp, B.H. Ern e, Donnan Potentials in Aqueous Phase Separated Polymer Mixtures, *Langmuir.* 30 (2014) 5755–5762.

- [27] Y. Liu, R. Lipowsky, R. Dimova, Concentration dependence of the interfacial tension for aqueous two-phase polymer solutions of dextran and polyethylene glycol, *Langmuir*. 28 (2012) 3831–3839.
- [28] R.S. King, H.W. Blanch, J.M. Prausnitz, Molecular thermodynamics of aqueous two-phase systems for bioseparations, *AIChE J.* 34 (1988) 1585–1594.
- [29] J.R. Luther, C.E. Glatz, Genetically engineered charge modifications to enhance protein separation in aqueous two-phase systems: Charge directed partitioning, *Biotechnol. Bioeng.* 46 (1995) 62–68.
- [30] H. Walter, K.E. Widen, Cell partitioning in two-polymer aqueous phase systems and cell electrophoresis in aqueous polymer solutions. Human and rat young and old red blood cells, *Biochim. Biophys. Acta.* 1194 (1994) 131–137.
- [31] H. Walter, F.A. Al-Romaihi, E.J. Krob, G. V Seaman, Fractionation of K-562 cells on the basis of their surface properties by partitioning in two-polymer aqueous-phase systems, *Cell Biophys.* 10 (1987) 217–32.
- [32] H. Walter, R.P. Coyle, Effect of membrane modification of human erythrocytes by enzyme treatment on their partition in aqueous dextran–polyethylene glycol two-phase systems, *Biochim. Biophys. Acta.* 165 (1968) 540–543.

**Table 1:** Summary of ATPS compositions used to investigate the influence of polymer molecular weight and TLL. All ATPS were buffered with 0.11 M sodium phosphate, pH 7.4. TLL: tie-line length.

#	Molecular Weight		Total System Composition		Bottom Phase Composition		Top Phase Composition		TLL	
	PEG [Da]	dextran [Da]	PEG [%(w/w)]	dextran [%(w/w)]	PEG [%(w/w)]	dextran [%(w/w)]	PEG [%(w/w)]	dextran [%(w/w)]	PEG [%(w/w)]	dextran [%(w/w)]
1	4,000	70,000	6.00	8.00	3.16	14.74	8.72	1.53	14.30	14.30
2	4,000	70,000	6.00	8.50	2.76	16.06	9.17	1.10	16.30	16.30
3	4,000	500,000	6.00	4.50	2.92	12.64	7.21	1.30	12.13	12.13
4	4,000	500,000	6.00	5.50	2.52	14.13	7.97	0.62	14.57	14.57
5	4,000	500,000	6.00	6.50	2.15	15.57	8.65	0.25	16.64	16.64
6	8,000	70,000	3.75	7.60	2.67	10.45	5.24	3.65	7.27	7.27
7	8,000	70,000	3.75	8.00	2.30	11.69	5.90	2.54	9.84	9.84
8	8,000	70,000	3.75	8.75	1.82	13.38	6.80	1.44	12.94	12.94
9	8,000	500,000	3.75	4.75	2.40	8.61	4.88	1.52	7.52	7.52
10	8,000	500,000	3.75	5.50	1.85	10.68	5.49	0.74	10.59	10.59
11	8,000	500,000	3.75	6.75	1.35	12.70	6.41	0.14	13.55	13.55
12	20,000	70,000	3.00	5.20	1.38	9.24	3.98	2.76	6.99	6.99
13	20,000	70,000	3.00	6.00	1.02	10.57	4.94	1.53	9.86	9.86
14	20,000	70,000	3.00	7.50	0.58	12.60	6.30	0.55	13.34	13.34
15	20,000	500,000	2.75	3.25	1.02	7.96	3.49	1.23	7.17	7.17
16	20,000	500,000	2.75	4.75	0.72	9.55	4.60	0.37	9.97	9.97
17	20,000	500,000	2.75	6.50	0.35	12.11	5.50	0.08	13.08	13.08



---

High-throughput downstream process development for  
cell-based products using aqueous two-phase systems – A case  
study

Sarah Zimmermann<sup>1</sup>, Christian Scheeder<sup>1</sup>, Philipp K Zimmermann<sup>1</sup>, Are  
Bogsnes<sup>2</sup>, Mattias Hansson<sup>3</sup>, Arne Staby<sup>4</sup>, Jürgen Hubbuch<sup>1</sup>

<sup>1</sup> Karlsruhe Institute of Technology (KIT), Institute of Process Engineering in Life Science, Section IV: Biomolecular Separation Engineering (MAB), Karlsruhe, Germany

<sup>2</sup> Novo Nordisk A/S, Biopharm Purification Development & Virology, Gentofte, Denmark

<sup>3</sup> Novo Nordisk A/S, Diabetes Research, Måløv, Denmark

<sup>4</sup> Novo Nordisk A/S, CMC Project Planning & Management, Bagsværd, Denmark

**Correspondence:** Prof. Dr. Jürgen Hubbuch, Karlsruhe Institute of Technology (KIT), Institute of Process Engineering in Life Science, Section IV: Biomolecular Separation Engineering (MAB), Engler-Bunte-Ring 3, 76131 Karlsruhe, Germany.

*E-mail:* juergen.hubbuch@kit.edu

## Abstract

The availability of preparative-scale downstream processing strategies for cell-based products presents a critical juncture between fundamental research and clinical development. Aqueous two-phase systems (ATPS) present a gentle, scalable, label-free, and cost-effective method for cell purification, and are thus a promising tool for downstream processing of cell-based therapeutics. Here, we report the application of a previously developed robotic screening platform that enables high-throughput cell partitioning analysis in ATPS. In the present case study we designed a purification strategy for two model cell lines based on high-throughput screening (HTS)-data and countercurrent distribution (CCD)-modeling, and validated the CCD-model experimentally. The obtained data show an excellent congruence between CCD-model and experimental data, indicating that CCD-models in combination with HTS-data are a powerful tool in downstream processing development. Finally, we showed that while cell cycle phase significantly influences cell partitioning, cell type specific differences in surface properties are the main driving force in charge-dependent separation of HL-60 and L929 cells. In order to design a highly robust purification process it is, however, advisable to maintain constant growth conditions.

**Keywords:** high-throughput screening (HTS), label-free cell separation, aqueous two-phase systems (ATPS), countercurrent distribution (CCD), cell cycle analysis

---

# 1 Introduction

In the past decade, the development of cell-based therapeutics has moved from academic research to pharmaceutical industry, and has reached clinical trials. The need for clinical-scale cell purification technologies thus has become more relevant than ever [1–5]. Aqueous two-phase systems (ATPS) present a gentle, scalable, label-free, and cost-effective method for cell purification, and are well established in downstream processing of biopharmaceuticals, such as protein- and DNA-based drugs [6–8]. In contrast to most state-of-the-art cell purification methods, ATPS-mediated cell separation does not require cost-intensive clinical-grade antibodies, and the associated regulatory obstacles cease to apply [4, 5, 9, 10]. Polymer-polymer ATPS, particularly polyethylene glycol (PEG)-dextran ATPS, have been extensively used to separate cells according to their physical and chemical surface properties [7, 11]. Using multi-step processes such as countercurrent distribution (CCD), even complex cell mixtures and closely related cell types can be separated with high resolution and selectivity [7, 12, 13]. While the mechanisms underlying cell partitioning in ATPS are not entirely understood, two main factors in cell separation have been identified: surface charge and membrane lipid composition. Surface charge-dependent cell separation can be achieved in ATPS containing phosphate (charge-sensitive ATPS), and partitioning coefficients of distinct cell types could be correlated to their electrophoretic mobility. Charge-independent cell separation is possible in ATPS containing sodium chloride (charge-insensitive ATPS), and partitioning coefficients of distinct cell types have been correlated with their membrane lipid composition [7, 11, 14, 15]. These phenomena are based on different partitioning properties of the respective salts. While sodium chloride partitions virtually equally between the phases, phosphate has a stronger affinity to the dextran-rich bottom phase, resulting in an interfacial electrostatic potential difference (Donnan potential). This in turn enables charge-independent and charge-dependent cell partitioning, respectively [7, 16, 17]. ATPS are thus a unique tool for cell separation and different cell types have been separated with high selectivity and resolution, including cell types differing only in age and cell cycle stage [7, 18, 19].

Nevertheless, the development of effective downstream processes for cell-based therapeutics requires the optimization of various different parameters, hampering the widespread application of ATPS in cell purification. In addition, it is unclear whether the high selectivity, e.g. resolution of cell cycle phases, interferes with the feasibility of a robust purification process. In former work, we developed an automated and miniaturized high-throughput screening (HTS) platform for the analysis of cell partitioning in ATPS [13]. We showed that the combination of HTS and CCD-modeling enables fast, cost-effective, and directed downstream process development for cell-based products. In the present work, we used this HTS-platform to conduct a case study with the model cell lines HL-60 and L929. We designed a purification strategy based on HTS-data and CCD-modeling and validated the CCD-model experimentally. Finally, we analyzed the influence of cell cycle phase on cell partitioning and the resolution of HL-60 and L929, which may interfere with the robustness of a purification process. As cells pass through the cell cycle a multitude of changes takes place, such as changes in cell volume, density, DNA content, protein expression, and consequently cell surface properties [19–22]. We thus evaluated to which extent cell cycle stage, and thus growth phase, influences a purification process.

## 2 Materials & Methods

### 2.1 Disposables

1.3 mL deep well plates (Nalgene Nunc, Rochester, NY, USA, cat. 260252) and 96-well U-bottom plates (BD Falcon™, Franklin Lakes, NJ, USA, cat. 353910) were used for ATPS preparation and flow cytometry, respectively. For any other purpose, polypropylene flat-bottom microplates (Greiner Bio-One, Kremsmuenster, Austria, cat. 655261) were used.

### 2.2 Software and data processing

The Tecan Freedom Evo 200 was controlled by Evoware 2.5 SP2 standard (Tecan, Crailsheim, Germany). For advanced applications, i.e. sampling and cell resuspension, visual basic scripts were fed into Evoware. Data evaluation and visualization was performed with Excel 2013 (Microsoft, Redmond, WA, USA) and Matlab R2014a (The MathWorks, Natick, ME, USA). Statistical data analysis was performed in Matlab R2014a. BD FACS-Diva 8.0 (BD Biosciences, San Jose, CA, USA) was used for raw data analysis, to control the BD LSR Fortessa Cell Analyzer, and to calculate compensation of spectral overlap. Visualization of flow cytometry data was performed in Flow Jo V10 (Tree Star, Ashland, OR, USA).

### 2.3 Preparation of buffers and stock solutions

All buffers and polymer solutions were prepared as previously described [13].

### 2.4 Cell culture

All cell culture reagents were purchased from Life Technologies™. HL-60 and L929 cells were cultured as previously described [13]. The suspension cell line HL-60 was split to a concentration of  $2 \times 10^5$  cells per mL every 3–4 days to a maximum passage number of 100. L929 cells were split every 3–4 days to a concentration of  $2 \times 10^4$  cells per cm<sup>2</sup> for a maximum of 20 passages.

### 2.5 Cell Tracker™, antibody and viability staining

For partitioning analysis of HL-60 and L929 cells, HL-60 cells were stained with Cell-Tracker™ Orange CMRA (Life Technologies™) as previously described [13]. For viability staining, cells were stained with 7-AAD (Biolegend, San Diego, CA, USA) according to the manufacturer's instructions.

### 2.6 Cell quantification using high-throughput flow cytometry

Cells were quantified using high-throughput flow cytometry as described in previous work [13, 23].

---

## 2.7 Automated high-throughput screening of cell partitioning in aqueous two-phase systems

The automated HTS-method was used as described in previous work [13]. The screening was performed on a Tecan Freedom Evo<sup>®</sup> 200 liquid-handling station (LHS). Next, the sample plates were transferred to the high-throughput sampler of the BD LSR Fortessa for cell quantification and analysis. ATPS were prepared in a 1.3 mL 96-well plate (final volume: 637  $\mu\text{L}$ ). After mixing and addition of cells ( $5 \times 10^5$  cells per well), phase separation was achieved by settling (30 minutes, RT) and sampling was performed as previously described [13]. During the sampling procedure samples were 5-fold diluted in staining buffer. Staining was subsequently performed by adding an equal volume of 2 x staining buffer containing 7-AAD. After incubation for 10 minutes at RT in the dark, flow cytometric analysis was performed.

## 2.8 Multi-stage partitioning

Multi-stage partitioning was performed manually in 1.5 mL Eppendorf tubes with a total volume of 637  $\mu\text{L}$  (equal volumes of top and bottom phase). Cells were prepared as described above and added in a volume of 13  $\mu\text{L}$  at a concentration of  $3.8 \times 10^7$  cells per mL. The ATPS were mixed by inverting the tubes five times, and the phases were allowed to separate by gravity (40 min, RT). Subsequently, the top phase was carefully removed and transferred to an equal volume of bottom phase. 30  $\mu\text{L}$  sample were taken and sample dilution and flow cytometric analysis was performed identically to the HTS-screening.

## 2.9 Cell cycle analysis

Cell cycle analysis was performed by DNA-content analysis with 4', 6-diamidino-2-phenylindole (DAPI). The experiment layout was the same as described above to ensure comparability between the experiments.  $3 \times 10^6$  cells per well in 13  $\mu\text{L}$  PBS were added to each well. After mixing and phase separation, 100  $\mu\text{L}$  were manually sampled from each well. The controls were resuspended before sampling. 2 x 8 control and ATPS samples were pooled to obtain sufficient cell numbers for cell cycle analysis. The pooled samples were washed twice with 15 mL PBS + 10% FBS and fixed with ice-cold 70% ethanol at 4°C overnight. Next, cells were washed twice and resuspended in 500  $\mu\text{L}$  staining buffer + 1  $\mu\text{g}/\text{mL}$  DAPI (Life Technologies<sup>™</sup>). After incubation for 30 minutes at 37°C, the samples were analyzed by flow cytometry. Measurement was performed at a maximum acquisition rate of 400 events per second, and 150.000 events were recorded per sample.

#### **2.10 Statistical data analysis**

Pre-processing of screening data was performed as described in a previous publication [13]. Mean comparison was performed by applying a two-sided student's  $t$ -test, provided that equal variances were asserted by an  $F$ -test. Error propagation was considered throughout our analyses [24]. DNA-content based cell cycle analysis was performed in FlowJo, using the Watson pragmatic model. Flow cytometry data were pre-processed to eliminate debris and aggregates. Discrimination between the two cell types was performed based on CellTracker<sup>TM</sup> Orange CMRA staining and DNA-content was determined by the DAPI signal.

### 3 Results

#### 3.1 Resolution of the two model cell lines HL-60 and L929 in dependence of salt composition, pH, and TLL

The aim of the first part of this case study was to optimize separation conditions for two model cell lines based on HTS-data. We chose the promyelocytic cell line HL-60 and the murine fibroblast cell line L929, since we expected these cell lines to differ significantly in their surface properties due to their different origins. In a series of screenings, we investigate the influence of tie-line length (TLL), salt composition, and pH on the resolution of the two cell lines. To enable multiplexing, we stained the HL-60 cells with Cell Tracker™ Orange CMRA. An overview of the staining and data deconvolution strategy is illustrated in **Figure 1**. In analogy to previous studies [13], we investigated the resolution of HL-60 and L929 cells in dependence of the ratio of sodium phosphate (NaPi) and sodium chloride (NaCl), pH, and TLL, representing conditions where both charge-dependent and charge-independent partitioning can be observed [7, 25].

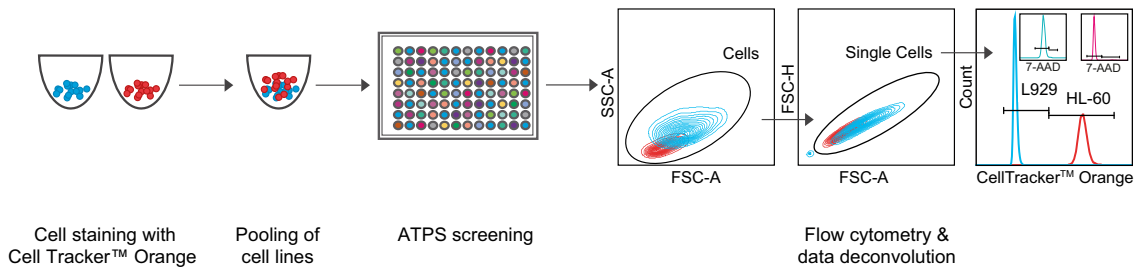


**Figure 1:** Multiplexing in HT-partitioning analysis in ATPS. HL-60 cells are stained with CellTracker™ Orange CMRA and pooled with unstained L929 cells before HT-partitioning analysis in ATPS. Cell quantification and analysis is performed by HT-flow cytometry. After data deconvolution, the partitioning coefficients of the two cell lines can be determined. The live cell population of each cell line was gated based on 7-AAD staining. FSC-A: Forward scatter peak area, SSC-A: side scatter peak area, FSC-H: Forward scatter peak height. HT: high-throughput.

The partitioning coefficient  $P$  of each cell line was defined as the fraction of cells in the top phase (equation 1). The partitioning coefficient for the bottom phase was determined accordingly.

$$P = \frac{Count_{TP} \times V_{TP}}{Count_C \times V_C} \quad (1)$$

*TP: top phase; C: PBS control; V: volume*

In **Figure 2A & B** the partitioning coefficients of each cell line in dependence of salt composition, pH, and TLL are summarized. ATPS compositions are summarized in **Table 1**. In addition, we determined enrichment/ depletion factors for the two cell lines. In **Figure 2C & D** the fold change of the percentage of each cell line in dependence of salt composition, pH, and TLL is summarized, which was determined using equation 2.

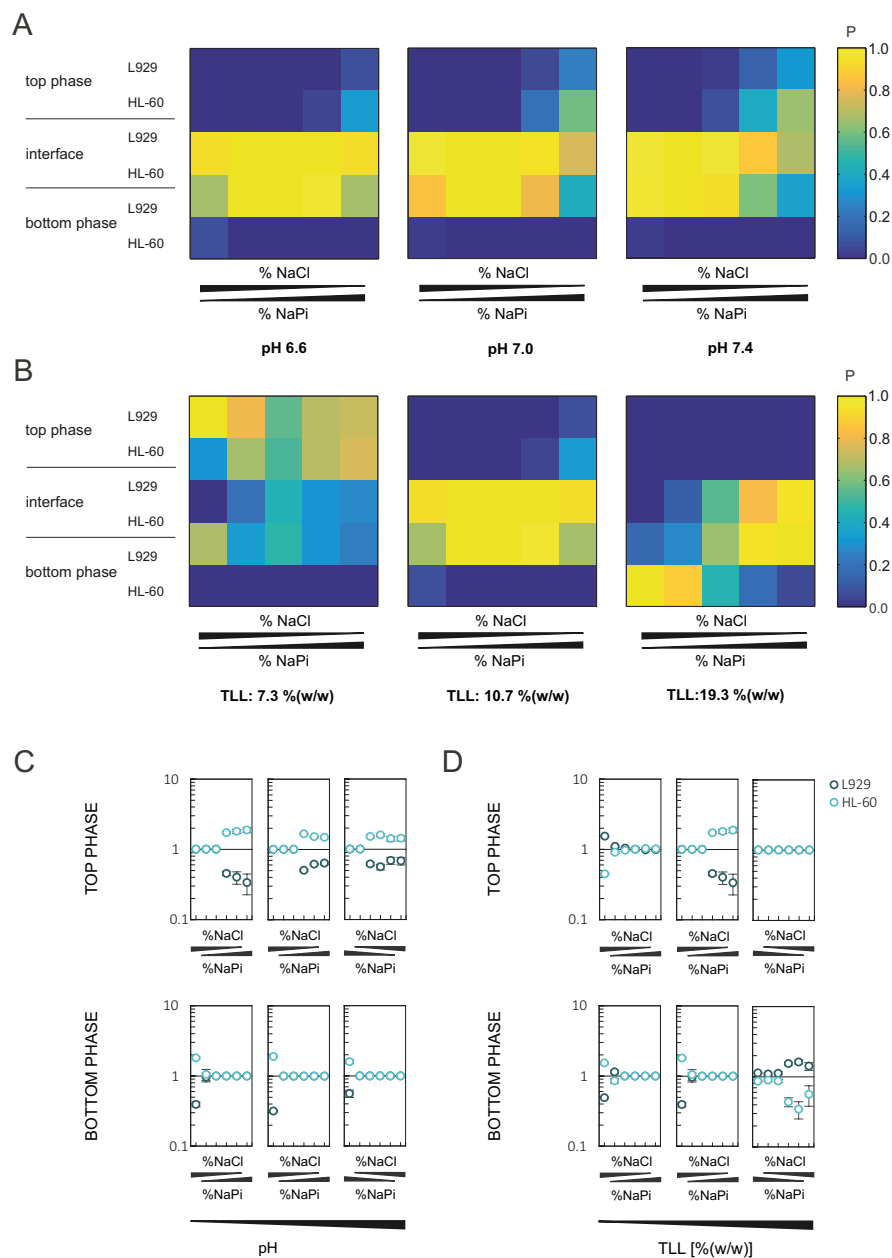


**Figure 2:** HT-partitioning analysis of the cell lines HL-60 and L929 in PEG-dextran ATPS, in dependence of salt composition, pH, and TLL. (A–B) Partitioning coefficients ( $P$ ) of HL-60 and L929. Cell partitioning was analyzed in PEG 8,000–dextran 500,000 ATPS with varying ratios of NaPi and NaCl. While the overall salt concentration was kept constant and isotonic, the molar ratio of NaPi and NaCl were varied (90%, 70%, 50%, 30%, 10% and 0% mM NaCl) at an intermediate TLL of 10.7% (w/w) at pH 6.6, 7.0 and 7.4 (A), and at three different TLL at pH 6.6 (B). The heat maps represent the mean partitioning coefficients ( $P$ ) of live cells in each phase ( $n=2$  technical replicates). (C–D) Fold change of the percentage of HL-60 and L929 compared to a PBS control at an intermediate TLL of 10.7 at pH 6.6, 7.0 and 7.4 (C), and at three different TLL (7.3, 10.7, and 19.3 % (w/w)) at pH 6.6 (D). Error bars represent s.d. ( $n=2$  technical replicates). TLL: tie-line length, HT: high-throughput.

$$\text{fold change} = \frac{\% \text{cell line } X_{\text{TP}}}{\% \text{cell line } X_{\text{BP}}} \quad (2)$$

As expected, we observed considerable differences in partitioning coefficients of HL-60 and L929. At an intermediate TLL of 10.7% (w/w), both cell lines partitioned increasingly to the top phase with increasing phosphate concentration. We found that HL-60 has significantly higher partitioning coefficients than L929 at high phosphate concentrations, i.e. in charge-sensitive ATPS. We further observed a slight pH-dependence, with an increase of partitioning coefficients with increasing pH (**Figure 2A**). The fold enrichment of HL-60 in the top phase, on the other hand, decreases with increasing pH (**Figure 2C**). Moreover, we observed excellent resolution of HL-60 and L929 in charge-sensitive ATPS at intermediate TLL (**Figure 2B & D, middle panel**), but not close to the critical point (**Figure 2B & D, left panel**).

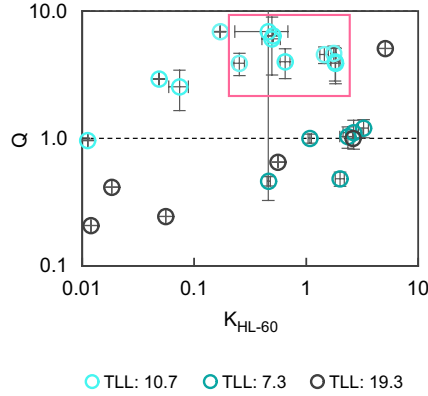


**Figure 3:** Selection of separation conditions for HL-60 and L929. The partitioning ratio of HL-60 ( $K_{\text{HL-60}}$ ) was plotted against the quotient of the partitioning ratios of HL-60 and L929 ( $Q$ ) obtained from the data shown in **Figure 2**. The red box indicates the conditions selected for multi-stage partitioning experiments. Error bars represent s.d. ( $n=2$  technical replicates).

At short TLL (7.3% (w/w)) and low phosphate concentrations, i.e. charge-insensitive ATPS, we observed a significant enrichment of L929 cells in the top phase (**Figure 2B & D, left panel**). Further, we observed no partitioning into the top phase at long tie-lines (13.3% (w/w)) (**Figure 2B, right panel**). At high phosphate concentrations, both cell lines accumulated at the interface. With decreasing phosphate concentration, however, we observed increasing partitioning into the bottom phase and an enrichment of L929 cells (**Figure 2B & D, right panel**). To select ATPS that enable maximal resolution, partitioning ratios ( $K$ ), and the quotient of the partitioning ratios of HL-60 and L929 ( $Q$ ) were calculated as follows:

$$K = \frac{P}{I} \quad (3)$$

$$Q = \frac{K_{\text{CD11b-negative}}}{K_{\text{CD11b-positive}}} \quad (4)$$

where  $P$  represents the fraction of cells in the top phase and  $I$  the fraction of cells at the interface. We investigated  $Q$  in dependence of  $K$  to select ATPS that give maximal resolution of the two cell lines (**Figure 3**). We obtained partitioning ratios over three orders of magnitude and  $Q$ -values between 0.2 and 6.9. As previously shown [13], ATPS that yield  $K$ -values around 1 and  $Q$ -values  $\ll 1 \gg$  enable maximal resolution in CCD. All ATPS that fulfill these criteria were ATPS with high phosphate concentrations and intermediate TLL (10.7% (w/w)). For further studies we chose an ATPS consisting of 4% PEG 8,000, 5% dextran 500,000, 0.11M NaPi, at pH 7.4, with  $K$ -values of  $0.5 \pm 0.1$  (mean  $\pm$  s.d.) and  $1.8 \pm 0.1$  for L929 and HL-60, respectively, and a  $Q$ -value of  $4.0 \pm 1.2$ . Based on earlier studies we prioritized  $K$ -values over  $Q$ -values, since this enabled maximal resolution in a CCD-model [13].

**Table 1.** Summary of ATPS-compositions.

ATPS	PEG 8,000	Dextran 500,00	Sodium Phosphate	Sodium Chloride	pH	Sodium Chloride
[#]	[% (w/w)]	[% (w/w)]	[mM]	[mM]	[-]	[% mM]
1	4	4	110	0	6.6	0
2	4	4	100	10	6.6	10
3	4	4	80	40	6.6	30
4	4	4	60	60	6.6	50
5	4	4	40	90	6.6	70
6	4	4	10	120	6.6	90
7	4	5	110	0	6.6	0
8	4	5	100	10	6.6	10
9	4	5	80	40	6.6	30
10	4	5	60	60	6.6	50
11	4	5	40	90	6.6	70
12	4	5	10	120	6.6	90
13	4	5	110	0	7.0	0
14	4	5	100	10	7.0	10
15	4	5	80	40	7.0	30
16	4	5	60	60	7.0	50
17	4	5	40	90	7.0	70
18	4	5	10	120	7.0	90
19	4	5	110	0	7.4	0
20	4	5	100	10	7.4	10
21	4	5	80	40	7.4	30
22	4	5	60	60	7.4	50
23	4	5	40	90	7.4	70
24	4	5	10	120	7.4	90
25	5	7	110	0	6.6	0
26	5	7	100	10	6.6	10
27	5	7	80	40	6.6	30
28	5	7	60	60	6.6	50
29	5	7	40	90	6.6	70
30	5	7	10	120	6.6	90

### 3.2 Validation of CCD-model

The aim of the second part of this case study was to validate a CCD-model based on batch-data. To facilitate manual handling, these experiments were performed in 1.5 mL Eppendorf tubes instead of 96-well plates. Since cell partitioning in ATPS is highly dependent on fill volume, vessel geometry, and mixing intensity, batch experiments were performed to optimize phase separation time and obtain accurate partitioning coefficients (**Figure 4A**).

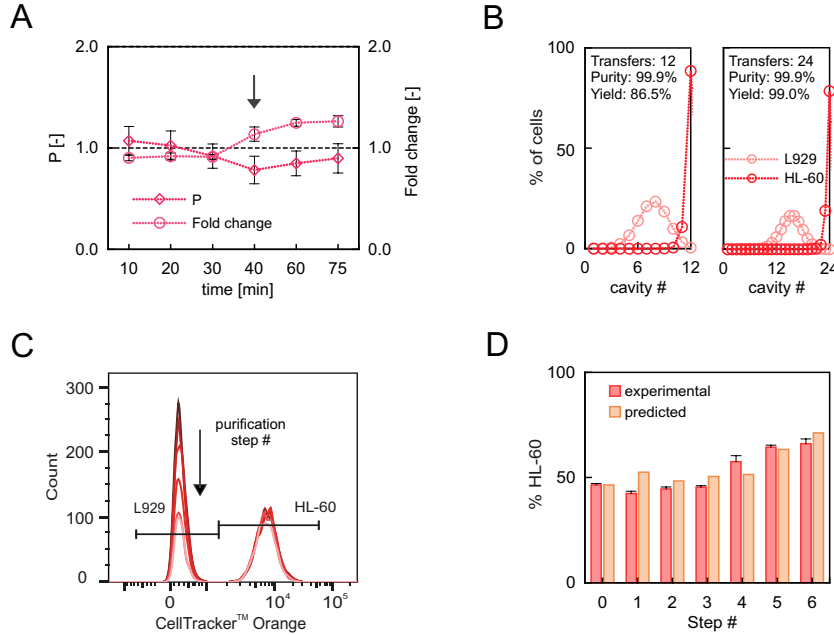


**Figure 4:** Validation of the CCD-model. (A) Selection of a suitable phase separation time for manual multi-stage partitioning experiments. Cell partitioning was analyzed in an ATPS consisting of 4% PEG 8,000, 5% dextran 500,000, 0.11 M NaPi, pH 7.4, as indicated in **Figure 3**. The partitioning coefficient for the entire cell population is shown on the primary ordinate and the fold change of HL-60 cells in the top phase is depicted on the secondary ordinate. The arrow represents the selected phase separation time. Error bars represent s.d. ( $n = 2$  technical replicates). (B) CCD-model with 12 (left panel) and 24 (right panel) theoretical transfers for the conditions indicated in (A). (C–D) Experimental validation of the CCD-model shown in (B). (C) Flow cytometric analysis of the ratio of HL-60 and L929 cells over 6 partitioning steps. The two cell lines were distinguished based on CellTracker™ Orange CMRA staining. Lighter colors were selected for increasing numbers of partitioning steps. (D) Comparison of theoretical and experimental CCD-data. Error bars represent s.d. ( $n = 2$  technical replicates).

As expected, we observed discrepancies in partitioning coefficients and fold change of the percentage of HL-60 cells in the top phase. In addition, the required phase separation time was significantly longer, with 60 instead of 30 minutes to obtain maximal resolution. For the experimental validation of the CCD-model, we chose a phase separation time of 40 minutes, which is the shortest phase separation time that enables resolution of the two cell lines. We determined partitioning coefficients of  $1.00 \pm 0.12$  (mean  $\pm$  s.d.) and  $0.64 \pm 0.15$  for HL-60 and L929, respectively. Based on these data the CCD-model was calculated as follows:

$$F(r) = \frac{n!}{r!(n-r)!} P^r (1-P)^{n-r} \quad (5)$$

where  $F$  represents the fraction of the total cell population appearing in each theoretical cavity ( $r$ ) of the CCD-apparatus, and  $n$  represents the total number of transfers. CCD-curves with 12 and 24 transfers are shown in **Figure 4B**. At a target purity of 99.9%,

86.5% and 99.0% yield can be achieved with 12 and 24 transfers, respectively. Due to the long phase separation times, only 5 consecutive transfers were performed manually. Flow cytometry data and the comparison of modeling and experimental data are shown in **Figure 4C & D**. Since the partitioning coefficient of HL-60 cells is 1.0, L929 cells are "washed-out" in each step, while the number of HL-60 cells remains almost constant (**Figure 4C**). In addition, the experimental data show excellent congruence with the CCD-model (**Figure 4D**). It should be noted that each purification step was modeled based on the results of the previous purification step, to avoid bias due to imprecise phase transfer.

### 3.3 Influence of cell cycle phase on partitioning in charge-sensitive ATPS

Aim of the third part of this case study was to investigate how cell cycle phase, and thus cell growth, influences cell partitioning in charge-sensitive ATPS. For this part of the study we selected conditions that enable maximal differences in partitioning coefficients and thus prioritized Q-values over K-values. The selected ATPS consisted of 4% PEG 8,000, 5% dextran 500,000, 0.11 M NaPi, at pH 6.6. Literature indicates that cell partitioning in charge-sensitive ATPS is dependent on cell cycle stage [19, 21], however, more comprehensive studies have not been conducted so far. We thus aimed to analyze to which degree cell partitioning is based on cell type specific properties, and to which degree on the cells cycle phase. This was done by analyzing cell cycle distribution of HL-60 and L929 cells after partitioning in ATPS, compared to PBS controls (**Figure 5**). As in previous screenings, discrimination between the two cell lines was performed based on CellTracker<sup>TM</sup> Orange CMRA staining and we observed a fold change of the percentage of HL-60 and L929 cells in the top phase of  $1.7 \pm 0.03$  and  $0.3 \pm 0.01$  (mean  $\pm$  s.d.), respectively (**Figure 5A**). Subsequently, DNA-content based cell cycle analysis was performed for each cell line individually, and cell cycle distribution after partitioning in ATPS was compared to PBS controls (**Figure 5B-D**). We observed a significant depletion ( $p < 0.05$ ) of S-phase cells from the top phase for both cell lines. The fold change of S-phase cells was  $0.8 \pm 0.04$  and  $0.7 \pm 0.08$  (mean  $\pm$  s.d.) for HL-60 and L929, respectively (**Figure 5D**). While the overall trends were comparable for both cell lines, a significant enrichment ( $p < 0.05$ ) of G<sub>2</sub>/M-phase cells was only observed for HL-60 cells with a fold change of  $1.3 \pm 0.06$  (mean  $\pm$  s.d.), while no significant enrichment was observed for L929 cells.

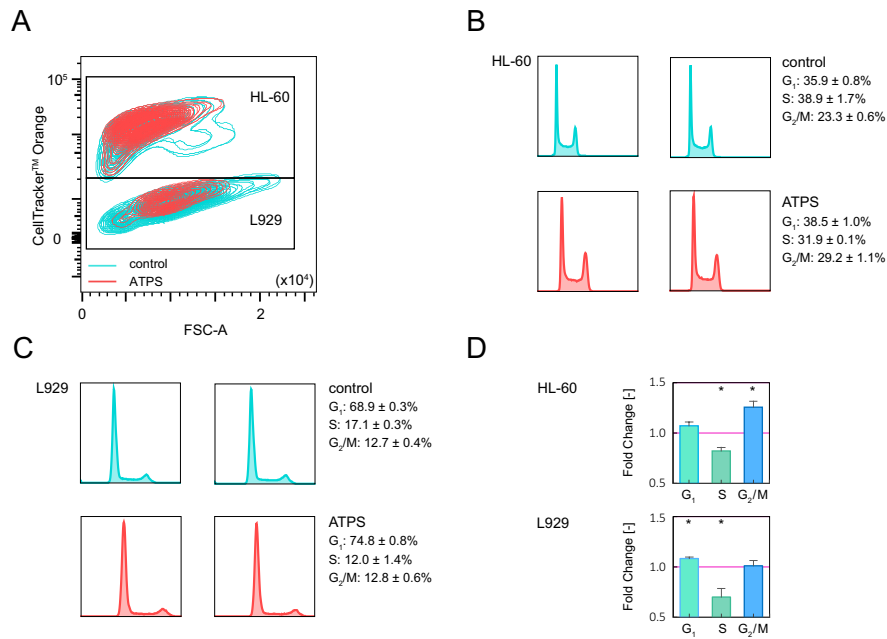


**Figure 5:** Influence of cell cycle stage on the partitioning in charge-sensitive ATPS. (A) The model cell lines HL-60 and L929 were stained with CellTracker™ Orange CMRA, and partitioning was analyzed in a charge-sensitive ATPS at a TLL of 10.7 (4% PEG 8,000, 5% dextran 500,000, 0.11 M NaPi, pH 6.6). (B–C) After data deconvolution, DNA-content dependent cell cycle distribution of both cell lines was analyzed based on the DAPI-signal using the Watson pragmatic model. Mean ± s.d. of the percentage of cells in each cell cycle phase (n=2 technical replicates) are indicated. (D) Fold change of the percentage of cells in each cell cycle phase compared to a PBS control. Asterisks indicate significant changes ( $p < 0.05$ ) as determined by a Student's *t*-test. Error bars represent s.d. (n= 2 technical replicates).

## 4 Discussion

The aim of this case study was to optimize separation conditions for the two model cell lines HL-60 and L929 based on HTS-data and CCD-modelling. Further, we aimed to validate the CCD-model experimentally and investigate the influence of cell cycle phase on cell partitioning.

In the first part of this study we performed a series of screenings to investigate the influence of TLL, salt composition, and pH on the resolution of the two cell lines (**Figure 2**). As expected, we observed the same overall trends described before [7, 13]. In addition, HL-60 cells showed significantly higher partitioning coefficients than L929 cells in charge-sensitive ATPS, indicating a higher net surface charge [7]. Since the electrostatic potential difference increases with increasing TLL [26–28], we observed excellent resolution of HL-60 and L929 in charge-sensitive ATPS, at intermediate TLL but not close to the critical point. In charge-insensitive ATPS, a significant enrichment of L929 cells was observed in the top phase, indicating differences in the membrane lipid composition of the two cell lines [7, 29]. Even though the electrostatic potential difference increases with increasing TLL [26–28], we observed no partitioning into the top phase at long tie-lines. This is due to the fact that at some distance from the critical point, the increase in interfacial tension offsets the increase in electrostatic potential difference [7]. Interestingly, we observed cell partitioning into the bottom phase and an enrichment of L929 cells at intermediate and long tie-lines at low phosphate concentrations. This has not been associated with specific cell surface characteristics so far. However, we observed an enrichment of HL-60 cells in all of the ATPS, indicating that charge-associated properties rather than membrane lipid associated properties are implied. Based on these HTS-data we selected ATPS that enable optimal separation using CCD (**Figure 3**) [13].

In the second part of this study we validated the CCD-model experimentally (**Figure 4**). This has been performed for small molecules and proteins but not for mammalian cells, however, it has been assumed that CCD-models are highly accurate if all relevant parameters are kept constant and the cell types to be separated are homogenous [7, 12, 30]. As previously described, cell partitioning and phase separation times are highly dependent on vessel geometry, fill volume, and mixing intensity [7, 11], thus, we observed significant differences in partitioning coefficients and phase separation times when using 1.5 mL Eppendorf tubes instead of 96-well plates. Experimental validation of the CCD-model showed excellent congruence between the model and experimental data. This indicates that predicted CCD-curves are highly accurate if all relevant parameters are kept constant and phase transfer is accurate. The strength of this HTS-platform is its versatility and applicability for most labware types, which enable direct optimization of all relevant parameters in high-throughput. Depending on target yield and purity, and maximal processing time, separation conditions can be further optimized and final purification conditions can be chosen. In future studies, the use of design of experiments (DoE) will enable the simultaneous optimization of numerous parameters, and the fast and cost-effective design of a purification process for various applications.

In the third part of this study we investigated the influence of cell cycle phase on a purification process. Our data show a significant decrease in partitioning coefficients of S-phase cells and an enrichment of cells in in G<sub>1</sub>- & G<sub>2</sub>/M-phase (**Figure 5**). The change of cell surface properties with cell growth and cell cycle phase has been described

---

in several publications [19–22]. Pinaev and Brent & Foster described an increase in electrophoretic mobility of mitotic / metaphase HeLa cells, as well as an increase of their partitioning coefficients in charge-sensitive ATPS, indicating an increase in cell surface charge. We observed this trend for HL-60 cells, but not for L929 cells. This may, however, be due to the low percentage of G<sub>2</sub>/M-phase cells of L929, which makes small changes in the percentage of G<sub>2</sub>/M-phase cells more difficult to detect. In addition, Walter et al. described an increase in partitioning coefficients of K-562 cells in late S-phase and G<sub>2</sub>/M-phase compared to cells in G<sub>0</sub>/G<sub>1</sub> and early M-phase. These findings are thus in excellent agreement with the data shown here. Moreover, our data show that while cell cycle phase significantly influences cell partitioning, cell type specific differences in surface properties have a much greater influence on cell partitioning. This is supported by the fact that the two cell lines showed almost ideal behavior in multi-stage partitioning. If the heterogeneity due to differences in cell cycle distribution had a major influence on cell partitioning we would have observed major discrepancies between theoretical and experimental CCD-data. It can, however, not be excluded that we may observe slight discrepancies at a higher number of transfers, due to differences in the partitioning based on cell cycle phase. To conclude, even though cell cycle phase significantly influences cell partitioning, cell type specific differences in surface properties have a much greater influence on partitioning. Nonetheless, growth phase should be kept constant in order to obtain a highly robust purification process.

## 5 References

- [1] Al-Rubeai, M., Naciri, M., *Stem Cells and Cell Therapy*, Springer Netherlands, 2014.
- [2] Trounson, A., McDonald, C., Stem Cell Therapies in Clinical Trials: Progress and Challenges. *Cell Stem Cell* 2015, 17, 11–22.
- [3] Fischbach, M.A., Bluestone, J.A., Lim, W.A., Cell-Based Therapeutics: The Next Pillar of Medicine. *Sci. Transl. Med.* 2013, 5, ps7.
- [4] Amos, P.J., Cagavi Bozkulak, E., Qyang, Y., Methods of cell purification: a critical juncture for laboratory research and translational science. *Cells. Tissues. Organs* 2012, 195, 26–40.
- [5] Rodrigues, G.M.C., Rodrigues, C.A.V., Fernandes, T.G., Diogo, M.M., et al., Clinical-scale purification of pluripotent stem cell derivatives for cell-based therapies. *Biotechnol. J.* 2015, 10, 1103–1114.
- [6] Cabral, J.M.S., Cell Partitioning in Aqueous Two-Phase Polymer Systems. *Adv. Biochem. Eng. Biotechnol.* 2007, 106, 151–171.
- [7] Walter, H., Brooks, D.E., Fisher, D., *Partitioning in Aqueous Two-Phase Systems – Theory, Methods, Uses, and Applications to Biotechnology*, Academic Press, Inc., 1985.
- [8] Soares, R.R.G., Azevedo, A.M., van Alstine, J.M., Aires-Barros, M.R., Partitioning in aqueous two-phase systems: Analysis of strengths, weaknesses, opportunities and threats. *Biotechnol. J.* 2015, 10, 1158–1169.
- [9] Chen, A., Ting, S., Seow, J., Reuveny, S., et al., Considerations in designing systems for large scale production of human cardiomyocytes from pluripotent stem cells. *Stem Cell Res. Ther.* 2014, 5, 12.
- [10] Fernandes, T.G., Rodrigues, C.A.V., Diogo, M.M., Cabral, J.M.S., Stem cell bioprocessing for regenerative medicine. *J. Chem. Technol. Biotechnol.* 2014, 89, 34–47.
- [11] Albertsson, P.A., *Partition of Cell Particles and Macromolecules*, John Wiley & Sons, New York, 1986.
- [12] Albertsson, P.A., Barid, G.D., Counter-Current Distribution of Cells. *Exp. Cell Res.* 1962, 28, 296–322.
- [13] Zimmermann, S., Gretzinger, S., Schwab, M.-L., Scheeder, C., et al., High-throughput downstream process development for cell-based products using aqueous two-phase systems. *J. Chromatogr. A* 2016, 1464, 1–11.
- [14] Walter, H., Cell partitioning in two-polymer aqueous phase systems. *TIBS* 1978, 3, 97–100.

- 
- [15] Gascoine, P.S., Fisher, D., The dependence of cell partition in two-polymer aqueous phase systems on the electrostatic potential between the phases. *Biochem. Soc. Trans.* 1984, *12*, 1085–1086.
- [16] Johansson, G., Partition of salts and their effects on partition of proteins in a dextran-poly(ethylene glycol)-water two-phase system. *BBA - Protein Struct.* 1970, *221*, 387–390.
- [17] Reitherman, R., Flanagan, D., Barondes, H., Electromotive Phenomena in Partition of Erythrocytes in Aqueous Polymer Two Phase Systems. *Biochim. Biophys. Acta* 1973, *297*, 193–202.
- [18] Walter, H., Krob, E.J., Garza, R., Ascher, G.S., Partition and countercurrent distribution of erythrocytes and leukocytes from different species. *Exp. Cell Res.* 1969, *55*, 57–64.
- [19] Walter, H., Al-Romaihi, F.A., Krob, E.J., Seaman, G. V, Fractionation of K-562 cells on the basis of their surface properties by partitioning in two-polymer aqueous-phase systems. *Cell Biophys.* 1987, *10*, 217–232.
- [20] Pinaev, G., Hoorn, B., Albertsson, P.A., Counter-Current Distribution of HeLa and Mouse Mast Cells in Different Stages of the Life Cycle. *Exp. Cell Res.* 1976, *98*, 127–135.
- [21] Brent, T.P., Forrester, J.A., Changes in Surface Charge of HeLa Cells during the Cell Cycle. *Nature* 1967, *215*, 92 – 93.
- [22] Gersten, D.M., Bosmann, H.B., Behaviour in Two-Phase Aqueous Polymer Systems of L5178Y Mouse Leukemic Cells. II. The Lag and Exponential Phases of Growth. *Exp. Cell Res.* 1974, *88*, 225–230.
- [23] Zimmermann, S., Gretzinger, S., Schwab, M.-L., Scheeder, C., et al., High-throughput cell quantification assays for use in cell purification development – Enabling technologies for cell production. *Biotechnol. J.* 2016, *11*, 676–686.
- [24] Bevington, P., Robinson, D.K., *Data reduction and error analysis for the physical sciences*, McGraw Hill, 2003.
- [25] Walter, H., Krob, E.J., Pedram, A., Subfractionation of cell populations by partitioning in dextran-poly (ethylene glycol) aqueous phases. "Discriminating" and "nondiscriminating" systems. *Cell Biophys.* 1982, *4*, 273–284.
- [26] Fan, W., Bakir, U., Glatz, C.E., Contribution of Protein Charge to Partitioning in Aqueous Two-Phase Systems. *Biotechnol. Bioeng.* 1998, *59*, 461–470.
- [27] King, R.S., Blanch, H.W., Prausnitz, J.M., Molecular thermodynamics of aqueous two-phase systems for bioseparations. *AIChE J.* 1988, *34*, 1585–1594.
- [28] Luther, J.R., Glatz, C.E., Genetically engineered charge modifications to enhance protein separation in aqueous two-phase systems: Charge directed partitioning. *Biotechnol. Bioeng.* 1995, *46*, 62–68.

### 3 PUBLICATIONS & MANUSCRIPTS

---

- [29] Walter, H., Krob, E.J., Brooks, D.E., Membrane surface properties other than charge involved in cell separation by partition in polymer, aqueous two-phase systems. *Biochemistry* 1976, *15*, 2959–2964.
- [30] Albertsson, P.A., Nyns, E.J., Counter-Current Distribution of Proteins in Aqueous Polymer Phase Systems. *Nature* 1959, *184*, 1465–1468.

---

## 4 Conclusion & Outlook

This thesis provides insights into novel tools for downstream processing of cell-based therapeutics. A main focus of this thesis was the development of preparative-scale downstream processing strategies using ATPS. The challenge of laborious empirical process optimizations and the lack of mechanistic understanding in ATPS research was addressed by the development of an integrated HTS-platform that enables HT-cell partitioning analysis in ATPS.

In this context, the following issues were addressed:

- Development of analytical technologies for HTS
- Design of an automated robotic screening platform
- Systematic investigation of key parameters in cell partitioning
- Development of downstream processing strategies based on HTS-data and experimental validation

In the first part of this work a comparative study on HT-cell quantification assays was performed, where sensitivity, dynamic range, and precision were evaluated for a number of state-of-the-art cell quantification methods that differ in their respective mechanism. This benchmark study was designed as a guide for selecting HT-cell quantification assays for a specific application. In addition, it identified HT-flow cytometry as an ideal tool for cell quantification and multi-parametric analysis in HT-DSP development for cell-based products.

In the second part of this thesis an automated robotic screening that enables HT-cell partitioning analysis in ATPS was developed and validated. The study demonstrated that this setup enables fast and systematic investigation of factors influencing cell partitioning. In combination with DoE approaches and CCD-modeling it thus presents a powerful enabling technology for translational research.

In the course of this thesis several case studies on HT-DSP development for cell-based products were conducted with numerous model cell lines. The development of a barcoding strategy enabled the multiplexing of numerous cell lines in HTS, which facilitated a significant reduction in time and material consumption. The case studies further identified numerous key parameters in ATPS-mediated cell separation, and provide a benchmark for future applications. The performed case studies demonstrated that the separability of numerous cell lines from a complex mixture, as well as, two distinct cell populations from a differentiation mix is feasible with excellent purity and yield in a CCD-setup. Experimental validation of the CCD-model demonstrated excellent accuracy of the model. The studies further revealed that cell type specific differences are the major driving forces in cell partitioning rather than cell cycle distribution, and that robust and reproducible purification processes are thus feasible.

Future exploitation of this platform will enable more directed DSP development and facilitate a better understanding of the mechanisms underlying cell partitioning in ATPS. Due to the versatility of Tecan LHS, the screening platform can easily be adapted to countless applications. Up- and downscaling can be performed by simply changing the labware type, and the influence of settling time, mixing intensity, fill volume, and vessel geometry can be studied. This enables the simultaneous optimization of numerous parameters for purification processes using a CCD-device. Likewise, various analytical methods, such as different PCR-techniques, ELISA, and high-content screenings (HCS) can be directly integrated into the screening process. The use of HTS-data in combination with DoE strategies and CCD-models will enable the simultaneous investigation of numerous parameters and the optimization of separation conditions for various applications.

The combination of HTS-data with numerous cellular parameters, e.g. surface parameters, such as zeta-potential, or complex spectral data, such as Raman-spectra, and the application of statistical tools, such as multivariate data analysis (MVDA), will provide a more detailed mechanistic understanding and will eventually enable a shift towards a more model-based DSP design.

In conclusion, the here developed technology has facilitated faster, cheaper, and more directed DSP development for cell-based therapeutics, and has demonstrated that ATPS are a promising tool for preparative-scale downstream processing of cell-based therapeutics.

---

## 5 References

Albertsson, P.A. (1986), *Partition of Cell Particles and Macromolecules*, John Wiley & Sons, New York.

Albertsson, P.A. and Barid, G.D. (1962), "Counter-Current Distribution of Cells", *Experimental Cell Research*, Vol. 28, pp. 296–322.

Al-Rubeai, M. and Naciri, M. (2014), *Stem Cells and Cell Therapy*, Springer Netherlands.

Amos, P.J., Cagavi Bozkulak, E. and Qyang, Y. (2012), "Methods of cell purification: a critical juncture for laboratory research and translational science.", *Cells, Tissues, Organs*, Vol. 195 No. 1–2, pp. 26–40.

An, W.F. and Tolliday, N. (2010), "Cell-based assays for high-throughput screening.", *Molecular Biotechnology*, Vol. 45 No. 2, pp. 180–6.

Baird, G., Albertsson, P.A. and Hofsten, B. (1961), "Separation of Bacteria by Counter-Current Distribution", *Nature*, Vol. 192, pp. 236–239.

Bensch, M., Schulze Wierling, P., von Lieres, E. and Hubbuch, J. (2005), "High Throughput Screening of Chromatographic Phases for Rapid Process Development", *Chemical Engineering & Technology*, Vol. 28 No. 11, pp. 1274–1284.

Bensch, M., Selbach, B. and Hubbuch, J. (2007), "High throughput screening techniques in downstream processing: Preparation, characterization and optimization of aqueous two-phase systems", *Chemical Engineering Science*, Vol. 62 No. 7, pp. 2011–2021.

Bluestone, J. A, Trotta, E. and Xu, D. (2015), "The therapeutic potential of regulatory T cells for the treatment of autoimmune disease", *Expert Opinion on Therapeutic Targets*, Vol. 8222 No. January, pp. 1–13.

Buckler, R.L., Kunkel, E.J., Thompson, M.L. and Ehrhardt, R.O. (2016), "Technological developments for small-scale downstream processing of cell therapies", *Cytotherapy*, Elsevier Inc., Vol. 18 No. 3, pp. 301–306.

Cabral, J.M.S. (2007), "Cell Partitioning in Aqueous Two-Phase Polymer Systems", *Advances in Biochemical Engineering/biotechnology*, Vol. 106, pp. 151–171.

Chen, A., Ting, S., Seow, J., Reuveny, S. and Oh, S. (2014), "Considerations in designing systems for large scale production of human cardiomyocytes from pluripotent stem cells.", *Stem Cell Research & Therapy*, Vol. 5, p. 12.

Coffman, J.L., Kramarczyk, J.F. and Kelley, B.D. (2008), "High-throughput screening of chromatographic separations: I. Method development and column modeling.", *Biotechnology and Bioengineering*, Vol. 100 No. 4, pp. 605–18.

Craig, L.C. and Post, H.O. (1949), "Apparatus for Countercurrent Distribution", *Analytical Chemistry*, Vol. 21, pp. 500–504.

Dahlberg, C.I.M., Sarhan, D., Chrobok, M., Duru, A.D. and Alici, E. (2015), "Natural killer cell-based therapies targeting cancer: Possible strategies to gain and sustain anti-

tumor activity”, *Frontiers in Immunology*, Vol. 6 No. NOV.

Daley, G.Q. and Scadden, D.T. (2008), ”Prospects for stem cell-based therapy.”, *Cell*, Vol. 132 No. 4, pp. 544–8.

Darkins, C.L. and Mandenius, C.-F. (2013), ”Design of large-scale manufacturing of induced pluripotent stem cell derived cardiomyocytes”, *Chemical Engineering Research and Design*, Institution of Chemical Engineers, No. August, pp. 1–11.

Diogo, M.M., da Silva, C.L. and Cabral, J.M.S. (2012), ”Separation technologies for stem cell bioprocessing.”, *Biotechnology and Bioengineering*, Vol. 109 No. 11, pp. 2699–709.

Dodson, B.P. and Levine, A.D. (2015), ”Challenges in the translation and commercialization of cell therapies”, *BMC Biotechnology*, *BMC Biotechnology*, Vol. 15 No. 1, p. 70.

Dove, A. (2003), ”Cell-based therapies go live”, *Nature Biotechnology*, Vol. 20, pp. 339–343.

Fan, W., Bakir, U. and Glatz, C.E. (1998), ”Contribution of Protein Charge to Partitioning in Two-Phase Systems”, *Biotechnology and Bioengineering*, Vol. 59 No. 4, pp. 461–470.

Fernandes, T.G., Rodrigues, C.A. V., Diogo, M.M. and Cabral, J.M.S. (2014), ”Stem cell bioprocessing for regenerative medicine”, *Journal of Chemical Technology and Biotechnology*, Vol. 89 No. 1, pp. 34–47.

Fischbach, M.A., Blustone, J.A. and Lim, W.A. (2013), ”Cell-Based Therapeutics: The Next Pillar of Medicine ”, *Science Translational Medicine*, Vol. 5 No. 179, p. ps7.

Fliervoet, L.A.L. and Mastrobattista, E. (2016), ”Drug delivery with living cells”, *Advanced Drug Delivery Reviews*, Elsevier B.V., pp. 1–10.

Forciniti, D., Hall, C.K. and Kula, M.R. (1990), ”Interfacial tension of polyethyleneglycol–dextran–water systems: influence of temperature and polymer molecular weight”, *Journal of Biotechnology*, Vol. 16, pp. 279–296.

Gascoine, P.S. and Fisher, D. (1984), ”The dependence of cell partition in two-polymer aqueous phase systems on the electrostatic potential between the phases”, *Biochemical Society Transactions*, Vol. 12, pp. 1085–1086.

González-González, M., Vázquez-Villegas, P., García-Salinas, C. and Rito-Palomares, M. (2012), ”Current strategies and challenges for the purification of stem cells”, *Journal of Chemical Technology & Biotechnology*, Vol. 87 No. 1, pp. 2–10.

Hatti-Kaul, R. (2000), *Aqueous Two-Phase Systems*, Vol. 11, Humana Press, New Jersey.

Heathman, T.R.J., Nienow, A.W., McCall, M.J., Coopman, K., Kara, B. and Hewitt, C.J. (2015), ”The Translation of Cell-Based Therapies: Clinical Landscape and Manufacturing Challenges.”, *Regenerative Medicine*, Vol. 10 No. 1, pp. 49–64.

---

Hertzberg, R.P. and Pope, A.J. (2000), "High-throughput screening: new technology for the 21st century.", *Current Opinion in Chemical Biology*, Vol. 4 No. 4, pp. 445–51.

Hoffmann, P., Boeld, T.J., Eder, R., Albrecht, J., Doser, K., Piseshka, B., Dada, A., et al. (2006), "Isolation of CD4+CD25+ regulatory T cells for clinical trials.", *Biology of Blood and Marrow Transplantation: Journal of the American Society for Blood and Marrow Transplantation*, Vol. 12 No. 3, pp. 267–74.

Johansson, G. (1998), "Multistage Countercurrent Distribution", *Encyclopedia of Analytical Sciences*, pp. 1398–1405.

King, R.S., Blanch, H.W. and Prausnitz, J.M. (1988), "Molecular thermodynamics of aqueous two-phase systems for bioseparations", *AIChE Journal*, Vol. 34 No. 10, pp. 1585–1594.

Lacki, K.M. (2014), "High throughput process development in biomanufacturing", *Current Opinion in Chemical Engineering*, Vol. 6, pp. 25–32.

Leader, B., Baca, Q.J. and Golan, D.E. (2008), "Protein therapeutics: a summary and pharmacological classification.", *Nature Reviews. Drug Discovery*, Vol. 7 No. 1, pp. 21–39.

Lee, D.W., Kochenderfer, J.N., Stetler-Stevenson, M., Cui, Y.K., Delbrook, C., Feldman, S.A., Fry, T.J., et al. (2015), "T cells expressing CD19 chimeric antigen receptors for acute lymphoblastic leukaemia in children and young adults: A phase 1 dose-escalation trial", *The Lancet*, Elsevier Ltd, Vol. 385 No. 9967, pp. 517–528.

Luther, J.R. and Glatz, C.E. (1995), "Genetically engineered charge modifications to enhance protein separation in aqueous two-phase systems: Charge directed partitioning", *Biotechnology and Bioengineering*, Vol. 46 No. 1, pp. 62–68.

Macarron, R., Banks, M.N., Bojanic, D., Burns, D.J., Cirovic, D. a, Garyantes, T., Green, D.V.S., et al. (2011), "Impact of high-throughput screening in biomedical research.", *Nature Reviews. Drug Discovery*, Nature Publishing Group, Vol. 10 No. 3, pp. 188–95.

Mount, N.M., Ward, S.J., Kefalas, P., Hyllner, J. and Mount, N.M. (2015), "Cell-based therapy technology classifications and translational challenges".

Oelmeier, S.A., Ladd Effio, C. and Hubbuch, J. (2012), "High throughput screening based selection of phases for aqueous two-phase system-centrifugal partitioning chromatography of monoclonal antibodies.", *Journal of Chromatography. A*, Elsevier B.V., Vol. 1252, pp. 104–14.

Pierige, F., Serafini, S., Rossi, L. and Magnani, M. (2008), "Cell-based drug delivery.", *Advanced Drug Delivery Reviews*, Vol. 60 No. 2, pp. 286–95.

Ratcliffe, E., Glen, K.E., Naing, M.W. and Williams, D.J. (2013), "Current status and perspectives on stem cell-based therapies undergoing clinical trials for regenerative medicine: case studies.", *British Medical Bulletin*, Vol. 108, pp. 73–94.

Reitherman, R., Flanagan, D. and Barondes, H. (1973), "Electromotive Phenomena in

Partition of Erythrocytes in Aqueous Polymer Two Phase Systems”, *Biochimica et Biophysica Acta*, Vol. 297, pp. 193–202.

Rodrigues, G.M.C., Rodrigues, C.A. V, Fernandes, T.G., Diogo, M.M. and Cabral, J.M.S. (2015), ”Clinical-scale purification of pluripotent stem cell derivatives for cell-based therapies”, *Biotechnology Journal*, Vol. 10, pp. 1103–1114.

Sart, S., Schneider, Y.-J., Li, Y. and Agathos, S.N. (2014), ”Stem cell bioprocess engineering towards cGMP production and clinical applications”, *Cytotechnology*, Vol. 66 No. 5, pp. 709–722.

Schriebl, K., Lim, S., Choo, A., Tscheliessnig, A. and Jungbauer, A. (2010), ”Stem cell separation: a bottleneck in stem cell therapy.”, *Biotechnology Journal*, Vol. 5 No. 1, pp. 50–61.

Schulz, T.C. (2015), ”Enabling Technologies for Cell-Based Clinical Translation Concise Review: Manufacturing of Pancreatic Endoderm Cells for Clinical Trials in Type 1 Diabetes”, *Stem Cells Translational Medicine*, Vol. 4 No. 8, pp. 927–931.

Schulz, T.C., Young, H.Y., Agulnick, A.D., Babin, M.J., Baetge, E.E., Bang, A.G., Bhoumik, A., et al. (2012), ”A scalable system for production of functional pancreatic progenitors from human embryonic stem cells”, *PLoS ONE*, Vol. 7 No. 5.

Soares, R.R.G., Azevedo, A.M., van Alstine, J.M. and Aires-Barros, M.R. (2015), ”Partitioning in aqueous two-phase systems: Analysis of strengths, weaknesses, opportunities and threats”, *Biotechnology Journal*, Vol. 10, pp. 1158–1169.

Sousa, A.F., Andrade, P.Z., Pirzgalska, R.M., Galhoz, T.M., Azevedo, A.M., da Silva, C.L., Aires-Barros, M.R., et al. (2011), ”A novel method for human hematopoietic stem/progenitor cell isolation from umbilical cord blood based on immunoaffinity aqueous two-phase partitioning.”, *Biotechnology Letters*, Vol. 33 No. 12, pp. 2373–7.

Spohn, G., Wiercinska, E., Karpova, D., Bunos, M., Hümmer, C., Wingefeld, E., Sorg, N., et al. (2015), ”Automated CD34+ cell isolation of peripheral blood stem cell apheresis product”, *Cytotherapy*, Elsevier Inc, Vol. 17 No. 10, pp. 1465–1471.

Stemberger, C., Dreher, S., Tschulik, C., Piossek, C., Bet, J., Yamamoto, T.N., Schiemann, M., et al. (2012), ”Novel serial positive enrichment technology enables clinical multiparameter cell sorting.”, *PloS One*, Vol. 7 No. 4, p. e35798.

Takahashi, K. and Yamanaka, S. (2006), ”Induction of Pluripotent Stem Cells from Mouse Embryonic and Adult Fibroblast Cultures by Defined Factors”, *Cell*, Vol. 126 No. 4, pp. 663–676.

Tang, Q. and Bluestone, J.A. (2013), ”Regulatory T-cell therapy in transplantation: Moving to the clinic”, *Cold Spring Harbor Perspectives in Medicine*, Vol. 3 No. 11, pp. 1–16.

Tohyama, S., Hattori, F., Sano, M., Hishiki, T., Nagahata, Y., Matsuura, T., Hashimoto, H., et al. (2013), ”Distinct metabolic flow enables large-scale purification of mouse and human pluripotent stem cell-derived cardiomyocytes”, *Cell Stem Cell*, Elsevier Inc., Vol.

---

12 No. 1, pp. 127–137.

Tomlinson, M.J., Tomlinson, S., Yang, X.B. and Kirkham, J. (2013), "Cell separation: Terminology and practical considerations", *Journal of Tissue Engineering*, Vol. 4, pp1–15.

Trounson, A. and McDonald, C. (2015), "Stem Cell Therapies in Clinical Trials: Progress and Challenges", *Cell Stem Cell*, Elsevier Inc., Vol. 17 No. 1, pp. 11–22.

Turner, M., Leslie, S., Martin, N.G., Peschanski, M., Rao, M., Taylor, C.J., Trounson, A., et al. (2013), "Toward the development of a global induced pluripotent stem cell library", *Cell Stem Cell*, Elsevier Inc., Vol. 13 No. 4, pp. 382–384.

Vis, M., Peters, V.F.D., Tromp, R.H. and Ern , B.H. (2014), "Donnan Potentials in Aqueous Phase Separated Polymer Mixtures.", *Langmuir*, Vol. 30, pp. 5755–5762.

Walter, H. (1978), "Cell partitioning in two-polymer aqueous phase systems", *TIBS*, Vol. 3.2, pp. 97–100.

Walter, H., Brooks, D.E. and Fisher, D. (1985), *Partitioning in Aqueous Two-Phase Systems - Theory, Methods, Uses, and Applications to Biotechnology*, Academic Press, Inc.

Weil, B.D. and Veraitch, F.S. (2014), "Bioprocessing Challenges Associated with the Purification of Cellular Therapies", *Stem Cells and Cell Therapy*, pp. 129–156.

Wiendahl, M., Schulze Wierling, P., Nielsen, J., Fomsgaard Christensen, D., Krarup, J., Staby, A. and Hubbuch, J. (2008), "High Throughput Screening for the Design and Optimization of Chromatographic Processes – Miniaturization, Automation and Parallelization of Breakthrough and Elution Studies", *Chemical Engineering & Technology*, Vol. 31 No. 6, pp. 893–903.

Willoughby, N. (2009), "Too big to bind: Will the purification of large and complex therapeutic targets spell the beginning of the end for column chromatography?", *Journal of Chemical Technology & Biotechnology*, Vol. 84, pp. 145–150.

Ye, Z. and Mahato, R.I. (2008), "Emerging trends in cell-based therapies.", *Advanced Drug Delivery Reviews*, Vol. 60 No. 2, pp. 89–90.

Zang, Y., Kammerer, B., Eisenkolb, M., Lohr, K. and Kiefer, H. (2011), "Towards protein crystallization as a process step in downstream processing of therapeutic antibodies: screening and optimization at microbatch scale.", *PloS One*, Vol. 6 No. 9, p. e25282.

Zhu, B. and Murthy, S.K. (2013), "Stem Cell Separation Technologies.", *Current Opinion in Chemical Engineering*, Vol. 2 No. 1, pp. 3–7.

## 5 REFERENCES

---

---

## 6 Abbreviations

Abbreviation	Definition
ALL	Acute lymphoblastic leukemia
ALS	Amyotrophic lateral sclerosis
ASC	Adult stem cells
ATMP	Advanced therapy medicinal product
ATP	Adenosine triphosphate
ATPS	Aqueous two-phase systems
BSA	Bovine serum albumin
CAR	Chimeric antigen receptor
CCC	Countercurrent chromatography
CCD	Countercurrent distribution
CNS	Central nervous system
CPC	Centrifugal partition chromatography
CV	Coefficient of variation
DAPI	4', 6-diamidino-2-phenylindole
DC	Dendritic cells
DEP	Dielectrophoresis
DL	Detection limit
DMSO	Dimethyl sulfoxide
DNA	Deoxyribonucleic acid
DoE	Design of experiments
DPBS	Dulbecco's phosphate buffered saline
dsDNA	double-stranded DNA
DSP	Downstream process
EDTA	Ethylenediaminetetraacetic acid
ELISA	Enzyme-linked immuno sorbent assay
ESC	Embryonic stem cells
FACS	Fluorescence activated cell sorting
FDA	U.S. food and drug administration
FFF	Field flow fractionation
GvHD	Graft-vs-host disease
HBSS	Hank's balanced salt solution
HCS	High-content screening
hESC	Human embryonic stem cells
hiPSC	Human induced pluripotent stem cells
HLA	Human leukocyte antigen
HSC	Hematopoietic stem cells
HT	High-throughput
HTPD	High-throughput process development
HTS	High-throughput screening
iPSC	Induced pluripotent stem cells
kDa	kilo dalton
mAb	Monoclonal antibody
MACS	Magnetic activated cell sorting

## 6 ABBREVIATIONS

---

MSC	Mesenchymal stem cells
MVDA	Multivariate data analysis
MW	Molecular weight
NaCl	Sodium chloride
NaPi	Sodium phosphate
NK	Natural killer cells
NSC	Neural stem cells
PBMC	Peripheral blood mononuclear cells
PCR	Polymerase chain reaction
PEG	Polyethylene glycol
pH	Pondus hydrogenii
PSC	Pluripotent stem cells
QL	Quantitation limit
STL	Slope of tie-line
TLL	Tie-line length
Tregs	Regulatory T-cells
UV	Ultraviolet
$w_i$	Weighting factor